

UC Irvine

UC Irvine Electronic Theses and Dissertations

Title

Complementarity in Dark Matter Phenomenology

Permalink

<https://escholarship.org/uc/item/5xm0h8rj>

Author

Wijangco, Alexander Matthew

Publication Date

2015

Peer reviewed|Thesis/dissertation

UNIVERSITY OF CALIFORNIA,
IRVINE

Complementarity in Dark Matter Phenomenology

DISSERTATION

submitted in partial satisfaction of the requirements
for the degree of

DOCTOR OF PHILOSOPHY

in Physics

by

Alexander Matthew Wijangco

Dissertation Committee:
Professor Arvind Rajaraman, Chair
Professor Tim Tait
Associate Professor Yuri Shirman

2015

Chapter 2 © 2011 Physical Review D
Chapter 3 © 2013 Physics of the Dark Universe
Chapter 4 © 2014 Physical Review D
Chapter 5 © 2014 Physical Review D
All other materials © 2015 Alexander Matthew Wijangco

DEDICATION

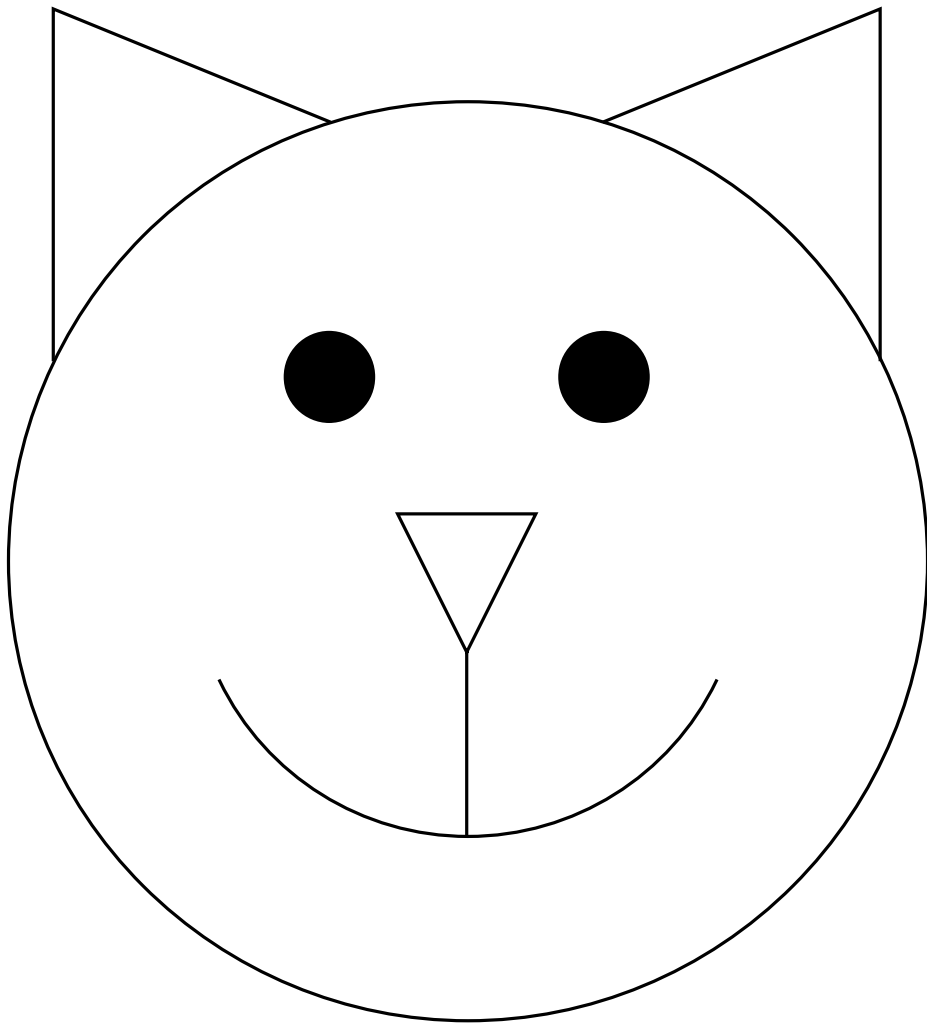


TABLE OF CONTENTS

	Page
LIST OF FIGURES	vi
LIST OF TABLES	x
ACKNOWLEDGMENTS	xi
CURRICULUM VITAE	xii
ABSTRACT OF THE DISSERTATION	xiv
1 Introduction	1
2 LHC Bounds on Interactions of Dark Matter	6
2.1 Introduction	6
2.2 Model Description	9
2.3 Collider Searches	12
2.3.1 Tevatron Constraints	13
2.3.2 LHC Constraints	14
2.3.3 LHC Future Reach	15
2.4 Direct Detection	16
2.5 Conclusion	19
2.6 Acknowledgements	23
3 Effective Theories of Gamma-ray Lines from Dark Matter Annihilation	25
3.1 Introduction	25
3.2 Effective Field Theory	27
3.3 Line Cross Sections	30
3.3.1 Dimension 6 Operators	31
3.3.2 Dimension 7 Operators	32
3.3.3 Dimension 8 Operators	34
3.4 Summary	35
3.5 Outlook	37
3.6 Acknowledgments	39

	4 Particle Physics Implications and Constraints on Dark Matter Interpretations of the CDMS Signal	40
4.1	Introduction	40
4.2	Simplified Model Framework	42
4.3	DM Observables	44
4.4	Collider & Low-Energy Constraints	48
	4.4.1 Mono-Objects	48
	4.4.2 Heavy-Flavor Searches	50
	4.4.3 B-Factory Constraints	52
	4.4.4 Exotic Higgs Decays	52
4.5	Discussion	54
4.6	Acknowledgments	55
5	Hidden On-Shell Mediators for the Galactic Center Gamma-ray Excess	58
5.1	Introduction	58
	5.1.1 From Effective Theories to Simplified Models	60
	5.1.2 The Gamma-ray Excess Suggests Light Mediators	61
	5.1.3 Annihilation to On-shell Mediators	62
5.2	On-Shell Simplified Models	64
	5.2.1 Parity Versus Chirality	65
	5.2.2 Mediators Versus s-wave Annihilation	66
	5.2.3 Requirements for On-Shell Mediators	68
	5.2.4 Estimates for the Gamma-ray Excess	70
5.3	The Gamma-Ray Excess from On-Shell Mediators	71
	5.3.1 Mediator Spectra	72
	5.3.2 Generating Gamma-Ray Spectra	73
	5.3.3 Fitting the Gamma-Ray Excess	74
5.4	Experimental Bounds on the SM Coupling	77
	5.4.1 Indirect Detection	77
	5.4.2 Direct Detection	79
	5.4.3 Collider bounds	80
5.5	Viability as a Thermal Relic	82
	5.5.1 s-wave Cross Section	83
	5.5.2 s-channel and p-wave Corrections	84
	5.5.3 MSPs Can Save Freeze-Out	85
	5.5.4 Conditions for Thermal Equilibrium	86
5.6	Comments on UV Completions and Model Building	86
	5.6.1 Minimal Flavor Violation	86
	5.6.2 Gauge symmetries	88
	5.6.3 Renormalizability	89
	5.6.4 Self-Interacting Dark Matter	90
	5.6.5 Prototypes for UV models	90
	5.6.6 Exceptions	91
5.7	Conclusions and Outlook	92

5.8	Acknowledgements	93
5.9	Appendix: The Spectrum of Spectra	94
6	Conclusion	98
	Bibliography	100

LIST OF FIGURES

	Page	
2.1	The collider bounds on the down-type quark operators with scalar Lorentz structures. Operators M1d, M2d, M3d, M4d, are in red, blue, green, and black respectively. The dashed-dotted, dashed, and solid lines are the Tevatron constraints, LHC constraints, and LHC discovery reach. The shaded region is where the effective theory breaks down. Models M1d and M3d are largely degenerate, as are models M2d and M4d.	13
2.2	The same as Fig. 2.1, for up-type quark operators M1u, M2u, M3u, and M4u.	14
2.3	The collider bounds on the down-type quark coupling operators mediated by a heavy scalar. Models M5d, M6d are in red, black respectively. The dashed-dotted, dashed, and solid lines are the Tevatron constraints, LHC constraints, and LHC discovery reach. The shaded region is where the effective theory breaks down. Models M5d and M6d are largely degenerate.	15
2.4	The same as Fig. 2.3, although now the up-type quark coupling operators M5u and M6u are displayed.	16
2.5	Spin-dependent nucleon scattering cross section assuming only the up-type quark operator M6u is present. The red and blue lines are the constraints from the Tevatron search and 7 TeV LHC search. The green lines are the 14 TeV LHC discovery reach. The solid lines are the proton coupling cross section and the dotted lines are the neutron coupling cross section. The dashed black line is the Xenon 10 constraint on the neutron cross section [1] and the solid black line is the SIMPLE constraint on the proton cross section [2].	18
2.6	The same as Fig. 2.5 but for the down-type quark coupling.	19
2.7	Spin dependent nucleon coupling cross section assuming equal down and up type couplings. The red and blue lines are the constraints from the Tevatron search and 7 TeV LHC search. The green line is the 14 TeV LHC discovery reach. The dashed black line is the XENON10 constraint on the neutron cross section [1], the solid black line is the SIMPLE constraint on the proton cross section.[2]	20
2.8	Spin independent proton scattering cross section assuming only up-type quark coupling. The red line is the constraint from the Tevatron search. The blue lines are the LHC 7 TeV constraint and LHC 14 discovery reach, which are dashed and solid respectively. The brown line is the XENON100 constraint [3]. The black lines (both solid and dashed) are the CDMS constraints [4, 5]. The orange region is CoGeNT favored results.[6]	21

2.9	The same as Fig. 2.8 but for the down-type coupling.	22
2.10	Spin independent coupling assuming both down and up type couplings such that the proton and neutron coupling is equal. The blue lines are the LHC 7 TeV constraint and LHC 14 discovery reach, which are dashed and solid respectively. The brown line is the XENON100 constraint.[3] The black lines (both solid and dashed) are the CDMS constraints.[4, 5] The orange region is CoGeNT favored results.[6]	23
2.11	Spin independent coupling assuming both down and up type coupling such that the neutron to proton coupling ratio is -0.7. The red line is the constraint from the Tevatron search. The blue lines are the LHC 7 TeV constraint and LHC 14 discovery reach, which are dashed and solid respectively. The green line is the XENON100 constraint.[3] The black lines (both solid and dashed) are the CDMS constraints.[4, 5] The orange region is CoGeNT favored results.[6]	24
4.1	Spin-Independent Scattering and Relic Density. The blue band denotes SI scattering cross-sections within the range Eqn. 4.2 (darker and lighter regions describing the extent of 1σ and 2σ ellipses in the result [7], respectively). The red band shows where our χ 's relic density is $\Omega_\chi \approx \Omega_{CDM}$. In the upper panels g_u and g_d are related such that $f_n = f_p$ (IP), while in the lower panels $f_n/f_p = -0.7$ (IV).	47
4.2	Monojet and $t\bar{t}$ + MET bounds on our model in the $g_\chi g_d$ vs. m_ϕ plane (IP left panel, IV right panel). The blue bands gives scattering cross-sections in the desired range, as in Fig. 4.1, while the gray regions are excluded by the ATLAS monojet search [8] and the ATLAS $t\bar{t}$ + MET search [9] (both at 95% confidence) as noted in the figure. The limits in this plot were generated with fixed $g_d = 1$	49
4.3	Heavy Flavor bounds on our model in the $t\bar{t}b$ channel (IP left panel, IV right panel). As this search depends only on the coupling g_d we display, in red and blue bands, the favored regions for scattering with $g_\chi = 0.01$ and $g_\chi = 1$, respectively. The gray region denotes parameter space for which the $t\bar{t}\phi$ production cross-section is greater than that for $t\bar{t}H$ production of the SM Higgs (our rough criterion for exclusion given the result [10]).	51
4.4	Bounds from the radiative Υ -decays to hadronic and di-tau final states. Gray regions are excluded by <i>BaBar</i> analyses [11] and [12] (as noted in the figure) at 90% confidence. The red and blue bands give direct detection favored regions for $g_\chi = 0.01$ and $g_\chi = 1$ as in Fig. 4.3. Favored regions are calculated for both IP (left) and IV (right) cases.	53
4.5	Combined bounds in the $g_\chi g_d$ vs. m_ϕ plane. Bounds from $t\bar{t}$ + MET, $t\bar{t}$ +b-jet and radiative Υ decays (in both hadronic and τ channels) are labelled accordingly. Monojet bounds are irrelevant, given the axes ranges plotted. We choose $g_\chi = 1$ ($g_\chi = 0.1$) in the upper (lower) panels to translate bounds that only depend on g_d onto this plane. Left and right panels correspond to IP and IV scenarios, respectively. We use a dashed line to remind the reader that the $t\bar{t}$ +b-jet bound is particularly rough (as described in the text). . . .	56

4.6	As in Figure 4.5, but with the inclusion of direct detection and <i>Planck</i> favored bands in blue and red, respectively.	57
5.1	(a) Annihilation, (b) Direct Detection, (c) Collider. Complimentary modes of dark matter detection. Annihilation sets both the thermal relic abundance and the present-day indirect detection rate.	59
5.2	(a) Annihilation, (b) Direct Detection, (c) Collider. DM complimentarity for on-shell mediators; compare to Fig. 5.1. (a) The annihilation rate is independent of the mediator coupling to the Standard Model. (b) Direct detection remains 2-to-2, here N is a target nucleon. (c) Colliders can search for the presence of the mediator independently of its DM coupling.	63
5.3	Dark matter annihilates to on-shell mediators, which in turn decay into $b\bar{b}$ pairs. Each step is controlled by a separate coupling, λ . See text for details.	64
5.4	(a) $\chi\bar{\chi} \rightarrow VV \rightarrow 4b$, (b) $\chi\bar{\chi} \rightarrow 3\varphi$, (c) $\chi\bar{\chi} \rightarrow 3\varphi \rightarrow 6b$. Energy spectrum with arbitrary normalization from DM annihilation for (a) b quarks from two on-shell spin-1 mediators, (b) pseudoscalar mediators, (c) b quarks from three on-shell pseudoscalar mediators. (a) corresponds to $m_\chi = 80$ GeV while (b,c) corresponds to $m_\chi = 120$. Lines correspond to $m_V = 15, 30, 55, 60$ GeV or $m_\phi = 15, 45, 55, 60$ GeV from red (solid) to blue (most dashed). The ‘box’ width in (a) is not monotonically decreasing with m_V , as evidenced by the 30 GeV line (orange).	72
5.5	(a) Comparison, (b) Spin-1, (c) Spin-0. Predicted spectra for the galactic center γ -ray excess (GCE) for (a) the best fit models categorized by the number of final state b quarks, (b) a range of spin-1 mediator masses, (c) a range of spin-0 mediator masses. Overlaid is the measured γ -ray spectrum from [13], bars demonstrate an arbitrary measure of goodness-of-fit. See Sec. 5.3.3 for details.	73
5.6	Fits for on-shell annihilation through spin-1 mediators. LEFT: best fit values of λ_{DM} . RIGHT: fit significance highlighting the best $(m_\chi, m_{\text{med.}})$ values. See text for details.	74
5.7	Fits for on-shell annihilation through spin-0 mediators. LEFT: best fit values of λ_{DM} . RIGHT: fit significance highlighting the best $(m_\chi, m_{\text{med.}})$ values. See text for details.	76
5.8	(a) Spin-1 (b -philic), (b) Spin-1 (q -democratic), (c) Spin-0. Fits including s -channel diagrams to the case of a (a) spin-1 mediator coupling only to b , (b) spin-1 mediator coupling to all quarks equally, and (c) pseudoscalar mediator. Plots assume that the s -channel diagrams are s -wave, see Tab. 5.2. Smaller values correspond to better fits, see (5.13).	78
5.9	Estimated direct detection bounds on the mediator–SM coupling (λ_{SM}) for interactions $\mathcal{O}_\chi \otimes \mathcal{O}_q$ defined in (5.1). The dashed (solid) lines assume the benchmark value $m_\chi = 120$ (80) GeV for spin-0 (1) mediators and the median DM couplings in (5.11–5.12).	79

5.10	Fits for on-shell annihilation through spin-1 mediators assuming universal coupling to all quarks; compare to Fig. 5.6 which assumed a coupling to only b quarks. LEFT: best fit values of λ_{DM} . RIGHT: fit significance highlighting the best ($m_\chi, m_{\text{med.}}$) values. See Section 5.3.3 for details.	88
5.11	(a) $\chi\bar{\chi} \rightarrow gg$, (b) $\chi\bar{\chi} \rightarrow gg$ (67%) or $b\bar{b}$ (33%), (c) $\chi\bar{\chi} \rightarrow \tau\bar{\tau}$, (d) $\chi\bar{\chi} \rightarrow \tau\bar{\tau}$ (85%) or $b\bar{b}$ (15%), (e) $\chi\bar{\chi} \rightarrow 6g$, (f) $\chi\bar{\chi} \rightarrow 2 \times [\tau\bar{\tau}$ (85%) or $b\bar{b}$ (15%)]. Spectra for various final states, including branching ratios to different final states. 4-(6-)body final states originate from on-shell mediators with masses m_V (m_φ) shown. For visual comparison with other plots in this work, the gray $2b$ line is the $\chi\bar{\chi} \rightarrow b\bar{b}$ best fit spectrum and dots are the measured galactic center γ -ray excess spectrum (GCE) assuming a $b\bar{b}$ signal template from [13]. Bars demonstrate an arbitrary measure of goodness-of-fit with respect to this spectrum. Note that the γ -ray excess data depends on the template used for the DM γ -ray spectrum so these data points are mainly for comparative purposes and are not necessarily representative of the goodness-of-fit to the γ -ray excess. See Sec. 5.3.3 for details.	95

LIST OF TABLES

		Page
2.1	The list of the effective operators defined in Eq. (2.2).	11
3.1	List of effective interactions for complex scalar dark matter and the type of line signals ($\gamma\gamma$, γZ , and/or γh) that they produce.	28
3.2	List of effective interactions for Dirac fermion dark matter and the type of line signals ($\gamma\gamma$, γZ , and/or γh) that they produce.	29
3.3	The strength of the first and second (when applicable) gamma ray line signals for each operator described in the text.	38
5.1	Contact operators between Dirac DM and quarks or gluons [14] that support s -wave annihilation and the constraint for the galactic center. See [15] for a recent technical analysis.	61
5.2	Annihilation to mediators. S,P,V,A correspond to scalar, pseudoscalar, vector, and axial vector interactions with DM. Also shown: the leading velocity (partial wave) dependence, whether the process may occur on-shell, and the approximate mass for 40 GeV final state b quarks. The off-shell axial coupling is s - or p -wave for axial/vectorlike SM coupling respectively [16].	66
5.3	Best fit parameters assuming b -philic couplings for the spin-0 mediator and universal quark couplings for the spin-1 mediator. The upper bound for λ_{SM} for the $\gamma^5 \otimes \gamma^5$ is a conservative estimate for the 8 TeV mono- b reach at the LHC (see Section 5.4.3); the other bounds come from direct detection. In the last column, we indicate whether consistency with a thermal relic abundance suggests a tighter DM profile ($\gamma = 1.3$) or some population of millisecond pulsars (MSP), see Section 5.5.	92

ACKNOWLEDGMENTS

I would like to thank the UCI particle theory faculty: Mu-Chun Chen, Jonathan Feng, Herbert Hamber, Yuri Shirman, Tim Tait, and in particular my advisor Arvind Rajaraman. Through their tutelage, support, and care I have learned to appreciate the quantum world, the beauty of symmetry, and elegance of the structure that binds our world.

I would like to thank the post docs and fellow graduate students whom I have had the pleasure of working with. I believe many of the finest moments in my education came from when we learned from one another.

I would like to thank the GAANN Fellowship, the UCI Department of Physics and Astronomy, and the UCI Particle Theory Group for their financial support during my graduate career. Fundamental science research is only possible with the continued financial support of society, and they have my gratitude for affirmation that this endeavor is worth their support.

I would like to acknowledge the journals Physical Review D and Physics of the Dark Universe, in which some portions of this thesis have been published.

Finally, I would like to thank my family. It is with them that I started my pursuit of knowledge, a quest which has become the focus of my life. I hold these beginning most dear, and they will always have my love and gratitude.

CURRICULUM VITAE

Alexander Matthew Wijangco

EDUCATION

Doctor of Philosophy in Physics University of California Irvine	2015 <i>Irvine, California</i>
Master of Science in Physics University of California Irvine	2012 <i>Irvine, California</i>
Bachelor of Science in Physics Case Western Reserve University	2010 <i>Cleveland, Ohio</i>
Bachelor of Arts in Mathematics Case Western Reserve University	2010 <i>Cleveland, Ohio</i>
Bachelor of Arts in Philosophy Case Western Reserve University	2010 <i>Cleveland, Ohio</i>
Bachelor of Arts in Psychology Case Western Reserve University	2010 <i>Cleveland, Ohio</i>

RESEARCH EXPERIENCE

Graduate Research Assistant University of California, Irvine	2010–2015 <i>Irvine, California</i>
--	---

TEACHING EXPERIENCE

Teaching Assistant University of California, Irvine	2010–2015 <i>Irvine, California</i>
---	---

PUBLICATIONS

- Hidden On-Shell Mediators for the Galactic Center
Gamma-Ray Excess** 2014
Phys.Rev., D90:035004, 2014
- Particle Physics Implications and Constraints on Dark
Matter Interpretations of the CDMS Signal** 2014
Phys.Rev., D90:013020, 2014.
- Large θ_{13} in a SUSY $SU(5)_X$ Model** 2014
JHEP, 1310:112
- Working Group Report: Dark Matter Complementarity** 2013
arXiv:1310.8621
- Dark Matter in the Coming Decade: Complementary
Paths to Discovery and Beyond** 2013
arXiv:1305.1605
- Compatibility of θ_{13} and the Type I Seesaw Model with
 A_4 Symmetry** 2013
JHEP, 1302:021, 2013
- Effective Theories of Gamma-ray Lines from Dark Mat-
ter Annihilation** 2013
Phys.Dark Univ., 2:17–21, 2013.
- LHC Bounds on Interactions of Dark Matter** 2011
Phys.Rev., D84:095013, 2011.

CONFERENCE TALKS

- Dark Matter and Complementarity** May 2014
2014 Phenomenology Symposium
- Particle Physics Implications and Constraints on Dark
Matter Interpretations of the CDMS Signal** Aug 2013
TeV Particle Astrophysics
- Dark Matter and Complementarity** June 2013
TASI Student Talks

ABSTRACT OF THE DISSERTATION

Complementarity in Dark Matter Phenomenology

By

Alexander Matthew Wijangco

Doctor of Philosophy in Physics

University of California, Irvine, 2015

Professor Arvind Rajaraman, Chair

The particle nature of dark matter remains an open question to the physics community, despite a monumental effort to determine its properties. These efforts have resulted in a wealth of experimental knowledge and a rich model space of possible explanations. Dark matter phenomenology stands at the intersection of these efforts, and this thesis contains a series of works that attempt to constrain or construct models based on the empirical data. The first of these works details the insights the initial results of the LHC had on isospin violating dark matter in the context of effective operators. The next work deals with the possible effective operators between Dirac dark matter and photon lines at indirect detection experiments. The third is about a model of light scalar mediators used to explain a possible signal at the CDMS experiment. The fourth and final work concerns itself with a particular annihilation topology generated by dark matter going to on-shell mediators.

Chapter 1

Introduction

Dark matter was a term coined in 1933 by Fritz Zwicky, who noticed discrepancies between various methods used to infer amount of mass in the Coma galaxy cluster (or extra-galactic nebulae, as he thought at the time) [17]. The difference arose when a gravitational measurement of the mass, based off the application of the viral theorem, was far larger than a luminous measurement, based on the amount of starlight observed. Zwicky conjectured that perhaps there was some other matter present that did not contribute to the luminous measurement (hence dark), but would still contribute to the gravitational measurement. This new mass component was called dark matter and has proven to be quite robust in its explanatory power. Since Zwicky, it is now understood that the mass of galaxy clusters are dominated by its dark component. For example, a more modern survey of the viral mass of over 1,000 galaxies have found that the average mass to light ratios of these objects to be about $300 hM_{\odot}/L_{\odot}$ [18]. Evidence for dark matter in galactic clusters come from a number of other, independent gravitational probes as well. Notable among these is the evidence from gravitational lensing, particularly in the case of the Bullet cluster [19]. The Bullet cluster consists of two galactic clusters which are currently in the later phases of a collision. During this collision, the two clusters pass through each other but different kinds of matter pass

through with different degrees of ease. Compared to conventional matter, dark matter is relatively collision-less and has passed through. The luminous matter is not, and one can observe the luminous matter being pulled away toward the otherwise invisible but dominant dark matter. Other lensing surveys confirm similar conclusions on the large presence of dark matter; for example see [20] for a survey of the Coma cluster.

The hypothesis of dark matter has more influence than at the scale of galactic clusters, and the evidence at these other scales adds to the robustness of the idea. In fact, the historically the next major piece of evidence for dark matter after Zwicky came in the form of galactic rotation curves. In 1969, Vera Rubin studied the velocities of objects within the Andromeda galaxy and found that they leveled off as one moves further away from the galactic center [21]. This implied that the density of matter scaled as $1/r^2$, a pattern that the luminous matter did not follow. However, this discrepancy could be resolved if dark matter were present, is also rather informative on the dark matter distribution of galaxies. As examples, see these measurements of M31 [22, 23] and this survey over a set of galaxies [24]. These surveys indicate that dark matter is in fact the dominate mass fraction of galaxies and play a key roll in holding together these galaxies. This is perhaps most clearly illustrated by the observation of dwarf satellite galaxies, which have the greatest ratios of dark matter mass to luminous matter mass observed [25, 26]. Dark matter's explanatory power extends to the largest scales too, with evidence for dark matter presenting itself in the cosmic microwave background (CMB). Measurements of the CMB indicate that the non-relativistic fraction of the universe's energy budget is far larger than the prediction for this quantity from just baryons. Dark matter is an excellent candidate to explain this discrepancy, and the most recent measurements indicate that there's about five times more dark matter in the universe than conventional matter [27]. Dark matter is further supported by simulation, indicating that dark matter is principally responsible for large scale structure formation. The most famous of these simulations being the Millennium project [28].

This mountain of evidence has convinced many scientists that dark matter exists, but little is known about dark matter outside of gravitational evidence. This would be principally done by the observation of other, non-gravitational interactions and has thus been the focus of a large fraction of dark matter research. A popular framework (although not the only framework) to model dark matter is to suppose that dark matter is comprised of Weakly Interacting Massive Particles (WIMPs). WIMPs are relatively simple and naturally generated in a large number of theoretical models. Moreover, WIMPs are particularly well suited for satisfying the amount of cosmological dark matter indicated through a process known as thermal freeze out and a choice of electroweak scale cross sections (known as the WIMP miracle). On the experimental side, the searches for WIMP interaction can be classified into one of three categories: direct detection, indirect detection, and collider searches (direct production). The idea behind direct detection is to observe WIMP-nucleon scattering using a man made target and the local dark matter abundance of the solar system. These efforts have yielded mixing results, with some experiments claiming to have observed candidate interaction events [29, 30, 31, 32, 33] with others contradict that claim and exclude large regions of the WIMP interaction parameter space [34, 35, 36, 7]. Indirect detection experiments attempt to observe the byproducts of WIMP annihilation or decays into visible objects. This will usually only be possible by looking at regions with large dark matter densities, with the popular candidate being the center of the Milky Way. Like direct detection, the results of these experiments are not completely straightforward to interpret. Some claim evidence for a signal [37, 13, 38] whereas other have result that indicatd these signals may be due to other astrophysical processes [39, 40]. Finally, collider searches attempt to produce either dark matter directly and infer this production by the recoil of visible particles. The results of different collider searches in this case are all in agreement: no WIMP production has yet to be observed [41, 42].

The theoretical side of dark matter is faced with a rather philosophical question of what kind of WIMP models are worth considering, as the number of properties one can ascribe to

a WIMP are quite large. Some have approached this problem with a data driven mindset, proposing models motivated by experimental hints of signals or models that are probable in the near future. Others choose to maximize the explanatory power of an idea, and relate dark matter to other problems in physics such as the gauge hierarchy problem or the strong CP problem. One can classify these different ideas on a spectrum that measures the amount of theoretical assumptions made. On one end of this continuum are "top down" ideas, which are often UV complete theories designed to explain more than just dark matter. These theories tend to require dark matter to couple in a particular fashion related to the nature of the UV physics. On the opposite end of the spectrum, the "bottom up" approach attempts to consider only the degrees of freedom relevant to dark matter interaction with the standard model. These approaches are usually more general, as many UV theories will often map to a particular bottom up framework. However, it is likely the case that a "bottom up" model would not tell the whole story of new physics. For a review on different dark matter candidates and the experimental reach for their parameter space, see [43, 44]. The focus of this thesis will be on a series of works featuring the "bottom up" approach, and highlight some of the insights that can be gained from such a methodology. This is particularly relevant given the aforementioned mixed experiment results, as apparent contradictions in nature imply a need for new theoretical frameworks to interpret the data.

This thesis will consist primarily of four works, this introduction, and some concluding remarks. The first two works will highlight the framework of effective operators, which restricts the degrees of freedom to only the particles that propagate at the energy scale relevant. For dark matter phenomenology, these typically include only the standard model and the dark matter candidate. The set of operators generated (or a subset, depending if there are additional symmetries present) will be the some subset of the operators generated in any UV theory that features the same dark matter candidate. This is particularly useful if the additional UV degrees of freedom are heavy compared to the energy scale in question, as the coefficient of these operators are dominated by these heavy masses. One can therefore pa-

parameterize the model without knowing the details of the heavy physics, and UV models will have a faithful map to the choice of parameterization so long as the energy scale remains well below any new degrees of freedom. An example of using this framework to probe an interesting area of parameter space for direct detection will be presented in chapter 2. Chapter 3 will feature this framework in the context of photon lines at indirect detection experiments. The remaining two chapters will feature another "bottom up" approach which has been termed "simplified models." In addition to the degrees of freedom used with effective operators, a UV complete model may include the propagators of these interactions, new symmetries and new particles to fill those multiplets, new dark sectors, and much more. However, most of these degrees of freedom may not be relevant to dark matter phenomenology. Simplified models attempt to characterize only the relevant degrees of freedom, such as a dark matter candidate and a mediator. This can result in models which naturally predict different cross sections than effective operators for experimental processes, an example of which will be illustrated in chapter 4, or entirely new signal topologies, an example of which will be in chapter 5. Chapter 6 will contain some concluding remarks.

Chapter 2

LHC Bounds on Interactions of Dark Matter

Arvind Rajaraman, William Shepherd, Tim M.P. Tait and Alexander M. Wijangco

2.1 Introduction

The evidence for the existence of dark matter in the universe is overwhelming [45], and models to incorporate dark matter into our understanding of the fundamental physics of the universe are myriad. Astrophysical observations tell us nothing about the mass of the dark matter particle or whether it interacts with the Standard Model (SM) particles in any way other than gravitationally. Models range in masses from keV to the GUT scale, and in coupling strength from slightly weaker than QCD couplings to purely gravitational interactions. The most popular models are driven by the WIMP(less) miracle [46], suggesting that the dark matter particle relic density should naturally be set by the thermal history of the universe and favoring a ratio of the mass and coupling strength. Such dark matter

candidates naturally appear in extensions of the Standard Model which are designed to address other theoretical issues, most notably the gauge hierarchy problem. Since WIMPs have fairly large couplings to SM fields to explain their relic density, it is possible to search for them interacting directly with normal matter, annihilating into normal matter, or being produced at high energy colliders.

Any WIMP which produces a signal in one of these searches would naively be expected to be seen in others as well, as a single coupling could be visible to all of them. Each type of experiments has a particular set of strengths and weaknesses associated with its ability to discover or exclude various models of dark matter. Direct detection experiments have a signal that is strongly peaked at very low energies, making it hard to distinguish from background effects and causing detector thresholds to be particularly troublesome when light candidate particles are considered. Indirect detection searches for dark matter annihilation products are able to observe locations which have much higher local densities of dark matter than our solar system, but then must contend with large astrophysical background uncertainties. Colliders have a fixed amount of energy available to them in the collisions (and do not take advantage of the dark matter already present in the galactic halo), and are thus unable to produce dark matter of very large mass, but have exceptional sensitivity to low mass WIMPs, which are ill constrained by the other two techniques. Any signal seen at colliders may be due to other new physics than dark matter, so astrophysical confirmation will be critical to being able to make robust claims regarding dark matter at colliders. However, colliders are able to make strong exclusion statements in the event of no signal [47, 48, 49, 50, 51, 52, 14, 53, 54, 55, 56, 57, 58, 59, 60, 61].

Currently there is much interest in light WIMP models, with masses of order $\lesssim 10$ GeV, motivated in large part by experimental results from the CoGeNT collaboration [6, 62] which can be explained by such a WIMP and appear to be tantalizingly close to the parameter space favored by a dark matter interpretation of the longstanding DAMA annual modulation

signal [36, 63, 64]. As the CoGeNT collaboration has recently reported that they also see annual modulation in their data [62], these results have only grown more interesting. These putative signals are, however, in significant tension with negative results from the Xenon 100 [3] and CDMS-II [65, 4, 5] collaborations, and the modulation exhibits an unexpected dependence on the recoil energy of the scattered nucleus [66, 67, 68].

In this work we extend previous studies [52, 14, 53, 54, 69] which use the framework of effective field theory to construct models of dark matter and constrain them from collider searches. These models make specific predictions for other dark matter searches as well, and allow the collider constraints to be drawn on a direct detection plane. Similarly, constraints from indirect searches can be interpreted in these models on the plane of direct detection [70, 71, 72]. We enlarge our previous set of effective theories to allow couplings to only one type of quarks at a time. This allows for the inclusion of effects which distinguish between quark charge in the model-independent framework which we previously presented and are more representative of the range of possible couplings present in models with minimal flavor violation (MFV) [73]. In particular, the dependence on $\tan\beta$ expected in type-II two Higgs doublet extensions of the SM (such as in the Minimal Supersymmetric Standard Model) can be easily represented in this set of models, in contrast to our previous work.

A recent proposal [74, 75] suggests that dark matter interactions may be sensitive to the specific proton and neutron content of the nucleus with which it is scattering, rather than just the net baryon number (the mass of the nucleus). For a WIMP whose couplings satisfy $\lambda_n/\lambda_p \sim -0.7$, one obtains consistency between the negative results of the Xenon collaboration and the putative signal seen at CoGeNT by largely canceling the coupling to xenon nuclei. This parameter point has the additional feature that it shifts the DAMA target region such that it moves from being close to but inconsistent with the CoGeNT signal, to a situation where CoGeNT and DAMA are fit by consistent choices of parameters. In a short time, many models predicting or utilizing this “isospin-violating” mechanism have appeared

in the literature [76, 77, 78, 79, 80, 81].

This article is organized as follows: In section 2.2 we discuss the effective field theory modeling of WIMP-SM interactions, in section 5.4.3 we calculate bounds on the strength of dark matter interactions using collider data and present future reach for the LHC, in section 2.4 we discuss the impact of these bounds on direct detection signals, and in section 2.5 we present our conclusions.

2.2 Model Description

In formulating our constraints on dark matter from collider searches we assume that the dark matter candidate is the only new particle which is accessible at the relevant experiments and that dark matter is a SM gauge singlet. Under these assumptions, only non-renormalizable couplings are possible between dark matter and the SM fields. We therefore focus on the operators which are of the lowest dimensionality, as these will give the strongest signals at energies below the scale which characterizes the interactions.

As with any effective field theory, the models of dark matter we construct in this way are only applicable below some cutoff scale where other new physics becomes relevant and renormalizability is regained. This cutoff is approximately at the mass of the lowest-lying state which is integrated out in the effective theory. This is related to the scale suppressing the higher-dimensional operators and the couplings of the fundamental theory as

$$M_* \sim \frac{M_\Phi}{g_\Phi}, \tag{2.1}$$

where Φ is the field which has been integrated out to give the interaction whose strength is

parametrized by M_* . Note that this relation tells us that below a certain value of M_* it is not possible to have a perturbative completion of the theory involving exchange of particles whose masses are all larger than the WIMP mass; we discard results in such regions as it is clear there is no perturbative UV completion of the effective theory in this regime [52].

In this work our primary focus is on the effect that isospin violation can have on collider constraints on dark matter, so we will specialize to the case of a Majorana WIMP, as constraints on the isospin violating couplings from colliders are not expected to depend sensitively on the nature of the dark matter candidate [52, 14, 53]. As we are particularly interested in relating to direct detection, we focus on couplings of dark matter to quarks in a similar fashion considered in [82]. Gluon couplings are also interesting for direct detection, but they are not able to differentiate between states of different isospin. We therefore do not consider couplings of dark matter to gluons in this work.

We construct all of the lowest-dimension operators that couple dark matter and quarks consistent with MFV, which helps ensure that the models which we produce are not in conflict with flavor physics observables [56]. This amounts to the assumption that any term which breaks $SU(2)_L$ of the SM must do so through the SM Yukawa couplings, leading to the suppression by the quark mass of any operator which flips the quark chirality. The leading operators are of the form

$$L_{Eff} = G_\chi \bar{\chi} \Gamma_\chi \chi \bar{q} \Gamma_q q \tag{2.2}$$

Name	G_χ	Γ_χ	Γ_q
M1	$m_q/2M_*^3$	1	1
M2	$im_q/2M_*^3$	γ_5	1
M3	$im_q/2M_*^3$	1	γ_5
M4	$m_q/2M_*^3$	γ_5	γ_5
M5	$1/2M_*^2$	$\gamma_5\gamma_\mu$	γ^μ
M6	$1/2M_*^2$	$\gamma_5\gamma_\mu$	$\gamma_5\gamma^\mu$

Table 2.1: The list of the effective operators defined in Eq. (2.2).

where

$$\Gamma_{\chi,q} \in \{1, \gamma^5, \gamma^\mu, \gamma^\mu\gamma^5, \sigma^{\mu\nu}\}. \quad (2.3)$$

Any other combination of bilinears are equivalent to a linear combination of this set through Fierz identities. Note that any Lorentz indices in Γ_χ must be contracted with indices in Γ_q to preserve Lorentz invariance. Thus our models contain no tensor terms, because it vanishes for Majorana particles and the alternatives are higher order in derivatives, and thus more suppressed in low energy reactions. The MFV assumption requires us to scale quark bilinears with no Lorentz indices by the quark mass, and to have no relative scaling between the couplings for different quarks in bilinears carrying a Lorentz index. However, we still have two independent coefficients for each operator structure associated with up- and down-type quark couplings, which are not constrained relative to each other by MFV.

The list of all operator Lorentz structures we consider are presented in Table 2.1. Note that the cases of up- and down-type couplings are distinguished in our notation by a trailing u

or d on the designator of the Lorentz structure. For example, operator M1u corresponds to

$$\mathcal{L}_{\text{M1u}} = \frac{1}{2M_*^3} \bar{\chi}\chi \sum_{q=u,c,t} m_q \bar{q}q. \quad (2.4)$$

2.3 Collider Searches

We constrain the operators by simulating the production of a pair of WIMPs and jets at colliders,

$$pp(p\bar{p}) \rightarrow \chi\chi + \text{jets} \quad (2.5)$$

As the WIMPs are invisible to the particle detectors, such a process would appear as a combinations of jets and missing energy. We estimate efficiencies for the signal to pass analysis cuts (outlined below) based on simulations using Madgraph 4.5.0, with showering and detector simulation performed by the Madgraph Pythia-PGS 2.8 package [83, 84, 85]. The dominant standard model background for such a signal is $Z + \text{jets}$, where the Z boson then decays to a pair of neutrinos. The next largest background is $W + \text{jets}$, where the W decays into a neutrino and a charged lepton which is mistagged to be a jet or lost [86, 87, 88].

We assume only one Lorentz structure is dominant at a time, and constrain each by assuming the others do not contribute to the cross section. Since the coupling of models with scalar Lorentz structures are proportional to quark mass, the cross sections from down-type operators are enhanced by the bottom quark mass (though moderated by the b parton distribution function), resulting in stronger bounds on operators M1d–M4d compared to M1u–M4u. For

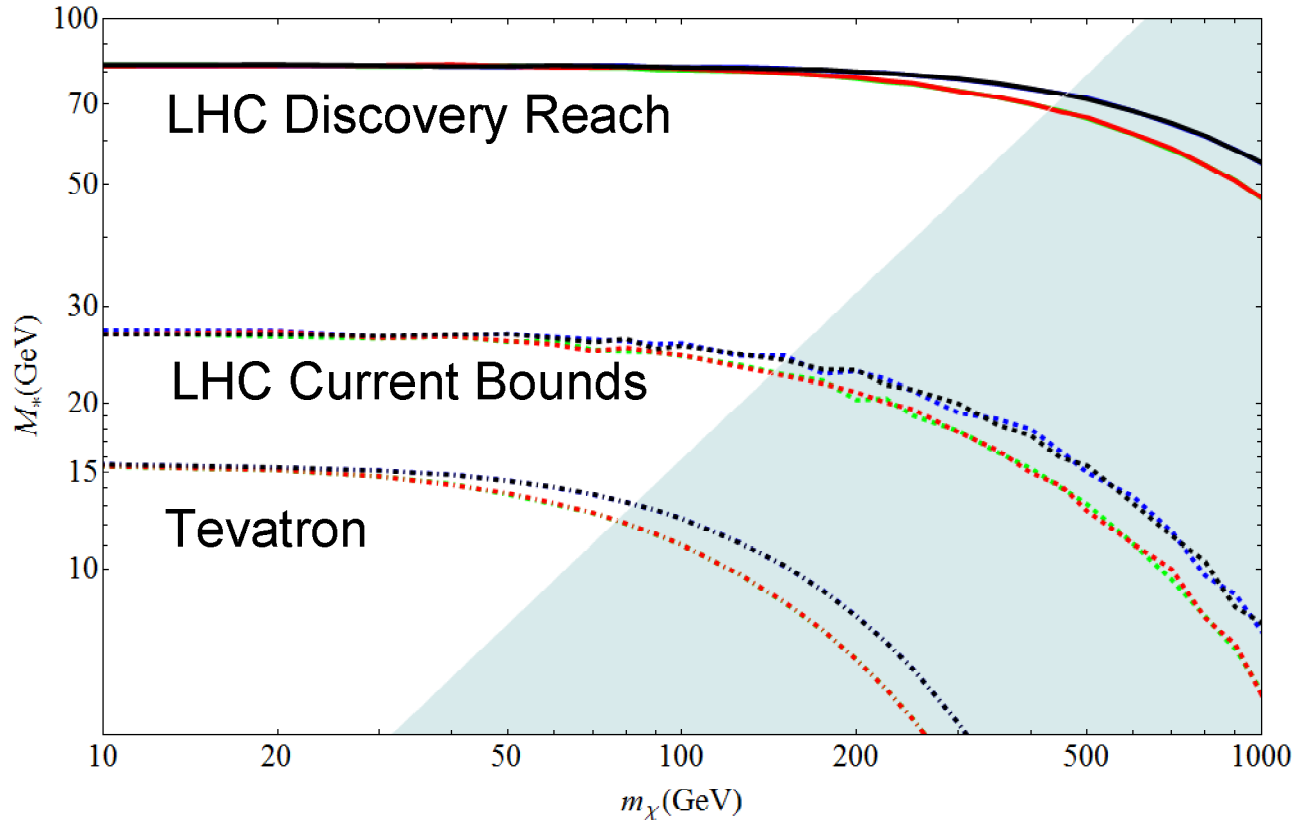


Figure 2.1: The collider bounds on the down-type quark operators with scalar Lorentz structures. Operators M1d, M2d, M3d, M4d, are in red, blue, green, and black respectively. The dashed-dotted, dashed, and solid lines are the Tevatron constraints, LHC constraints, and LHC discovery reach. The shaded region is where the effective theory breaks down. Models M1d and M3d are largely degenerate, as are models M2d and M4d.

models with vector Lorentz structure, the parton distribution functions are the dominant difference between the up-type and down-type operators, resulting in comparatively stronger constraints upon the up-type couplings.

2.3.1 Tevatron Constraints

The CDF collaboration has reported null results for a mono-jet search based on about 1 fb^{-1} of Tevatron run II data [87], constraining the size of additional contributions to missing energy + jets. The analysis selects events which have missing transverse momentum $\cancel{E}_T >$

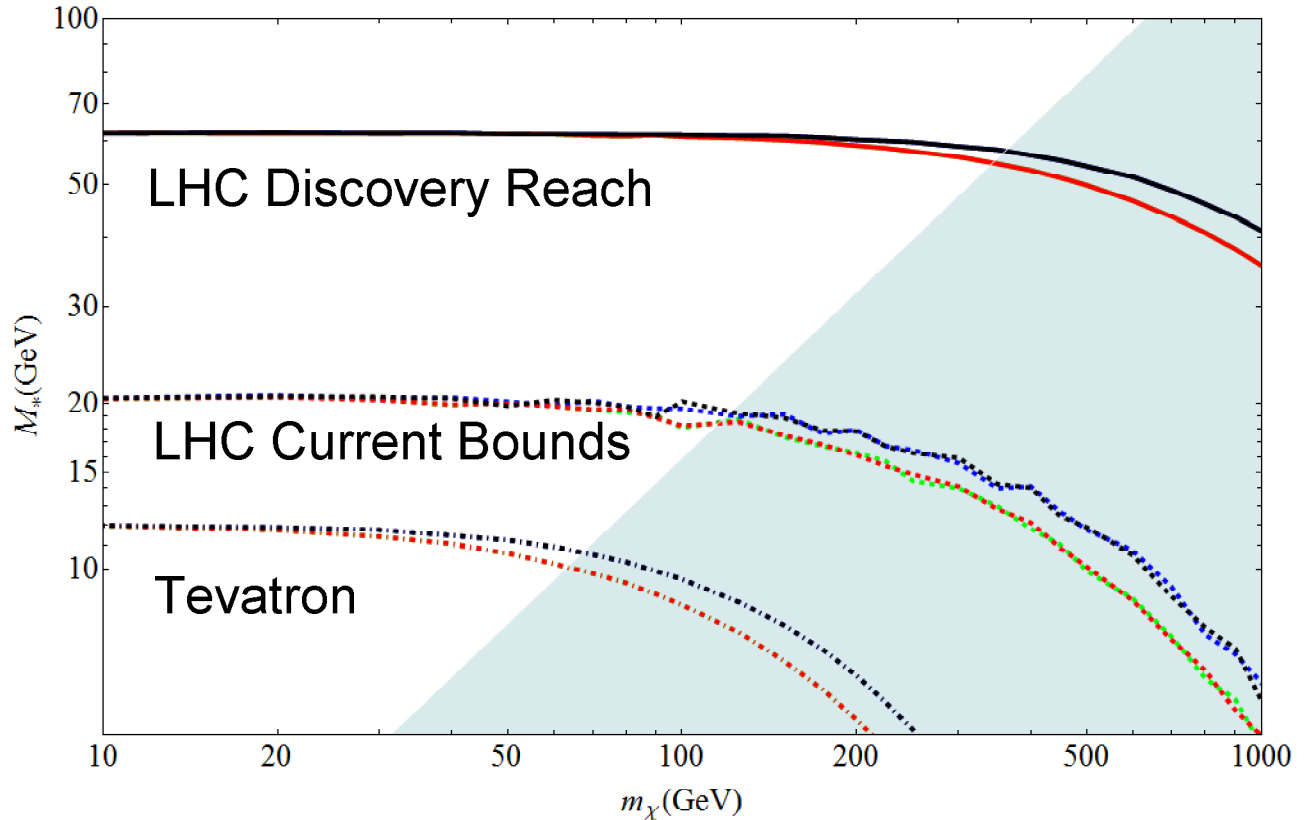


Figure 2.2: The same as Fig. 2.1, for up-type quark operators M1u, M2u, M3u, and M4u.

80 GeV together with a leading jet whose transverse momentum is $p_T > 80$ GeV. A second jet with $p_T < 30$ GeV is allowed, and any subsequent jets must have $p_T < 20$ GeV. In a sample size of 1 fb^{-1} , CDF found 8449 events while the Standard Model prediction was 8663 ± 332 events. To be within 2σ of these results, the accepted cross section of new physics can be at most 0.664 pb. In Figures 2.1 - 2.4, we translate the cross section limit into one on M_* for each operator, as a function of the dark matter mass.

2.3.2 LHC Constraints

The ATLAS Collaboration has very recently released the results of a search for anomalous production of jets and missing energy at $\sqrt{s} = 7$ TeV with an integrated luminosity of 1.00 fb^{-1} [88]. Events with $\cancel{E}_T > 120$ GeV and containing a leading jet with $p_T > 120$ GeV

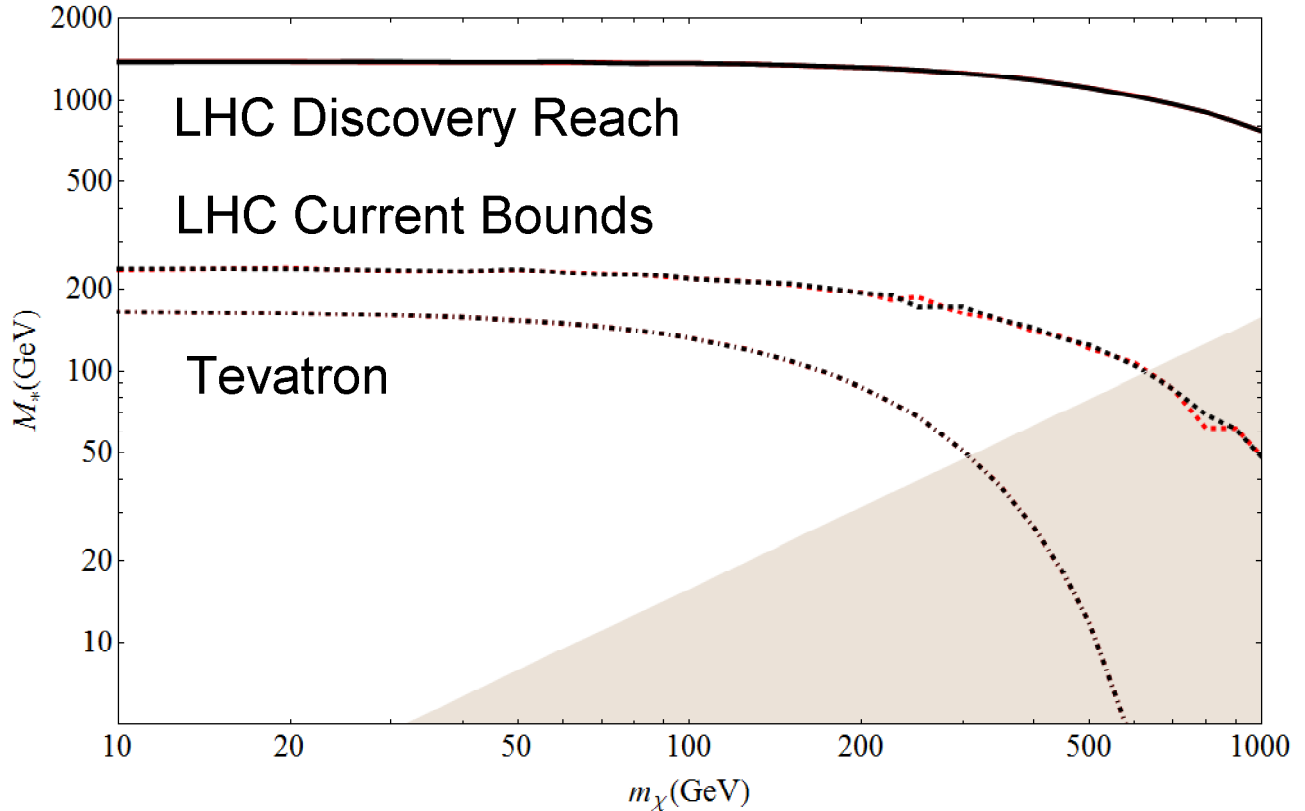


Figure 2.3: The collider bounds on the down-type quark coupling operators mediated by a heavy scalar. Models M5d, M6d are in red, black respectively. The dashed-dotted, dashed, and solid lines are the Tevatron constraints, LHC constraints, and LHC discovery reach. The shaded region is where the effective theory breaks down. Models M5d and M6d are largely degenerate.

and $|\eta| < 2$ were selected. A second jet with $p_T < 30$ GeV and $|\eta| < 4.5$ was allowed. 15740 events were observed, to be compared with an expected $15100 \pm 170(\text{stat.}) \pm 680(\text{syst.})$. This excludes an effective cross section of 1.7 pb, which we map to constraints upon M_* in Figures 2.1 - 2.4.

2.3.3 LHC Future Reach

We also investigate the 5σ discovery reach of such operators, using the analysis done in [89], which considered the LHC running at $\sqrt{s} = 14$ TeV and with an integrated luminosity of

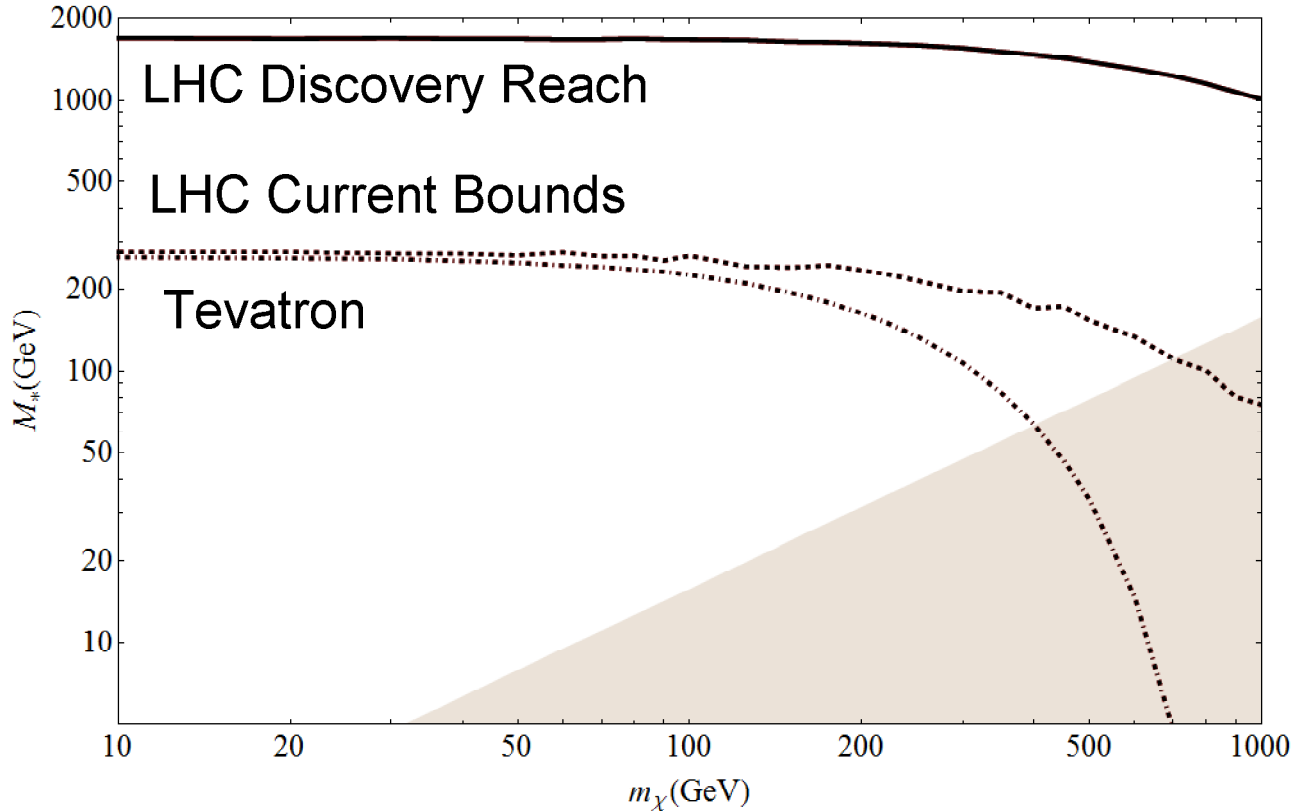


Figure 2.4: The same as Fig. 2.3, although now the up-type quark coupling operators M_{5u} and M_{6u} are displayed.

100 fb^{-1} . Events with missing $\cancel{E}_T > 500 \text{ GeV}$ and at least one a jet with $p_T > 500 \text{ GeV}$ were considered, but no secondary jet rejection cut was employed. Events with isolated charged leptons were rejected. Ref [89] predicts a Standard Model background of about $B = 3 \times 10^4$ events for this integrated luminosity. We determine the discovery reach by requiring that the significance of the new physics signal S passing the cuts satisfy $S/\sqrt{B} \geq 5$ and plot the resulting region in Figures 2.1 - 2.4.

2.4 Direct Detection

Our effective theory allows one to translate the collider bounds into the parameter space of direct detection experiments. In the non-relativistic limit, only operators M_{1d} , M_{1u} , M_{6d} ,

and M6u mediate unsuppressed scattering cross sections with nucleons. In terms of M_* , the resulting cross sections are

$$\sigma^{p,n;SD} = \frac{4\mu_\chi^2}{\pi} \left(\frac{\Delta_u^{p,n}}{M_{*,M6u}^2} + \frac{\Delta_d^{p,n} + \Delta_s^{p,n}}{M_{*,M6d}^2} \right)^2, \sigma^{p,n;SI} = \frac{\mu_\chi^2}{\pi} \left(\frac{\sum_u f_u^{p,n}}{M_{*,M1u}^3} + \frac{\sum_d f_d^{p,n}}{M_{*,M1d}^3} \right)^2, \quad (2.6)$$

where we have adopted the values [90, 91],

$$\begin{aligned} \Delta_u^p &= 0.78, & \Delta_d^p &= -0.48, & \Delta_s^p &= -0.15 \\ f_u^p &= 0.023, & f_d^p &= 0.033, & f_s^p &= 0.05, \\ f_u^n &= 0.018, & f_d^n &= 0.042, & f_s^n &= 0.05, \\ & & f_{c,b,t}^{p,n} &= 0.066, & & \end{aligned} \quad (2.7)$$

and the neutron and proton spin fractions are related by isospin symmetry.

In constructing models which have particular isospin behavior with respect to protons and neutrons in spin-independent scattering we solve the equation

$$\frac{\lambda_n}{\lambda_p} = \frac{\sum_d f_d^p}{\sum_u f_u^p} \frac{M_{*,M1u}^3}{M_{*,M1d}^3}, \quad (2.8)$$

where the ratio of neutron to proton couplings is taken as input and we calculate the ratio of suppression scales. The models are then constrained at colliders by noting that there is no interference at leading order between the up- and down-type couplings, which allows us to directly sum the signal cross section from each to find the total cross section expected for a given operator strength.

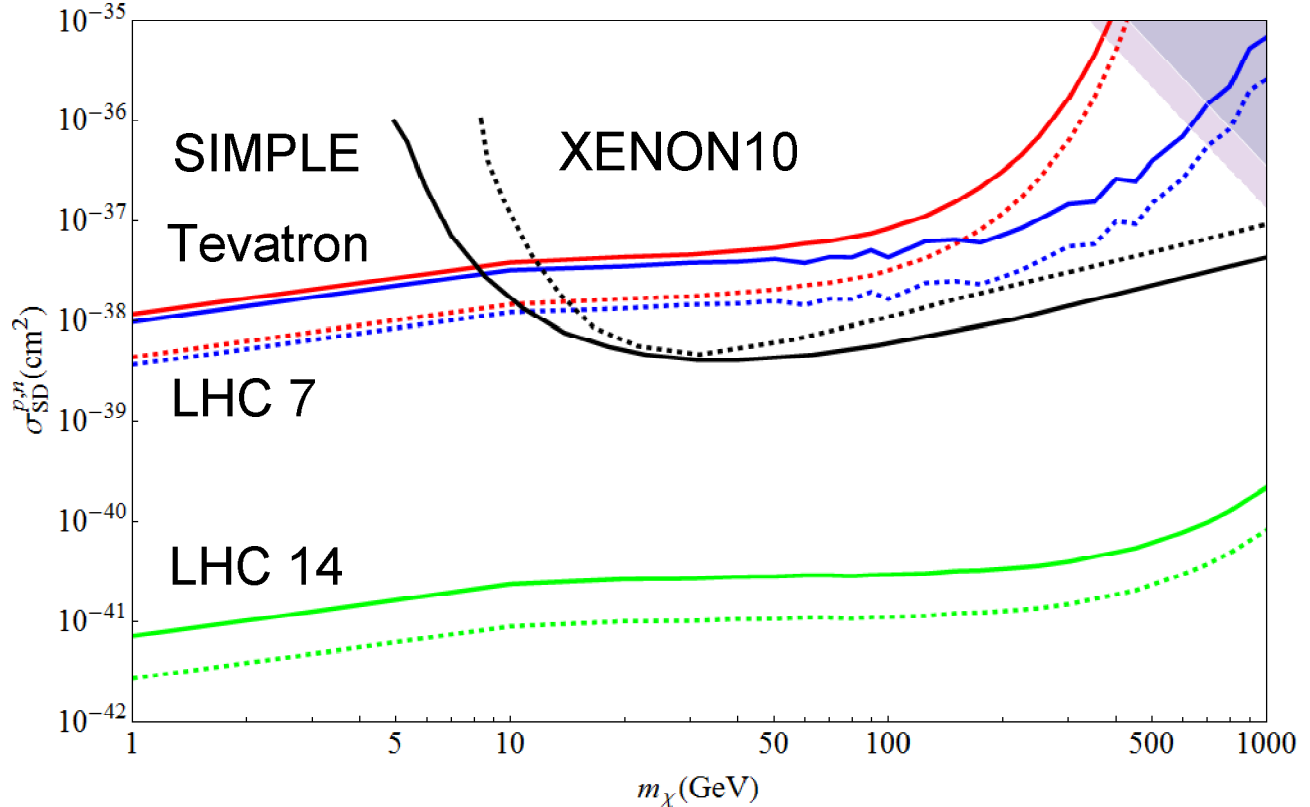


Figure 2.5: Spin-dependent nucleon scattering cross section assuming only the up-type quark operator $M6u$ is present. The red and blue lines are the constraints from the Tevatron search and 7 TeV LHC search. The green lines are the 14 TeV LHC discovery reach. The solid lines are the proton coupling cross section and the dotted lines are the neutron coupling cross section. The dashed black line is the Xenon 10 constraint on the neutron cross section [1] and the solid black line is the SIMPLE constraint on the proton cross section [2].

We translate collider bounds into limits on spin-dependent cross sections in Figures 2.5–2.7 for the cases where only the operator $M6u$ is present, the case where only the operator $M6d$ is present, and the case where $M6u$ and $M6d$ have equal couplings. The spin independent bounds are shown on Figures 2.8-2.11. The proton scattering cross section bounds for only operators $M1u$ or $M1d$ are plotted in Figure 2.8 and Figure 2.9, while Figure 2.10 shows the bounds assuming both $M1u$ and $M1d$ are present and weighted such that the coupling to the proton and neutron are equal. In Figure 2.11, we show bounds for $\lambda_n/\lambda_p = -0.7$, the central value for isospin violating couplings which reconcile CoGeNT and Xenon.

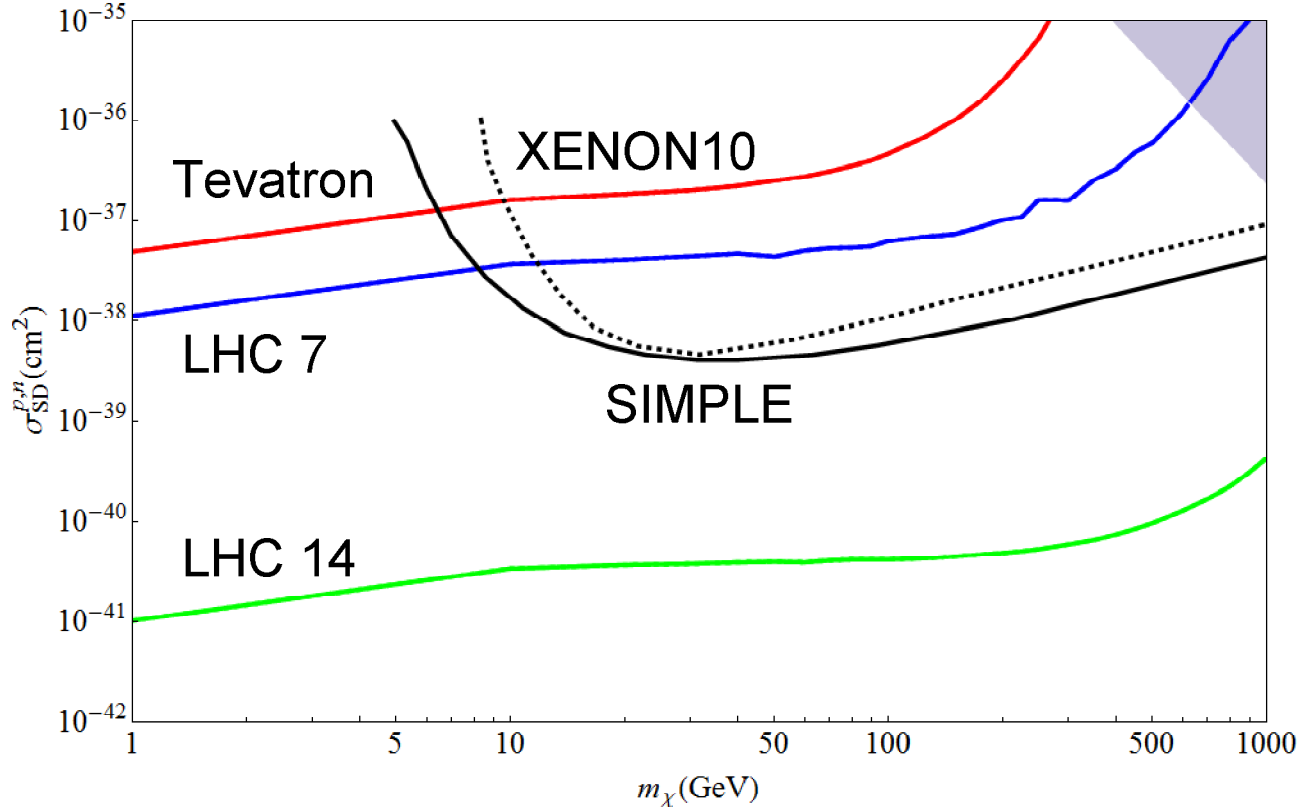


Figure 2.6: The same as Fig. 2.5 but for the down-type quark coupling.

2.5 Conclusion

We have extended previous studies of collider constraints on dark matter to include isospin-violating effects and updated them to make use of the recent null searches for jets plus missing energy based on 1 fb^{-1} of LHC data. Our effective theory description is structured based on MFV to ensure consistency with flavor physics observables and remain as model-independent as possible. In particular, it faithfully reproduces the physics when the particles mediating interactions between dark matter and the SM are significantly heavier than the dark matter particle. We find results which are qualitatively similar to (though quantitatively stronger than) our previous results, with collider limits being the strongest on models of very light dark matter and losing sensitivity as the mass of dark matter approaches the typical energy of collisions at the collider.

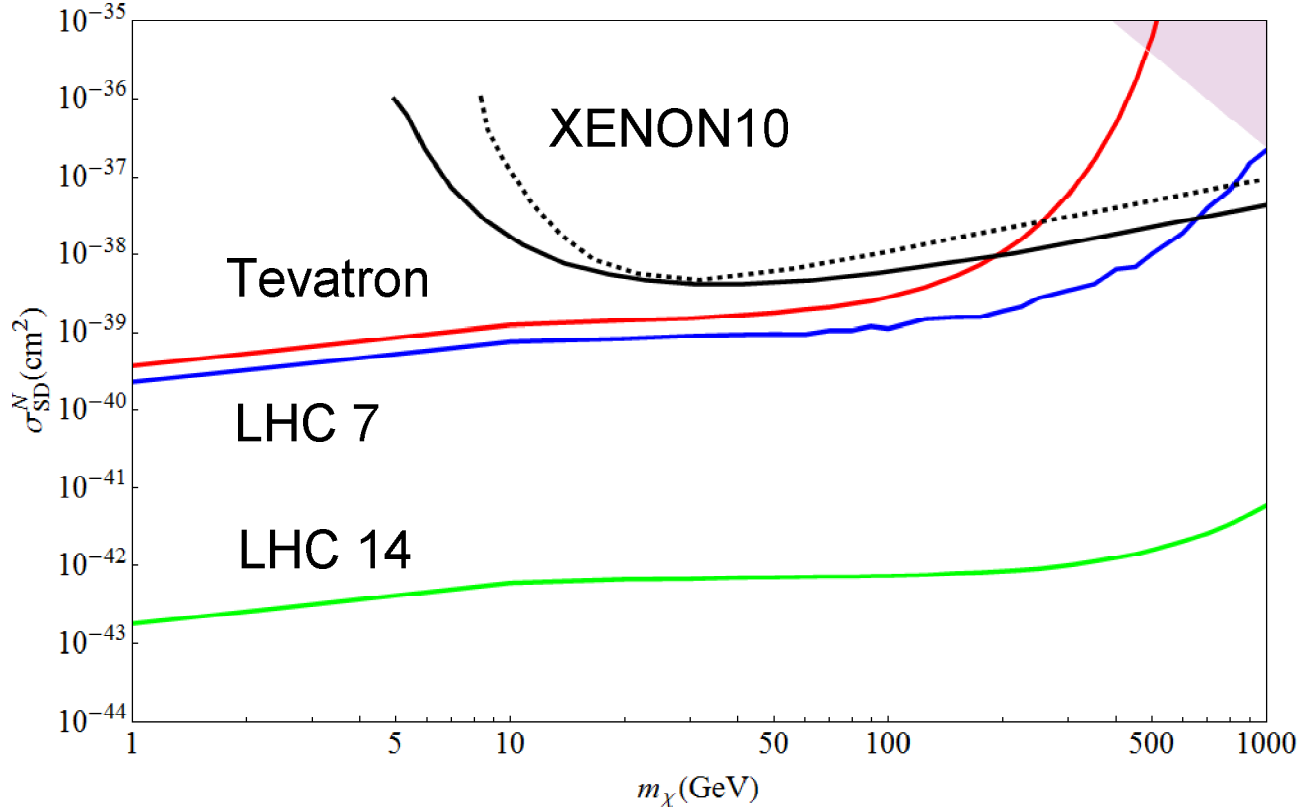


Figure 2.7: Spin dependent nucleon coupling cross section assuming equal down and up type couplings. The red and blue lines are the constraints from the Tevatron search and 7 TeV LHC search. The green line is the 14 TeV LHC discovery reach. The dashed black line is the XENON10 constraint on the neutron cross section [1], the solid black line is the SIMPLE constraint on the proton cross section.[2]

Collider constraints on spin-dependent scattering can be appreciably weakened by isospin violation in the UV couplings of dark matter to quarks. Suppressing the coupling to one type of quarks does not significantly change the production cross section at colliders for dark matter pairs, but it does remove destructive interference in the direct detection scattering cross section, leading to weaker limits from direct detection searches than for isospin conserving cases.

The effects of isospin violation in the spin-independent sector can either strengthen or weaken collider bounds. Suppressing couplings to the heavier down-type quarks significantly decreases the cross section at colliders for mass-suppressed operators, which are the main contributor to spin-independent scattering. However, taking the preferred value for isospin

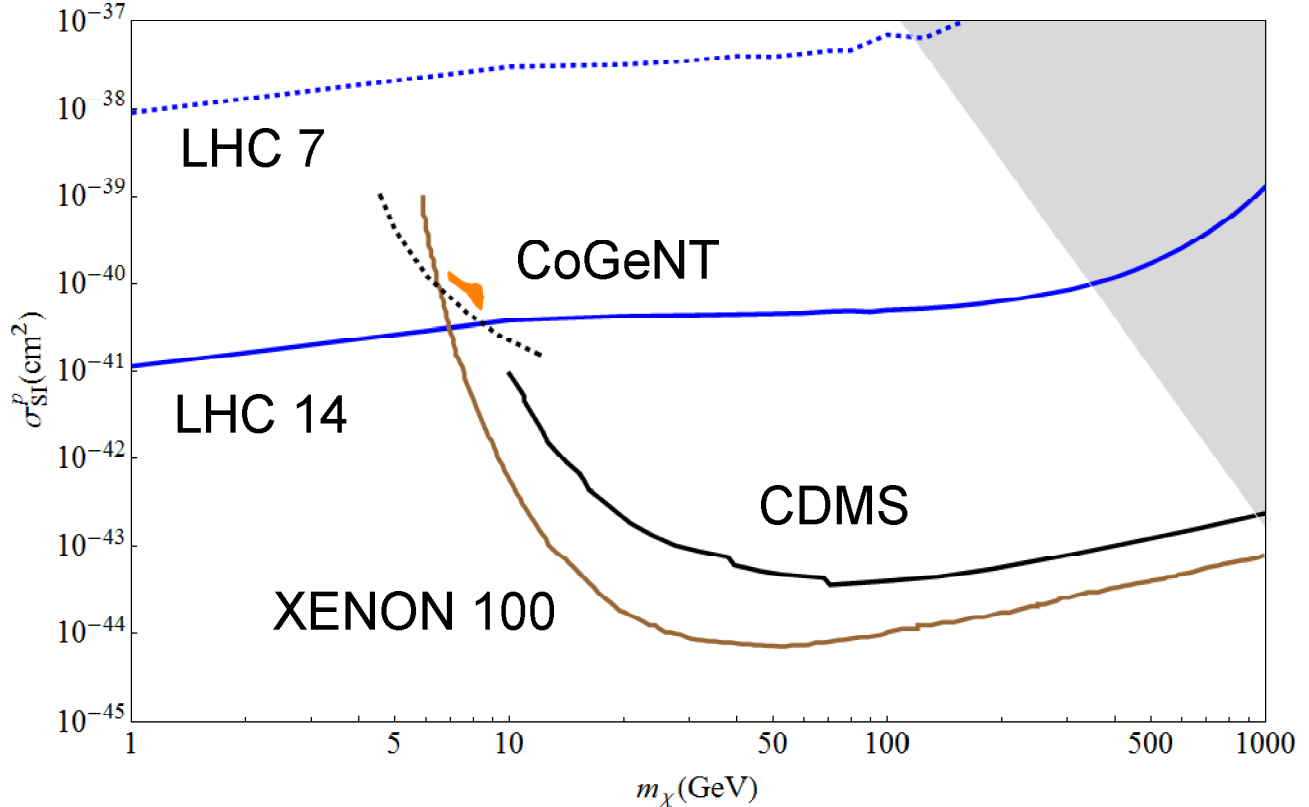


Figure 2.8: Spin independent proton scattering cross section assuming only up-type quark coupling. The red line is the constraint from the Tevatron search. The blue lines are the LHC 7 TeV constraint and LHC 14 discovery reach, which are dashed and solid respectively. The brown line is the XENON100 constraint [3]. The black lines (both solid and dashed) are the CDMS constraints [4, 5]. The orange region is CoGeNT favored results.[6]

violation which allows CoGeNT to be consistent with Xenon 100 results strengthens collider bounds considerably, as it leads to large destructive interference even within a single nucleon as compared to the usual case of isospin conservation. The bounds derived from colliders in this region of parameter space are not only stronger relative to the weakened direct detection experiments, but also stronger in the absolute sense by orders of magnitude. 7 TeV LHC results are already competitive with the strongest direct detection bounds through a large range of dark matter mass in this case, and future LHC reach is better up to masses beyond 1 TeV.

These results are sensitive to the assumption that the particle mediating the dark matter-SM interactions is heavy, and also to the assumption that such interactions obey the MFV

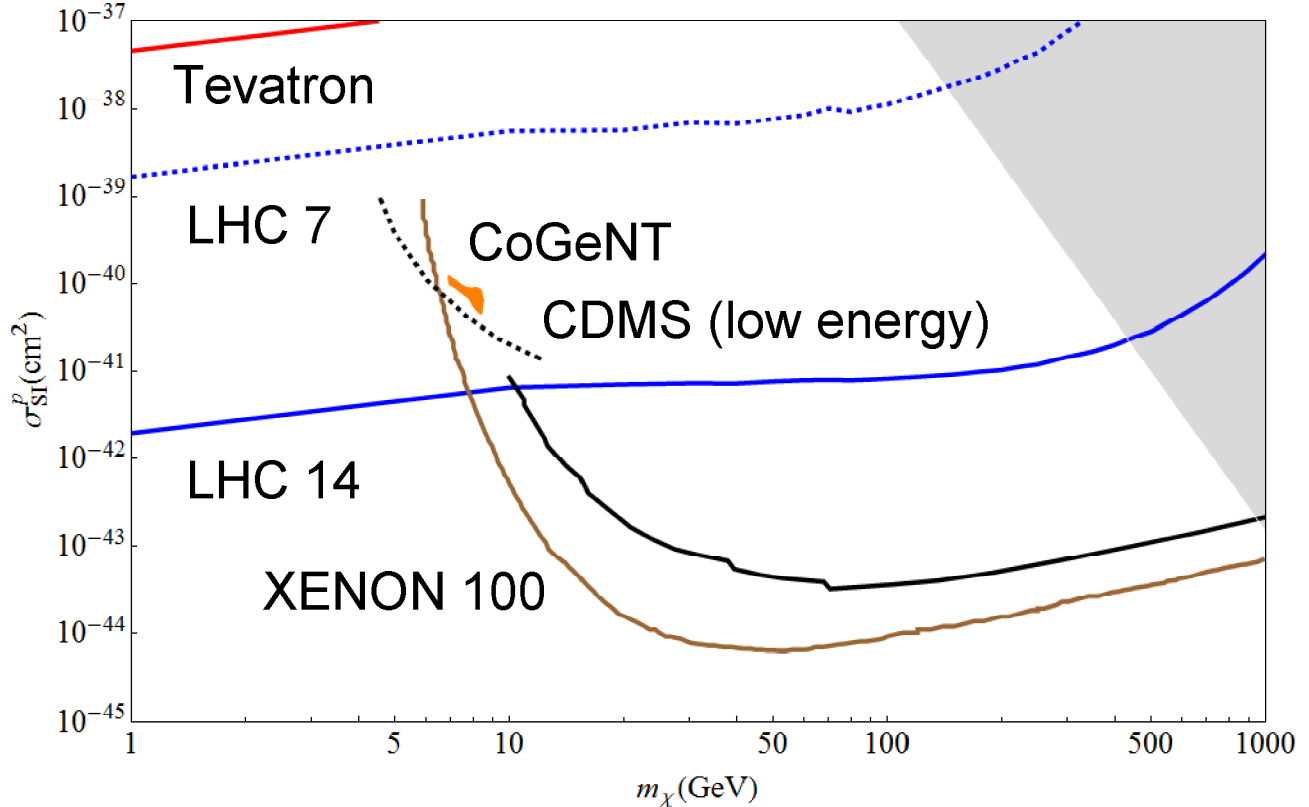


Figure 2.9: The same as Fig. 2.8 but for the down-type coupling.

hypothesis. In models which predict light mediators or more complicated flavor structures for these interactions those effects need to be taken into account directly, either through using a UV complete description of the dark matter scattering or altering the ratios of couplings between the generations away from the MFV assumptions. Our results indicate that any theory of dark matter which uses the paradigm of isospin violation to reconcile the CoGeNT and Xenon results must either have a collider-accessible mediator responsible for dark matter-SM interactions or have more complicated flavor structure in its couplings. In particular, theories which only couple the dark matter to up and down quarks, and not members of the other generations, are much more difficult to probe at colliders if they interact through mass-suppressed operators.

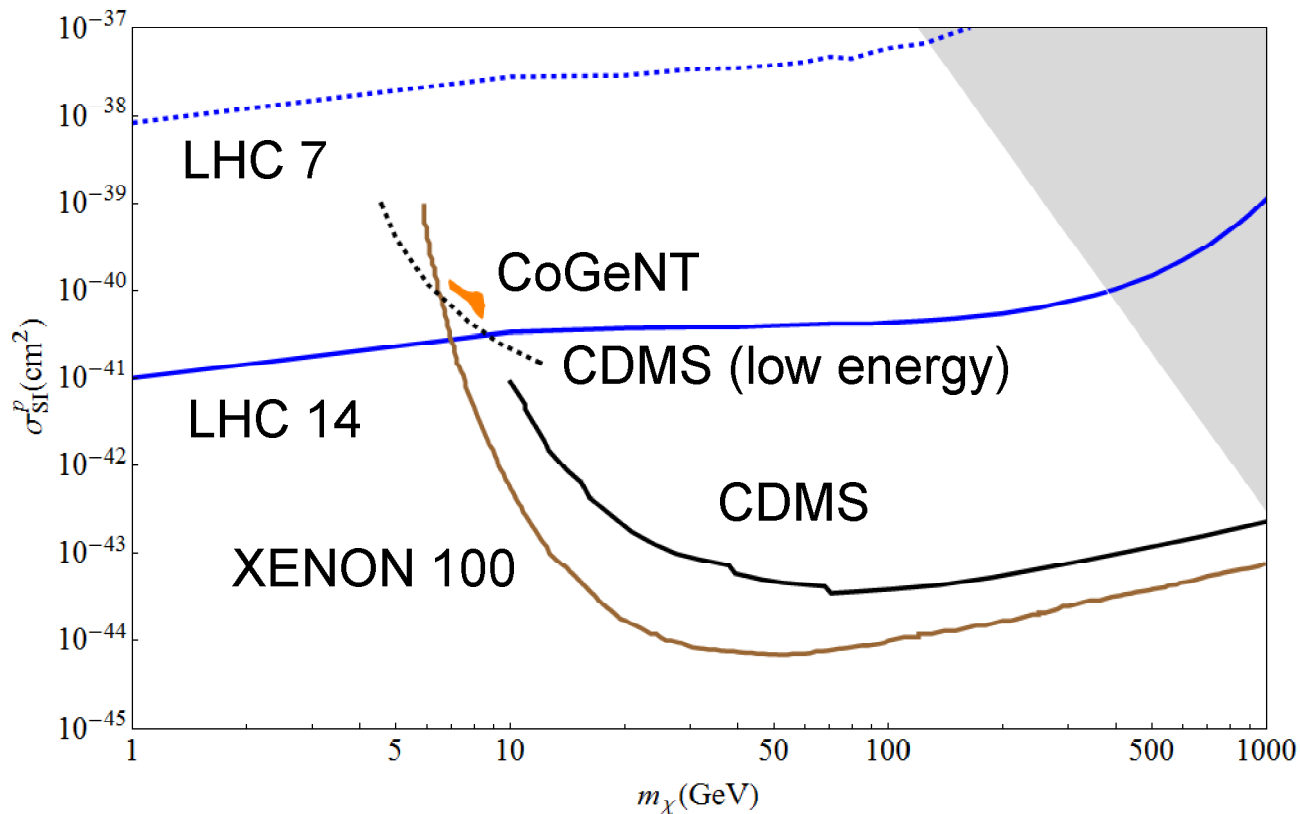


Figure 2.10: Spin independent coupling assuming both down and up type couplings such that the proton and neutron coupling is equal. The blue lines are the LHC 7 TeV constraint and LHC 14 discovery reach, which are dashed and solid respectively. The brown line is the XENON100 constraint.[3] The black lines (both solid and dashed) are the CDMS constraints.[4, 5] The orange region is CoGeNT favored results.[6]

2.6 Acknowledgements

We thank D. Sanford for helpful conversations. The work of AR is supported in part by NSF grant PHY-0653656. AR would also like to thank the Aspen Center of Physics, where part of this work was completed, for hospitality. The work of TT is supported in part by NSF grant PHY-0970171 and he gratefully acknowledges the hospitality of the SLAC theory group, where part of this work was completed. TT and WS acknowledge the hospitality of TASI-2011 at the University of Colorado, where some of this work was undertaken.

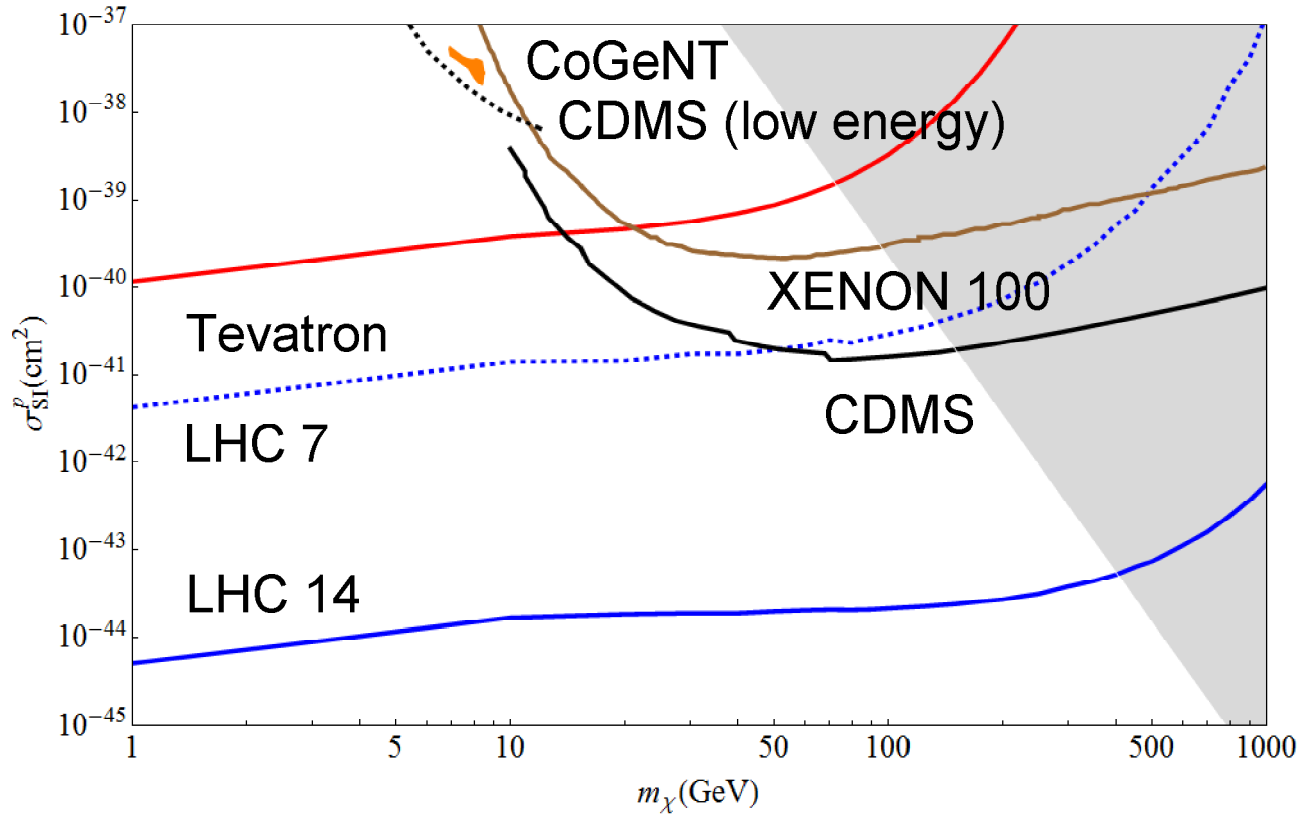


Figure 2.11: Spin independent coupling assuming both down and up type coupling such that the neutron to proton coupling ratio is -0.7 . The red line is the constraint from the Tevatron search. The blue lines are the LHC 7 TeV constraint and LHC 14 discovery reach, which are dashed and solid respectively. The green line is the XENON100 constraint.[3] The black lines (both solid and dashed) are the CDMS constraints.[4, 5] The orange region is CoGeNT favored results.[6]

Chapter 3

Effective Theories of Gamma-ray Lines from Dark Matter Annihilation

Arvind Rajaraman, Tim M.P. Tait, and Alexander M. Wijangco

3.1 Introduction

While the existence of dark matter is now secure, its nature remains elusive. Many experiments are searching for evidence of non-gravitational dark matter interactions through direct detection of its scattering off heavy nuclei, or by direct production in colliders. Yet another approach to search for dark matter indirectly is by looking for signals produced by its annihilation to Standard model (SM) particles. In particular, the Universe is transparent to ~ 100 GeV energy gamma rays on galactic distance scales, which allows one to use their distribution in the sky as well as in energy as handles to try to sift the signal from the (often poorly understood) astrophysical backgrounds.

Among the most striking potential signals one can imagine from dark matter annihilation is

a mono-energetic “line” of gamma rays. Such a process occurs when two (non relativistic) dark matter particles annihilate into a two-body final state, one of which is a photon. The most canonical of such signals would be annihilation into two photons, whose energies are expected to be very close to the mass of the dark matter particle. While such a process is usually suppressed compared to the continuum of gamma rays that result from dark matter annihilations into charged or hadronic particles, the signature is distinctive and difficult for more conventional astrophysics to mimic.

In fact, recent analysis of data obtained by the Fermi-LAT collaboration [92, 93] has found tentative indications of such a line at an energy of about 130 GeV, originating from close to the galactic center [94, 95, 96]. Such a signal is tantalizing, and the presence of what may be a fainter secondary line in the data whose energy is consistent with annihilation into a γZ final state [96, 97] lends some credence to an interpretation in terms of dark matter annihilation. On the other hand, searches for signs of a signal in targets away from the galactic center have yielded results which are confusing at best [98, 99, 100, 101, 102], there are significant limits on a continuum signal associated with the regions of the sky where the line appears brightest [103], and most seriously, there seems to be a hint of a feature in photons arriving from the direction of the Earth’s limb [96] raising the possibility that the feature in the data is the result of a subtle instrumental effect [104, 105, 106]. Perhaps less likely, the signal could also correspond to more prosaic astrophysical processes [107, 108, 109]. Despite these potential issues, the feature at 130 GeV is very interesting and worthy of investigation.

In this article, we examine dark matter annihilations as a source of multiple lines, using the powerful language of effective field theory developed in Ref. [97]. While we are inspired by the feature currently observed in the Fermi data, we will be more concerned with the generic systematics of multiple line signals, which can be applied both to the currently observed feature and to future searches.

3.2 Effective Field Theory

We will take the dark matter (denoted by χ) to be a singlet under all SM interactions, which implies that it couples to the electroweak gauge bosons (including the photon) through higher dimensional operators that result from integrating out electroweakly charged massive fields. We work at the level of this effective field theory containing the dark matter and the SM itself. We impose a Z_2 symmetry under which the dark matter is odd and the SM is even in order to insure that the dark matter is stable. We are interested in operators containing at least one photon, so as to result in an observable gamma ray line signal. The operators are organized by the energy dimension of the field content, since one generically expects operators corresponding to higher dimensions to be less relevant in low energy processes, being more suppressed by the masses of the heavy particles that were integrated out to produce them.

This last issue raises an important question – does one expect that effective field theory can capture the physics of dark matter annihilation into photons at all? Like any effective theory, our theory is valid at very low momentum transfer, but fails to capture the physics of high energy processes, for which the complete theory in the ultra-violet is required. For (non-relativistic) dark matter annihilation, the characteristic momentum transfer is of order the mass of the dark matter itself, and so this assumption boils down to the requirement that the particles mediating the interaction between the dark matter and electroweak bosons are heavier than m_χ . Since such mediator particles must be charged, their masses are bounded in general to be $\gtrsim 100$ GeV by LEP (or more by the LHC if they are stable on collider time scales [110]). However, in many theories the loop process connecting the dark matter to the weak bosons contains a mixture of SM as well as heavy mediator particles. For example, the line signal resulting from dark matter whose primary interaction is with SM light quarks is considered in Ref. [70].

Dimension 6 Operators		
B1+B2	$\frac{1}{\Lambda_{B1}^2} \chi \chi^* B_{\mu\nu} B^{\mu\nu} + \frac{1}{\Lambda_{B2}^2} \chi \chi^* W_{\mu\nu}^a W^{a\mu\nu}$	$\gamma\gamma, \gamma Z$
B3+B4	$\frac{1}{\Lambda_{B3}^2} \chi \chi^* B_{\mu\nu} \tilde{B}^{\mu\nu} + \frac{1}{\Lambda_{B4}^2} \chi \chi^* W_{\mu\nu}^a \tilde{W}^{a\mu\nu}$	$\gamma\gamma, \gamma Z$
Dimension 8 Operators		
D1+D2	$\frac{1}{\Lambda_{D1}^4} (\chi \partial_\mu \chi^* - \chi^* \partial_\mu \chi) B^{\mu\alpha} \Phi^\dagger D_\alpha \Phi + \frac{1}{\Lambda_{D2}^4} (\chi \partial_\mu \chi^* - \chi^* \partial_\mu \chi) \Phi^\dagger W_a^{\mu\alpha} T^a D_\alpha \Phi$	
D3+D4	$\frac{1}{\Lambda_{D3}^4} (\chi \partial_\mu \chi^* - \chi^* \partial_\mu \chi) \tilde{B}^{\mu\alpha} \Phi^\dagger D_\alpha \Phi + \frac{1}{\Lambda_{D4}^4} (\chi \partial_\mu \chi^* - \chi^* \partial_\mu \chi) \Phi^\dagger \tilde{W}_a^{\mu\alpha} T^a D_\alpha \Phi$	

Table 3.1: List of effective interactions for complex scalar dark matter and the type of line signals ($\gamma\gamma$, γZ , and/or γh) that they produce.

Nonetheless, even if there are light SM particles participating, the structure remains tightly constrained by $SU(2) \times U(1)$ electroweak gauge invariance. The presence of multiple lines thus remains generic and (provided the non-SM heavy mediators are sufficiently heavy compared to m_χ), the relative rates of various line processes such as $\gamma\gamma$ and γZ are not likely to show large deviations from an effective theory description, although the precise mapping of the EFT coefficients to the UV theory parameters becomes more murky.

Our effective field theory is constructed as the Standard Model, plus a dark matter particle χ which we allow to be either a complex scalar or Dirac fermion. The real and Majorana cases are simply related to our results. The interactions of interest contain at least one $SU(2)$ W_3^μ or hyper charge B^μ gauge field, which will become a photon after rotating to the mass eigenbasis,

$$B_\mu = A_\mu \cos \theta_W - Z_\mu \sin \theta_W \tag{3.1}$$

$$W_\mu^3 = A_\mu \sin \theta_W + Z_\mu \cos \theta_W$$

where A_μ and Z_μ are the photon and Z boson fields respectively, and θ_W is the electroweak mixing angle.

Dimension 5 Operators		
A1+A2	$\frac{1}{\Lambda_{A1}} \bar{\chi} \gamma^{\mu\nu} \chi B_{\mu\nu} + \frac{1}{\Lambda_{A2}} \bar{\chi} \gamma^{\mu\nu} \chi \tilde{B}_{\mu\nu}$	$\gamma\gamma, \gamma Z$
Dimension 7 Operators		
C1+C2	$\frac{1}{\Lambda_{C1}^3} \bar{\chi} \chi B_{\mu\nu} B^{\mu\nu} + \frac{1}{\Lambda_{C2}^3} \bar{\chi} \chi W_{\mu\nu}^a W^{a\mu\nu}$	
C3 + C4	$\frac{1}{\Lambda_{C3}^3} \bar{\chi} \chi B_{\mu\nu} \tilde{B}^{\mu\nu} + \frac{1}{\Lambda_{C4}^3} \bar{\chi} \chi W_{\mu\nu}^a \tilde{W}^{a\mu\nu}$	
C5+C6	$\frac{1}{\Lambda_{C5}^3} \bar{\chi} \gamma^5 \chi B_{\mu\nu} B^{\mu\nu} + \frac{1}{\Lambda_{C6}^3} \bar{\chi} \gamma^5 \chi W_{\mu\nu}^a W^{a\mu\nu}$	$\gamma\gamma, \gamma Z$
C7 + C8	$\frac{1}{\Lambda_{C7}^3} \bar{\chi} \gamma^5 \chi B_{\mu\nu} \tilde{B}^{\mu\nu} + \frac{1}{\Lambda_{C8}^3} \bar{\chi} \gamma^5 \chi W_{\mu\nu}^a \tilde{W}^{a\mu\nu}$	$\gamma\gamma, \gamma Z$
C9+C10	$\frac{1}{\Lambda_{C9}^3} \bar{\chi} \gamma^{\mu\nu} \chi B_{\mu\alpha} \tilde{B}^{\alpha\nu} + \frac{1}{\Lambda_{C10}^3} \bar{\chi} \gamma^{\mu\nu} \chi W_{\mu\alpha}^a \tilde{W}^{a\alpha\nu}$	γZ
C11+C12	$\frac{1}{\Lambda_{C11}^3} \bar{\chi} \gamma^{\mu\nu} \chi B_{\mu\nu} \Phi ^2 + \frac{1}{\Lambda_{C12}^3} \bar{\chi} \gamma^{\mu\nu} \chi \Phi^\dagger W_{\mu\nu}^a T^a \Phi$	γh
C13+C14	$\frac{1}{\Lambda_{C13}^3} \bar{\chi} \gamma^{\mu\nu} \chi \tilde{B}_{\mu\nu} \Phi ^2 + \frac{1}{\Lambda_{C14}^3} \bar{\chi} \gamma^{\mu\nu} \chi \Phi^\dagger \tilde{W}_{\mu\nu}^a T^a \Phi$	γh
Dimension 8 Operators		
D5+D6	$\frac{1}{\Lambda_{D5}^4} \bar{\chi} \gamma_\mu \chi B^{\mu\alpha} \Phi^\dagger D_\alpha \Phi + \frac{1}{\Lambda_{D6}^4} \bar{\chi} \gamma_\mu \chi \Phi^\dagger W_a^{\mu\alpha} T^a D_\alpha \Phi$	$\gamma Z, \gamma h$
D7+D8	$\frac{1}{\Lambda_{D7}^4} \bar{\chi} \gamma_\mu \chi \tilde{B}^{\mu\alpha} \Phi^\dagger D_\alpha \Phi + \frac{1}{\Lambda_{D8}^4} \bar{\chi} \gamma_\mu \chi \Phi^\dagger \tilde{W}_a^{\mu\alpha} T^a D_\alpha \Phi$	$\gamma Z, \gamma h$
D9+D10	$\frac{1}{\Lambda_{D9}^4} \bar{\chi} \gamma_\mu \gamma_5 \chi B^{\mu\alpha} \Phi^\dagger D_\alpha \Phi + \frac{1}{\Lambda_{D10}^4} \bar{\chi} \gamma_\mu \gamma_5 \chi \Phi^\dagger W_a^{\mu\alpha} T^a D_\alpha \Phi$	γZ
D11+D12	$\frac{1}{\Lambda_{D11}^4} \bar{\chi} \gamma_\mu \gamma_5 \chi \tilde{B}^{\mu\alpha} \Phi^\dagger D_\alpha \Phi + \frac{1}{\Lambda_{D12}^4} \bar{\chi} \gamma_\mu \gamma_5 \chi \Phi^\dagger \tilde{W}_a^{\mu\alpha} T^a D_\alpha \Phi$	γZ

Table 3.2: List of effective interactions for Dirac fermion dark matter and the type of line signals ($\gamma\gamma$, γZ , and/or γh) that they produce.

We consider the effective vertices shown in Tables 3.1 and 3.2 (for scalar and fermionic dark matter, respectively), which are built out of the dark matter fields, the field strengths $W_a^{\mu\nu}$ and $B^{\mu\nu}$ (and their duals \tilde{W} and \tilde{B}), the SM Higgs doublet Φ , and its covariant derivative

$$D_\alpha \Phi = \partial_\alpha \Phi - ig_2 T_a W_\alpha^a \Phi - i \frac{1}{2} g_1 B_\alpha \Phi, \quad (3.2)$$

where T^a are the generators of the doublet representation of $SU(2)$, and g_1 and g_2 are gauge couplings. We define $\gamma^{\mu\nu} \equiv [\gamma^\mu, \gamma^\nu]$. For our purposes, it will be sufficient to work in the unitary gauge, for which we may take,

$$\Phi \rightarrow \frac{1}{\sqrt{2}} \begin{pmatrix} 0 \\ V + h(x) \end{pmatrix}, \quad (3.3)$$

where $V \simeq 246$ GeV is the Higgs vacuum expectation value and $h(x)$ is the physical Higgs field.

This set of interactions is complete up to terms of dimension 8. A similar list was studied, including bounds from indirect and direct detection and LHC searches, in Refs. [111, 112].

3.3 Line Cross Sections

Since dark matter is expected to be highly non-relativistic (with velocity dispersion $v \sim 10^{-3}$) in the galactic halo, dark matter annihilation into photons may be simplified as an expansion in v^2 . We retain only the leading (v -independent) terms. In this limit, the operators C1 – C4 and D1 – D4 lead to vanishing cross sections, and thus are unlikely to lead to any observable line signal. Operators A1 and A2 (which correspond to magnetic/electric dipole moments for the dark matter) are strongly constrained by direct detection [55], and thus also unlikely to contribute to a large line signal¹. We leave consideration of all of these unpromising cases for future work.

We will denote p_1, p_2 to be the incoming dark matter particle momenta, p_3 will be a photon, and p_4 is either another photon, Z boson, or higgs boson. The differential cross section is written

$$\frac{d\sigma}{d\Omega} = \frac{E_3}{256\pi^2 E^3 v} |\overline{\mathcal{M}}|^2 \quad (3.4)$$

where $E = m_\chi + \mathcal{O}(v^2)$ is the energy of each dark matter particle, v is the dark matter velocity, and $E_3 = |\vec{p}_3|$ is the energy of the outgoing line photon. $|\mathcal{M}|^2$ is the matrix element \mathcal{M} averaged over initial dark matter spins (if any) and summed over final state particle spins.

¹An inelastically scattering dark matter particle with dipole interactions can evade direct detection constraints and might even explain the DAMA signal, see Refs. [70, 113, 114, 115, 116].

3.3.1 Dimension 6 Operators

Operators B1 – B4 and C1 – C18 all have the form $X F^{\mu\nu} F_{\mu\nu}$ or $X F^{\mu\nu} \tilde{F}_{\mu\nu}$, where $F^{\mu\nu} = B^{\mu\nu}$ or $W^{\mu\nu}$. For the $X F^{\mu\nu} F_{\mu\nu}$ operators, the matrix element will have the form $\mathcal{M} = -2Y(p_3 \cdot p_4 \epsilon_3 \cdot \epsilon_4)$ where Y is whatever the Feynman rules of X yield, and depends on the spin of the dark matter. If p_4 corresponds to another photon, we find

$$\sum_{\epsilon_3, \epsilon_4} |\mathcal{M}|^2 = 16YY^\dagger (p_3 \cdot p_4)^2 . \quad (3.5)$$

To obtain $\overline{|\mathcal{M}|^2}$, one averages this result over the dark matter spin states. In the case where p_4 corresponds to a massive gauge boson, we find:

$$\sum_{\epsilon_3, \epsilon_4} |\mathcal{M}|^2 = 12YY^\dagger (p_3 \cdot p_4)^2 . \quad (3.6)$$

For an operator of the form $X F^{\mu\nu} \tilde{F}_{\mu\nu}$ the matrix element will have the form: $\mathcal{M} = Y(p_3^\mu \epsilon_3^\nu - p_3^\nu \epsilon_3^\mu)(p_4^\rho \epsilon_4^\sigma - p_4^\sigma \epsilon_4^\rho) \epsilon_{\mu\nu\rho\sigma}$ Squaring this yields:

$$\sum_{\epsilon_3, \epsilon_4} |\mathcal{M}|^2 = 32YY^\dagger (p_3 \cdot p_4)^2 . \quad (3.7)$$

For the (complex) scalar dark matter dimension six operators, $YY^\dagger = \frac{1}{\Lambda^2}$ and the average over spin is trivial. The operators B1 and B2 interfere with one another, but are separate from B3 and B4. The resulting cross sections are:

$$|v|\sigma_{B1,2}(\chi\chi^* \rightarrow \gamma\gamma) = \frac{2m_\chi^2}{\pi} \left(\frac{\cos^4 \theta_W}{\Lambda_{B1}^4} + \frac{2 \cos^2 \theta_W \sin^2 \theta_W}{\Lambda_{B1}^2 \Lambda_{B2}^2} + \frac{\sin^4 \theta_W}{\Lambda_{B2}^4} \right), \quad (3.8)$$

$$|v|\sigma_{B1,2}(\chi\chi^* \rightarrow \gamma Z) = \frac{3 \cos^2 \theta_W \sin^2 \theta_W (4m_\chi^2 - m_Z^2)^3}{64\pi m_\chi^4} \left(\frac{1}{\Lambda_{B1}^4} - \frac{2}{\Lambda_{B1}^2 \Lambda_{B2}^2} + \frac{1}{\Lambda_{B2}^4} \right), \quad (3.9)$$

and

$$|v|\sigma_{B3,4}(\chi\chi^* \rightarrow \gamma\gamma) = \frac{4m_\chi^2}{\pi} \left(\frac{\cos^4 \theta_W}{\Lambda_{B3}^4} + \frac{2 \cos^2 \theta_W \sin^2 \theta_W}{\Lambda_{B3}^2 \Lambda_{B4}^2} + \frac{\sin^4 \theta_W}{\Lambda_{B4}^4} \right), \quad (3.10)$$

$$|v|\sigma_{B3,4}(\chi\chi^* \rightarrow \gamma Z) = \frac{\cos^2 \theta_W \sin^2 \theta_W (4m_\chi^2 - m_z^2)^3}{8\pi m_\chi^4} \left(\frac{1}{\Lambda_{B3}^4} - \frac{2}{\Lambda_{B3}^2 \Lambda_{B4}^2} + \frac{1}{\Lambda_{B4}^4} \right), \quad (3.11)$$

respectively.

3.3.2 Dimension 7 Operators

A Dirac fermion can annihilate into $\gamma\gamma$ and γZ through the dimension seven operators C5 – C8 (recall that C1 – C4 vanish at zero velocity). The matrix elements are identical to B1 – B4 as far as the final state, and the only difference is the average over initial WIMP spins.

The resulting cross sections are,

$$|v|\sigma_{C5,6}(\chi\bar{\chi} \rightarrow \gamma\gamma) = \frac{4m_\chi^4}{\pi} \left(\frac{\cos^4 \theta_W}{\Lambda_{C5}^6} + \frac{2 \cos^2 \theta_W \sin^2 \theta_W}{\Lambda_{C5}^3 \Lambda_{C6}^3} + \frac{\sin^4 \theta_W}{\Lambda_{C6}^6} \right), \quad (3.12)$$

$$|v|\sigma_{C5,6}(\chi\bar{\chi} \rightarrow \gamma Z) = \frac{3(4m_\chi^2 - m_Z^2)^3 \cos^2 \theta_W \sin^2 \theta_W}{32\pi m_\chi^2} \left(\frac{1}{\Lambda_{C5}^6} - \frac{2}{\Lambda_{C5}^3 \Lambda_{C6}^3} + \frac{1}{\Lambda_{C6}^6} \right), \quad (3.13)$$

and

$$|v|\sigma_{C7,8}(\chi\bar{\chi} \rightarrow \gamma\gamma) = \frac{8m_\chi^4}{\pi} \left(\frac{\cos^4 \theta_W}{\Lambda_{C7}^6} + \frac{2 \cos^2 \theta_W \sin^2 \theta_W}{\Lambda_{C7}^3 \Lambda_{C8}^3} + \frac{\sin^4 \theta_W}{\Lambda_{C8}^6} \right), \quad (3.14)$$

$$|v|\sigma_{C7,8}(\chi\bar{\chi} \rightarrow \gamma Z) = \frac{(4m_\chi^2 - m_Z^2)^3 (\cos^2 \theta_W \sin^2 \theta_W)}{4\pi m_\chi^2} \left(\frac{1}{\Lambda_{C7}^6} - \frac{2}{\Lambda_{C7}^3 \Lambda_{C8}^3} + \frac{1}{\Lambda_{C8}^6} \right). \quad (3.15)$$

The remaining dimension seven operators lead to single lines. For C9 and C10, the anti-symmetry of $\gamma^{\mu\nu}$ forces the $\chi\chi \rightarrow \gamma\gamma$ cross section to vanish identically, leaving only a γZ line:

$$|v|\sigma_{C9,10}(\chi\bar{\chi} \rightarrow \gamma Z) = \frac{(4m_\chi^2 - m_Z^2)^3 (4m_\chi^2 + m_Z^2) \cos^2 \theta_W \sin^2 \theta_W}{16m_\chi^4 \pi} \left(\frac{1}{\Lambda_{C9}^6} - \frac{2}{\Lambda_{C9}^3 \Lambda_{C10}^3} + \frac{1}{\Lambda_{C10}^6} \right). \quad (3.16)$$

Whereas operators C11 – C14 result in a single γh line,

$$|v|\sigma_{C11,12}(\chi\bar{\chi} \rightarrow \gamma h) = \frac{(4m_\chi^2 - m_h^2)^3 V^2}{64m_\chi^4 \pi} \left(\frac{\cos^2 \theta_W}{\Lambda_{C11}^6} - \frac{\cos \theta_W \sin \theta_W}{\Lambda_{C11}^3 \Lambda_{C12}^3} + \frac{\sin^2 \theta_W}{4\Lambda_{C12}^6} \right), \quad (3.17)$$

and

$$|v|\sigma_{C13,14}(\chi\bar{\chi} \rightarrow \gamma h) = \frac{(4m_\chi^2 - m_h^2)^3 V^2}{16m_\chi^4 \pi} \left(\frac{\cos^2 \theta_W}{\Lambda_{C13}^6} - \frac{\cos \theta_W \sin \theta_W}{\Lambda_{C13}^3 \Lambda_{C14}^3} + \frac{\sin^2 \theta_W}{4\Lambda_{C14}^6} \right). \quad (3.18)$$

3.3.3 Dimension 8 Operators

Dimension eight operators could in principle contribute to line signals from scalar dark matter, but in practice these operators lead to cross sections which vanish in the zero velocity limit. Thus, we limit our discussion to the case where the dark matter is a Dirac fermion, for which there are potentially both γZ and γh final states. For D5 – D8, we have two sets of interfering operators,

$$|v|\sigma_{D5,6}(\chi\bar{\chi} \rightarrow \gamma Z) = \frac{(4m_\chi^2 - m_Z^2)^3 (4m_\chi^2 + m_Z^2) V^4 (g_2 \cos \theta_W + g_1 \sin \theta_W)^2}{4096\pi m_\chi^4 m_Z^2} \quad (3.19)$$

$$\times \left(\frac{\cos^2 \theta_W}{\Lambda_{D5}^8} - \frac{\cos \theta_W \sin \theta_W}{\Lambda_{D5}^4 \Lambda_{D6}^4} + \frac{\sin^2 \theta_W}{4\Lambda_{D6}^8} \right),$$

$$|v|\sigma_{D5,6}(\chi\bar{\chi} \rightarrow \gamma h) = \frac{(4m_\chi^2 - m_h^2)^3 V^2}{1024m_\chi^2 \pi} \left(\frac{\cos^2 \theta_W}{\Lambda_{D5}^8} - \frac{\cos \theta_W \sin \theta_W}{\Lambda_{D5}^4 \Lambda_{D6}^4} + \frac{\sin^2 \theta_W}{4\Lambda_{D6}^8} \right), \quad (3.20)$$

and

$$|v|\sigma_{D7,8}(\chi\bar{\chi} \rightarrow \gamma Z) = \frac{(4m_\chi^2 - m_Z^2)^3 (24m_\chi^2 + m_Z^2) V^4 (g_2 \cos \theta_W + g_1 \sin \theta_W)^2}{1024\pi m_\chi^4 m_Z^2} \quad (3.21)$$

$$\times \left(\frac{\cos^2 \theta_W}{\Lambda_{D7}^8} - \frac{\cos \theta_W \sin \theta_W}{\Lambda_{D7}^4 \Lambda_{D8}^4} + \frac{\sin^2 \theta_W}{4\Lambda_{D8}^8} \right),$$

$$|v|\sigma_{D7,8}(\chi\bar{\chi} \rightarrow \gamma h) = \frac{(4m_\chi^2 - m_h^2)^3 V^2}{256\pi m_\chi^2} \left(\frac{\cos^2 \theta_W}{\Lambda_{D7}^8} - \frac{\cos \theta_W \sin \theta_W}{\Lambda_{D7}^4 \Lambda_{D8}^4} + \frac{\sin^2 \theta_W}{4\Lambda_{D8}^8} \right). \quad (3.22)$$

For operators D9 – D12, the γh line vanishes in the limit of zero velocity, leaving a single

bright γZ line from each set of operators. The cross sections are,

$$|v|\sigma_{D9,10}(\chi\bar{\chi} \rightarrow \gamma Z) = \frac{(4m_\chi^2 - m_Z^2)^3 V^4 (g_2 \cos \theta_W + g_1 \sin \theta_W)^2}{16384 m_\chi^4 \pi} \quad (3.23)$$

$$\times \left(\frac{\cos^2 \theta_W}{\Lambda_{D9}^8} - \frac{\cos \theta_W \sin \theta_W}{\Lambda_{D9}^4 \Lambda_{D10}^4} + \frac{\sin^2 \theta_W}{4\Lambda_{D10}^8} \right),$$

and

$$|v|\sigma_{D11,12}(\chi\bar{\chi} \rightarrow \gamma Z) = \frac{(4m_\chi^2 - m_Z^2)^3 V^4 (g_2 \cos \theta_W + g_1 \sin \theta_W)^2}{4096 m_\chi^4 \pi} \quad (3.24)$$

$$\times \left(\frac{\cos^2 \theta_W}{\Lambda_{D11}^8} - \frac{\cos \theta_W \sin \theta_W}{\Lambda_{D11}^4 \Lambda_{D12}^4} + \frac{\sin^2 \theta_W}{4\Lambda_{D12}^8} \right).$$

3.4 Summary

We are now in a position to summarize the various possible annihilation modes for each operator class. The processes resulting from each operator which are not suppressed by the dark matter velocity are listed in the third column of Tables 3.1 and 3.2. As is evident from the table, any operator which can produce a $\gamma\gamma$ line will (modulo interference between two operators) also result in a γZ one, whereas some of the higher dimension operators are able to produce γZ or γh lines in isolation. Of course, a specific UV theory of dark matter may result in more than one operator being turned on. Typically one expects that relevant operators of the lowest dimension will dominate the size of each line with corrections from higher order terms being controlled by m_χ/Λ_i to the appropriate power.

Our results are suggestive of new ways to interpret the results of line searches. Given a choice of dark matter mass and now that the Large Hadron Collider has measured the Higgs

boson mass, the energy of each line is determined,

$$E_{\gamma\gamma} = m_\chi \tag{3.25}$$

$$E_{\gamma Z} = \frac{4m_\chi^2 - m_Z^2}{4m_\chi} \tag{3.26}$$

$$E_{\gamma h} = \frac{4m_\chi^2 - m_h^2}{4m_\chi} \tag{3.27}$$

where it should be clear that the energy in each case refers to the energy of the final state photon, and the label applies to the process which produced the gamma ray. Since multiple lines are a fairly generic feature, it would be interesting to recast single line searches into searches for multiple lines based on a given value of m_χ . For example, a search for lines related to a scalar dark matter particle could search simultaneously for two lines with energies $E_{\gamma\gamma}$ and $E_{\gamma Z}$ based on operators B1 and B2. At each putative dark matter mass, a bound can be placed in the Λ_{B1} - Λ_{B2} plane.

Alternately, if one has a particular UV theory in mind such that either one operator or the other (or some linear combination with a fixed ratio) is generated, one can improve the sensitivity by searching for two lines at correlated energies with a fixed intensity ratio for the two. In Table 3.3, we list, for each operator, the strength of the first (lowest energy) and second line implied by each set of operators. For convenience, we have introduced the short

hand notation:

$$f_1(\Lambda_1, \Lambda_2, n) \equiv \left(\frac{\cos^4 \theta_W}{\Lambda_1^{2n}} + \frac{2 \cos^2 \theta_W \sin^2 \theta_W}{\Lambda_1^n \Lambda_2^n} + \frac{\sin^4 \theta_W}{\Lambda_2^{2n}} \right), \quad (3.28)$$

$$f_2(\Lambda_1, \Lambda_2, n) \equiv \cos^2 \theta_W \sin^2 \theta_W \left(\frac{1}{\Lambda_1^{2n}} - \frac{2}{\Lambda_1^n \Lambda_2^n} + \frac{1}{\Lambda_2^{2n}} \right), \quad (3.29)$$

$$f_3(\Lambda_1, \Lambda_2, n, m) \equiv \left(\frac{\cos^2 \theta_W}{\Lambda_1^{2n}} - \frac{\cos \theta_W \sin \theta_W}{\Lambda_1^n \Lambda_2^n} + \frac{\sin^2 \theta_W}{4 \Lambda_2^{2n}} \right) (g_2 \cos \theta_W + g_1 \sin \theta_W)^m. \quad (3.30)$$

The operator groups D5+D6 and D7+D8 each predict a fixed ratio between the two lines, regardless of the specifics of the relative coefficients of the operators within each category.

The ratios are:

$$\frac{|v| \sigma_{D5,6}(\chi\chi \rightarrow \gamma Z)}{|v| \sigma_{D5,6}(\chi\chi \rightarrow \gamma h)} = \left(\frac{4m_\chi^2 - m_Z^2}{4m_\chi^2 - m_h^2} \right)^3 \frac{(4m_\chi^2 + m_Z^2) V^2 (g_2 \cos \theta_W + g_1 \sin \theta_W)^2}{4 m_\chi^2 m_Z^2}, \quad (3.31)$$

$$\frac{|v| \sigma_{D7,8}(\chi\chi \rightarrow \gamma Z)}{|v| \sigma_{D7,8}(\chi\chi \rightarrow \gamma h)} = \left(\frac{4m_\chi^2 - m_Z^2}{4m_\chi^2 - m_h^2} \right)^3 \frac{(24m_\chi^2 + m_Z^2) V^2 (g_2 \cos \theta_W + g_1 \sin \theta_W)^2}{4 m_\chi^2 m_Z^2}. \quad (3.32)$$

3.5 Outlook

Gamma ray line searches make up a crucial part of searches for the indirect detection of dark matter. We have studied using the tools of effective field theory the generic multi-line signatures of dark matter annihilation. While our specific analytic results apply only in the case where the particles mediating the interactions between the dark matter and photons

Operator	First Line	Second Line
B1+B2	$\frac{3(4m_\chi^2 - m_Z^2)^3}{64\pi m_\chi^4} f_2(\Lambda_{B1}, \Lambda_{B2}, 2)$	$\frac{2m_\chi^2}{\pi} f_1(\Lambda_{B1}, \Lambda_{B2}, 2)$
B3+B4	$\frac{(4m_\chi^2 - m_Z^2)^3}{8\pi m_\chi^4} f_2(\Lambda_{B3}, \Lambda_{B4}, 2)$	$\frac{4m_\chi^2}{\pi} f_1(\Lambda_{B7}, \Lambda_{B8}, 2)$
C5+C6	$\frac{3(4m_\chi^2 - m_Z^2)^3}{32\pi m_\chi^2} f_2(\Lambda_{C5}, \Lambda_{C6}, 3)$	$\frac{4m_\chi^4}{\pi} f_1(\Lambda_{C5}, \Lambda_{C6}, 3)$
C7+C8	$\frac{(4m_\chi^2 - m_Z^2)^3}{4\pi m_\chi^2} f_2(\Lambda_{C7}, \Lambda_{C8}, 3)$	$\frac{8m_\chi^4}{\pi} f_1(\Lambda_{C7}, \Lambda_{C8}, 3)$
C9+C10	$\frac{(4m_\chi^2 - m_Z^2)^3 (4m_\chi^2 + m_Z^2)}{16m_\chi^4 \pi} f_2(\Lambda_{C9}, \Lambda_{C10}, 3)$	N/A
C11+C12	$\frac{(4m_\chi^2 - m_h^2)^3 V^2}{64m_\chi^4 \pi} f_3(\Lambda_{C11}, \Lambda_{C12}, 3, 0)$	N/A
C13+C14	$\frac{(4m_\chi^2 - m_h^2)^3 V^2}{16m_\chi^4 \pi} f_3(\Lambda_{C13}, \Lambda_{C14}, 3, 0)$	N/A
D5+D6	$\frac{(4m_\chi^2 - m_h^2)^3 V^2}{1024m_\chi^2 \pi} f_3(\Lambda_{D5}, \Lambda_{D6}, 4, 0)$	$\frac{(4m_\chi^2 - m_Z^2)^3 (4m_\chi^2 + m_Z^2) V^4}{4096\pi m_\chi^4 m_Z^2} f_3(\Lambda_{D5}, \Lambda_{D6}, 4, 2)$
D7+D8	$\frac{(4m_\chi^2 - m_h^2)^3 V^2}{256\pi m_\chi^2} f_3(\Lambda_{D7}, \Lambda_{D8}, 4, 0)$	$\frac{(4m_\chi^2 - m_Z^2)^3 (24m_\chi^2 + m_Z^2) V^4}{1024\pi m_\chi^4 m_Z^2} f_3(\Lambda_{D7}, \Lambda_{D8}, 4, 2)$
D9+D10	$\frac{(4m_\chi^2 - m_Z^2)^3 V^4}{16384m_\chi^4 \pi} f_3(\Lambda_{D9}, \Lambda_{D10}, 4, 2)$	N/A
D11+D12	$\frac{(4m_\chi^2 - m_Z^2)^3 V^4}{4096m_\chi^4 \pi} f_3(\Lambda_{D11}, \Lambda_{D12}, 4, 2)$	N/A

Table 3.3: The strength of the first and second (when applicable) gamma ray line signals for each operator described in the text.

are much heavier than the dark matter itself, the central result that there are multiple lines, and their relative intensities, are the consequence of $SU(2) \times U(1)$ gauge invariance, and thus rather generic.

We have examined the set of lowest operators which can contribute to $\gamma\gamma$, γZ , and γh lines, for dark matter which is a complex scalar or Dirac fermion. Our results suggest that an interesting extension of the current suite of searches for photon lines at gamma ray telescopes would include the simultaneous search for two lines at fixed relative energies. Such a search should improve the sensitivity to specific UV theories of dark matter in many cases, which fix the ratio between the interfering operators of a given dimensionality. Should a set of lines be discovered, the energies and relative intensities of the set provide key information as to the possible responsible operators, and thus the first clues as to the nature of the dark matter responsible.

3.6 Acknowledgments

TMPT acknowledges the Aspen Center for Physics (supported by the NSF grant PHY-1066293) where part of this work was completed. and the theory group of SLAC National Lab for their support of his many visits. The work of AR and TMPT is supported in part by NSF grants PHY-0970173 and PHY-0970171.

Chapter 4

Particle Physics Implications and Constraints on Dark Matter Interpretations of the CDMS Signal

Randel C. Cotta, Arvind Rajaraman, Tim M.P. Tait, and Alexander M. Wijangco

4.1 Introduction

Astronomical and cosmological probes of dark matter not only exist, but indicate that dark matter is five times as prevalent in the universe than the conventional forms of matter described by the Standard Model [27]. Despite this abundance however, knowledge of dark matter remains perplexingly incomplete. Principle among these unknowns are the mass of the dark matter (DM) particle and the nature of its interactions with the Standard Model (SM), both of which are unconstrained over many orders of magnitude.

A diversity of theoretical models has grown to accompany the diversity of allowed phe-

nomenology [117]. Extremely light and weakly-coupled axions [118, 119] are a canonical scenario of DM with phenomenology that differs drastically from that of the more usually discussed WIMPs [120, 121, 122, 123, 124, 125], though essentially arbitrary phenomenology can be obtained from hidden sector models [126, 127, 46, 128], which may be designed to solve problems unrelated to dark matter (*e.g.*, generation of cosmic baryon number [129, 130, 131]).

Given this diversity, the experimental effort to measure such interactions has become increasingly creative. In addition to the traditional three-pronged experimental program consisting of direct detection, which seeks to measure DM-nucleon scattering, colliders searches for DM production and indirect detection searches for the energetic products of DM annihilation in astroparticle experiments, are studies of even more diverse effects, *e.g.*, observed and simulated shapes of DM halos [132], the detailed nature of the CMB [133, 134, 135] and primordial element abundances [136] and cooling of astrophysical objects [137].

Recently, the CDMS collaboration has made the interesting observation of an excess of 3 events over an expected background of 0.4 events, that can be interpreted as a signal detection with $\sim 2\sigma$ significance [7]. Such a result is clearly inconclusive on its own and should be subjected to the utmost scrutiny, especially as the favored mass $m_{DM} \simeq 8.6\text{GeV}$ coincides with the sensitivity threshold of the experiment. Despite these considerations, the result is very interesting in light of similar anomalous results, such as from CoGeNT [6], and in the favored-region's proximity to the predictions of some well-motivated theoretical models [138].

Describing a light DM particle with such (relatively) large interactions with the SM and that wouldn't have already been seen elsewhere is a phenomenological challenge. There exist several "portals" (in effective operator language: SM-singlet operators built only out of SM fields) by which such DM may easily communicate with the SM, each of which may naturally suggest vector, scalar or fermionic mediators and have been studied in some detail in the context of light DM [139, 140, 138, 141, 142, 143]. In this work we will consider a

generic model of Dirac fermionic DM interacting with the Standard Model via a relatively light scalar mediator particle. For such a model to avoid being ruled out from the outset we consider our mediator to be coupled to SM fermions in minimal-flavor-violating (MFV [144]) fashion, suggesting a natural connection between the physics that generates our DM and messenger to the physics of the Higgs sector and electroweak symmetry breaking. We will describe regions of parameter space for which our model obtains scattering in the range of the CDMS result, where the annihilations in our model are sufficient for equalling the cosmological DM relic density and regions that are already ruled out by collider and low-energy experiments.

The rest of this paper is divided into four sections. In Section 4.2 we describe and discuss our simplified model framework, in Section 4.3 we describe our model’s DM phenomenology, in Section 4.4 we describe collider and low-energy bounds that can be placed on the parameter space of our model and in Section 4.5 we present a concluding discussion.

4.2 Simplified Model Framework

We work in the framework of a simplified model consisting of the Standard Model supplemented by a Dirac DM particle χ and a CP-even scalar messenger ϕ . CP-even scalars induce s-wave scattering cross sections between WIMP and nucleons, which is favorable for modeling a direct detection signal. Since the CDMS signal is suggestive of a WIMP whose mass is well below $M_Z/2$, we restrict ourselves to considering dark matter which is an electroweak singlet in order to avoid large contributions to the invisible width of the Z boson [145]. Fitting the CDMS signal region will imply $\mathcal{O}(0.1 - 1)$ coupling between ϕ and $\bar{\chi}\chi$, suggesting that ϕ should also be an electroweak singlet. The mass of the χ is fixed by the CDMS signal to $m_\chi \simeq 8.5$ GeV. In the discussion below, we fix the dark matter mass to this value and comment where appropriate as to how our results would change for different masses.

In order to evade very strong bounds from flavor-violating observables, we invoke minimal flavor violation [144] with regard to the ϕ coupling to quarks,

$$\mathcal{L}_{int} = g_\chi \phi \bar{\chi} \chi + \sum_i g_d \lambda_i^d \phi \bar{d}_i d_i + \sum_i g_u \lambda_i^u \phi \bar{u}_i u_i \quad (4.1)$$

where λ_i^d and λ_i^u are the down-type and up-type Yukawa interactions. In addition to the masses m_χ and m_ϕ , the model is specified by the dimensionless couplings to dark matter g_χ , to down-type quarks (scaled by the appropriate Yukawa interaction) g_d , and similarly defined coupling to up-type quarks g_u . In what follows we will work primarily in the 3-dimensional space (m_ϕ, g_χ, g_d) . We consider two distinct cases for g_u :

- $g_u \sim 1.8 g_d$, leading to iso-spin preserving (IP) elastic scattering in direct detection experiments; or
- $g_u \sim -1.015 g_d$, leading to isospin-violating (IV) scattering with $f_n/f_p \sim -0.7$, designed to maximally weaken the sensitivity of Xenon-based searches [74].

It is worth noting that even for $g_u \sim g_d$, the elastic scattering cross section will be similar for protons and neutrons, owing to the relatively small contribution of the up and down quarks because of their small Yukawa interactions. One could also write down (and put bounds on) a coupling between ϕ and leptons, but such an interaction is largely orthogonal to a discussion of the CDMS signal. Where relevant, we will comment on the bounds on such a coupling below.

There are also potentially renormalizable interactions between ϕ and the Standard Model Higgs doublet, H . In general, the details of the scalar potential are not very important for the phenomena of interest here, and we leave a detailed analysis for future work. However, it is worth noting that mixing between ϕ and the Higgs boson allows for ϕ to be produced

via typical Higgs production modes, including ϕZ at LEP II. For masses less than about 110 GeV, null results of Higgs searches at LEP generically imply that the mixing is no larger than $\mathcal{O}(10\%)$ [146], although there are windows of mass where bounds are weaker, and might even be interpreted as not very significant hints for a positive signal [147].

While we remain agnostic as to the origin of the simplified model framework, it is worth noting that one can imagine a simple UV-completion of the scalar sector based on a two Higgs doublet model augmented by a gauge singlet scalar. The two Higgs doublets provide sufficient freedom in the Yukawa couplings so as to realize g_u and g_d in the desired ranges, with the (mostly singlet) ϕ inheriting the couplings through modest mixing with a combination of the physical CP even Higgs bosons. Perhaps the most studied model containing these ingredients is the NMSSM [148, 149]. It has been pointed out that one can find limits in the NMSSM parameter space that attain large scattering cross-sections with a low DM mass [150, 151, 152] although there may be some tension with other constraints as, in supersymmetric models like these, large cross-sections tend to come hand-in-hand with sizable couplings to W^\pm/Z^0 [153]. Variations of supersymmetric models consisting of the MSSM plus a singlet super-field can realize suitable cross sections [154, 155, 156]. For an example of a non-supersymmetric UV completion see [157].

4.3 DM Observables

In this section we focus on finding regions of our parameter space that are attractive from a DM standpoint: light DM with large elastic scattering cross-sections. Although we are particularly interested in scattering, we also calculate relic density and discuss current annihilation cross-sections for our χ to give a sense of the cosmological history necessary in such a scenario. We consider messenger masses in a wide range, $1\text{GeV} \lesssim m_\phi \lesssim 100\text{GeV}$, anticipating (as is confirmed below) that mediator masses above $\sim 100\text{GeV}$ will be non-trivially

constrained by collider monojet searches¹. We use *MicrOMEGAs v2.4* [159] for all elastic scattering and annihilation cross section calculations.

For our direct detection calculation we use a local DM density $\rho_0 = 0.3\text{GeV}/\text{cm}^3$ and nuclear form factors:

$$\begin{aligned} f_u^p &= 0.023, & f_d^p &= 0.033, & f_s^p &= 0.05, \\ f_u^n &= 0.018, & f_d^n &= 0.042, & f_s^n &= 0.05. \end{aligned}$$

Appropriate values for the strange-flavored scalar form factors are hotly-debated at current [160, 161, 162, 163, 164, 165, 166, 167], the choice $f_s^N \approx 0.05$ is on the low side of proposed values, making it a conservative choice for our purposes. The uncertainty coming from the strange quark is anyway not critical for our purposes: we consider a wide range of elastic scattering cross-sections²,

$$10^{-6}\text{pb} \lesssim \sigma_{\text{SI,N}} \lesssim 3 * 10^{-4}\text{pb}, \tag{4.2}$$

as interesting for our purposes. Since the transfer energy of scattering is much less than m_ϕ , the scattering cross section depends on m_ϕ and the couplings as a function of $g_\chi g_d/m_\phi^2$.

We calculate the thermal relic density of our χ assuming that the only relevant processes at freezeout are those in our simplified model. As always, this is a fairly heavy-handed assumption and may or may not be relevant in any particular completion of our model. Despite this, our thermal relic calculation remains useful for denoting regions of parameter

¹For mediator masses heavier than typical LHC center-of-mass energies the limit should be essentially the same as the stringent EFT bounds derived in [158]

²This range corresponds to the lower-most and upper-most values on the 2σ ellipse of the result [7].

space where extra theoretical structure³ may be necessary to increase or decrease the relic density with respect to our minimal scenario and where our model saturates the *Planck* collaboration’s measurement [27], $\Omega_{CDM}h^2 \approx 0.1146$, on its own. Annihilations proceed through t-channel $\chi\bar{\chi} \rightarrow \phi\phi$ (when kinematically available) and through s-channel $\chi\bar{\chi} \rightarrow f\bar{f}$, the former depending on the couplings only as g_χ^2 and the latter as $g_\chi g_d$. Both of these processes are actually p-wave processes at leading order (suppressed by $v^2 \sim 10^{-6}$) so current annihilations from our simplified model are predicted to be much below the canonical $\langle\sigma v\rangle \sim 3 * 10^{-26}\text{cm}^3/\text{s}$. Similarly low rates are calculated in the resonant region $2m_\chi \approx m_\phi$, although *Planck*-level relic densities are achieved for much lower coupling values. Such processes also fall below the bound found in [168]. If our model were to also include a pseudo-scalar state, a , then there would be available s-wave processes giving current annihilations close to the canonical value⁴. Such pseudo-scalars are not hard to come by theoretically (*e.g.*, in approximately SUSY-preserving multiplets) and would have no effect on scattering rates (momentum suppressed) but potentially sizable effects on the other observables, such as collider production.

In Figure 4.1 we map out the combinations of g_χ and m_ϕ for which scattering cross sections are within the range Eqn. 4.2 and for which the relic density matches the *Planck* value for both IP and IV cases and for several values of g_d . The shape of the signal region can be understood as a restriction of $g_\chi g_d/m_\phi^2$ to a particular interval. The features of the relic density band are easy to understand: there is a sharp upturn where the $\chi\chi \rightarrow \phi\phi$ channel becomes phase space suppressed ($m_\phi \approx m_\chi$) and a sharp downturn in the resonant annihilation region ($m_\phi \approx 2m_\chi$). Annihilation cross-sections (not shown) are $\langle\sigma v\rangle \lesssim 3 * 10^{-30}\text{cm}^3/\text{s}$ on the *Planck* band. In principle it is possible for m_ϕ to be sufficiently light such that tension arises with measurements of N_{eff} . However, the smallest value of m_ϕ we consider is 1 GeV. At these masses ϕ decays away before BBN and does not affect the CMB. In the IV

³*e.g.*, non-thermal evolution or dark sector states that participate in the thermal calculation

⁴As may be desired given the current (inconclusive, but interesting) hints of $\sim 10\text{GeV}$ DM particles annihilating to b ’s or τ ’s contributing to the γ -ray spectrum at the Galactic Center [169, 170].

case, scattering cross-sections are reduced by destructive interference and we observe a shift of the favored region for scattering toward larger coupling values. We observe regions where both large scattering cross-sections and $\Omega_\chi \approx \Omega_{CDM}$ can be obtained simultaneously, for essentially any choice of g_d . While this happens both for very light mediators ($m_\phi < 10\text{GeV}$) and for very heavy mediators ($m_\phi > 20\text{GeV}$), we expect these regions to be in danger either from Υ -decay data or from collider searches. In contrast, regions of overlap in the $m_\Upsilon < m_\phi < 2m_\chi$ range are particularly hard to constrain. In principle, an s-wave $\chi\chi$ scattering is also introduced, although we do not consider the consequences of this interaction in this work.

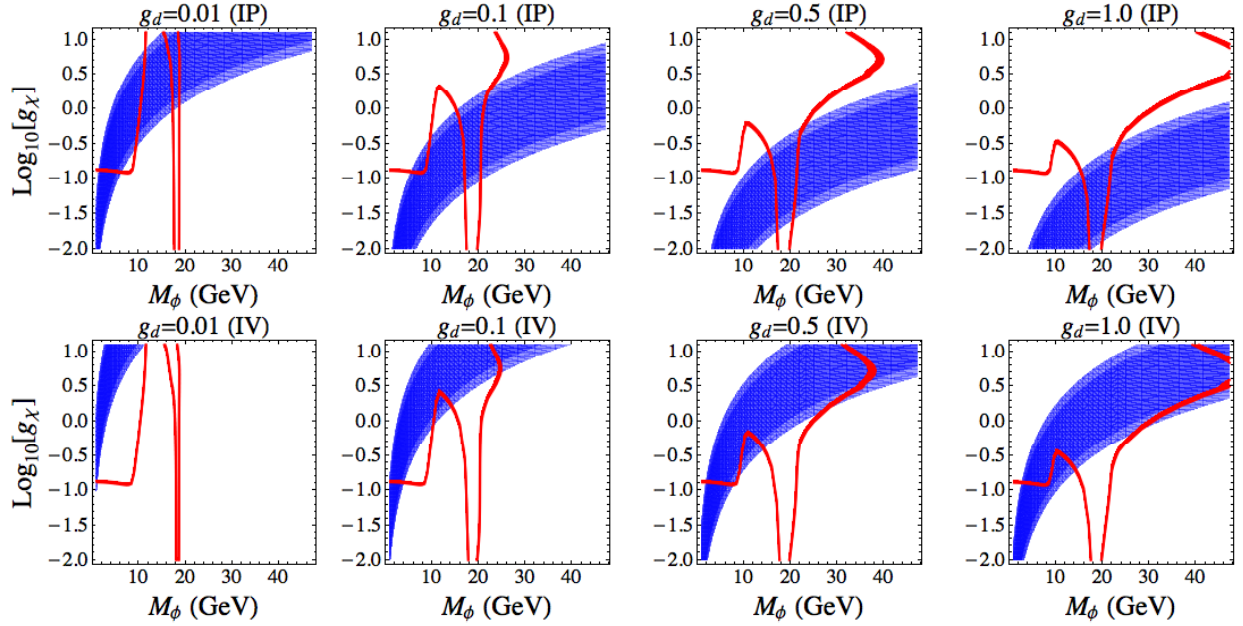


Figure 4.1: Spin-Independent Scattering and Relic Density. The blue band denotes SI scattering cross-sections within the range Eqn. 4.2 (darker and lighter regions describing the extent of 1σ and 2σ ellipses in the result [7], respectively). The red band shows where our χ 's relic density is $\Omega_\chi \approx \Omega_{CDM}$. In the upper panels g_u and g_d are related such that $f_n = f_p$ (IP), while in the lower panels $f_n/f_p = -0.7$ (IV).

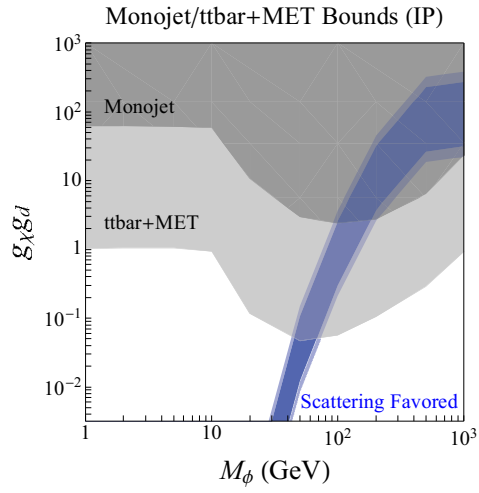
4.4 Collider & Low-Energy Constraints

4.4.1 Mono-Objects

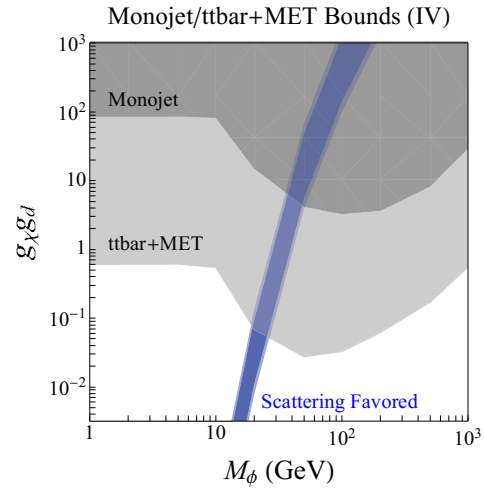
Intuition garnered from DM effective theory analyses over the last few years suggests that collider searches may have the final say on the viability of this scenario [50, 52, 14, 53, 158, 54, 171, 172, 111, 173, 174]. Such searches typically look for DM direct production by studying single objects (monojets, monophotons, etc.) recoiling off of a missing transverse momentum vector and, unlike direct detection experiments, remain sensitive to arbitrarily small DM masses. The caveat to these searches is the efficacy of the EFT description, which can give either an overly-conservative or an overly-optimistic sense of the collider reach in light-mediator scenarios. For our mediators, with the DM mass fixed at $m_\chi = 8.5\text{GeV}$, there are roughly three regimes for collider production: *(i)* the mediator is very heavy compared to typical machine center-of-mass energies, *(ii)* the mediator is light compared to collider center of mass energies but heavier than $2m_\chi$ and *(iii)* the mediator is lighter than $2m_\chi$. Scenario *(i)* is the regime where the EFTs should give basically the right answer, in scenario *(ii)* the mediator can be produced on-shell so we would expect the EFT bounds to be conservative relative to the exact bounds and in scenario *(iii)* the mediator can never be put on-shell, the production cross-section is a rapidly falling function of the mono-object's p_T and the EFT bounds would suggest much tighter constraints than what one would actually get in the full calculation. Of course these regimes bleed into each other a bit, here we seek to describe this behavior. For studies involving light vector mediators, see Refs. [175, 176, 177, 178].

Here we focus on LHC monojet searches, which we expect to provide the tightest constraints in this class of experiments. Monojet bounds from the Tevatron were checked (*c.f.*, [53]) as well and they are not competitive with those coming from the LHC⁵. We mimic cuts

⁵Monophoton bounds from LEP are irrelevant unless our mediator were to have large couplings to the electron, which seems unlikely in our construction.



$t\bar{t} + \text{MET}$



$g_\chi g_d \quad m_\phi$

$t\bar{t} + \text{MET}$

$g_d = 1$

$m_\phi < 2m_\chi$

$m_\phi = 2m_\chi$

$g_\chi g_d \sim 4\pi$

$t\bar{t} + \text{MET}$

m_ϕ

4.4.2 Heavy-Flavor Searches

While the MFV structure of our messenger’s couplings keep direct collider production of ϕ ’s highly-suppressed, the large couplings to top and bottom quarks suggest large rates for ϕ ’s radiated off of the final states in heavy flavor (HF) production. Since our ϕ ’s may be made to decay either dominantly to missing transverse energy (for $g_\chi \gg g_d$) or to $b\bar{b}$ (for $g_d \gg g_\chi$), heavy flavor searches both with and without associated MET may be applicable. HF searches with MET are typical of the suite of SUSY searches for third-generation squarks (*e.g.*, [9]), while HF searches without MET are not nearly as common. An example of the latter is the search for signals of Higgs production in the $t\bar{t}H \rightarrow t\bar{t}b\bar{b}$ channel (in practice, the $t\bar{t}$ +b-jet channel [10, 180]). Here we investigate bounds on our model’s parameter space that can be derived from these two searches. Another recent work that considered heavy-flavored final states and dark matter is [181]

The ATLAS analysis [9], uses 13 fb^{-1} of 8TeV data to place very stringent constraints, $\mathcal{O}(1\text{fb})$, on $t\bar{t} + \text{MET}$ from BSM sources. Here we use the full *MPP* analysis chain to simulate the SM background to this search and to get a sense of the acceptance profile for tagging the two tops in our signal. To calculate the signal rate we assume that the acceptance (more precisely, the part of which comes from top-tagging) for signal events is essentially the same as that for the SM background. This allows us to do an initial calculation of the signal at parton level, before applying the more involved m_{T2} cut to accurately reproduce the MET acceptance (the quantity that is really sensitive to the kinematics of our signal events) in reasonable computational time. The particular MET and p_T cuts that we used were those of the “110 SR” signal region defined in [9]. The resulting excluded region is described in Figure 4.2 and is seen to be stronger for all m_ϕ than that from the monojet search. Our model’s mediator mass is bounded to be $m_\phi \lesssim 45\text{GeV}$ (IP) or $m_\phi \lesssim 20\text{GeV}$ (IV), in both cases far smaller than the model’s ultimate perturbativity bound $g_\chi g_d \lesssim 4\pi$.

$t\bar{t}b$

$t\bar{t}b$

$t\bar{t}j$

b

j

4.7 fb^{-1}

7 TeV

$t\bar{t}b$ $t\bar{t}j$

1.4σ

125GeV

$t\bar{t}b$

$t\bar{t}\phi$

$t\bar{t}H$

$t\bar{t}\phi$

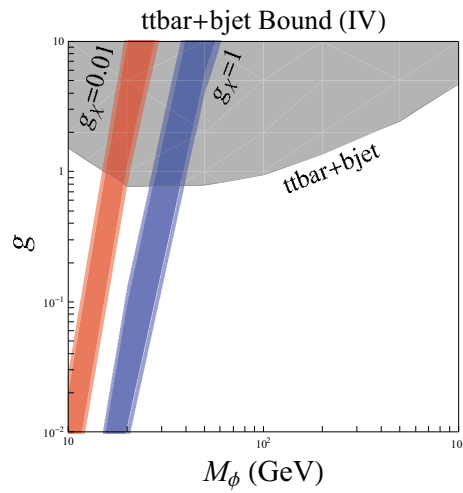
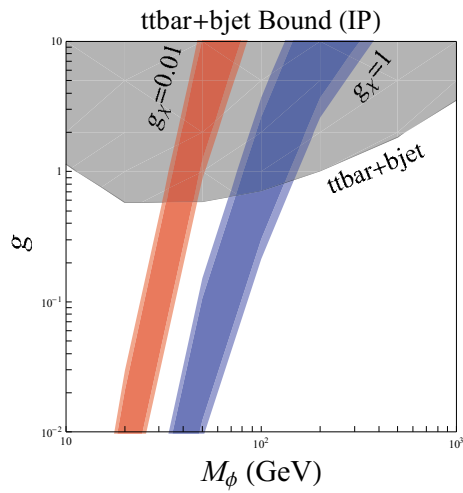
$t\bar{t}H$

g_χ $g_\chi = 0.01$

$g_\chi = 1$

$t\bar{t}\phi$

g_d



$t\bar{t}b$

g_d

$g_\chi = 1$

$g_\chi = 0.01$

$t\bar{t}\phi$

$t\bar{t}H$

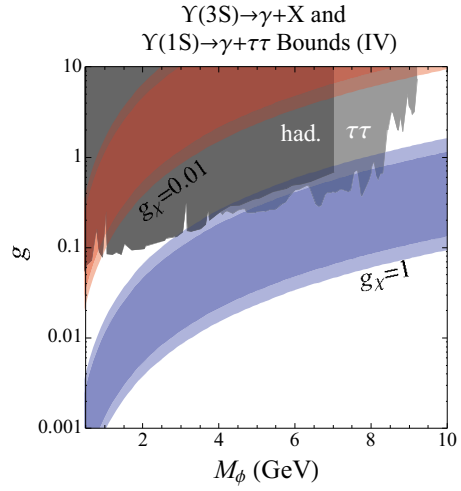
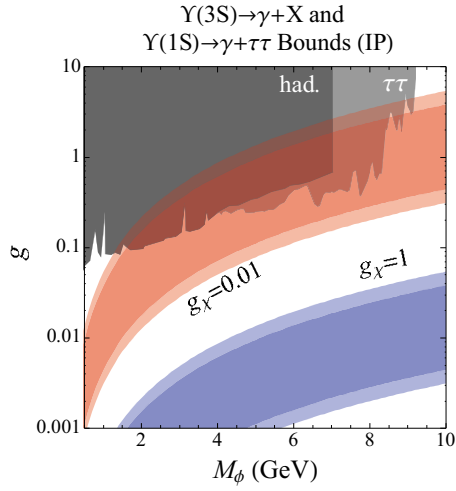
4.4.3 B-Factory Constraints

For mediators with $m_\phi \lesssim m_\Upsilon \approx 10\text{GeV}$ one must consider the possible signatures of our model in $\Upsilon(nS)$ decay processes. Since our DM has $2m_\chi > m_\Upsilon$ we do not expect signatures in Υ decays with invisible products (although these would become relevant for $m_\chi \lesssim 5\text{GeV}$), instead we consider radiative Υ decays, $\Upsilon(nS) \rightarrow \gamma\phi \rightarrow \gamma X$ where⁷ X is some visible system recoiling off of a monochromatic γ . We consider two *BaBar* collaboration analyses: [11], a search for photon resonances in $\Upsilon(3S) \rightarrow \gamma + \text{hadrons}$ and [12], a search for photon resonances in $\Upsilon(1S) \rightarrow \gamma + \tau^+\tau^-$. Both of these results provide a bound on g_d (independent of g_χ), the former considering only quark coupling while the latter requires the model-dependent assumption that $g_l = g_d$. We calculate the associated rates in our model space, following closely the work [182]. The resulting bounds are shown in Figure 4.4. The Υ data limits the g_d coupling to be generally $g_d \lesssim 0.1$ for models with $m_\phi \lesssim 10\text{ GeV}$, ruling out favored parts of parameter space where g_χ is small. There is a large dependence on the choice of IP or IV scattering, the latter being constrained much more tightly at a given scattering cross-section by the Υ data.

4.4.4 Exotic Higgs Decays

Given the necessarily small mixing between our messenger and the SM Higgs, we expect that the current constraint on the Higgs invisible width (about 40%, per [183]) is not tight enough to constrain our model. If our mediator is light, $m_\phi \ll m_H$, then, as in many NMSSM discussions, we may imagine producing a pair of boosted ϕ 's and searching for pairs of boosted objects from their decays. While the rate of such events depends on the details of the UV physics that give rise to our simplified model, the resultant striking signature may be the first place in which such a model can be discovered.

⁷Of course, “ ϕ ” here refers to our mediator, not the light unflavored meson.



Υ

$g_\chi = 0.01$ $g_\chi = 1$

τ

ϕ

p_T/m_j

$\sigma_s = 0.5 \text{ fb}$

$\sigma_b = 0.12 \text{ fb}$

$S/\sqrt{B} = 5$

$\mathcal{L} = 12 \text{ fb}^{-1}$ 14TeV

$\tau\tau \sim \mathcal{O}(10\%)$

g_d $BR(\phi \rightarrow$
 $g_{h\phi\phi} = \sqrt{4\pi}$

g_d g_l $BR(\phi \rightarrow \tau\tau) \sim \mathcal{O}(100\%)$
 $\mathcal{L} = 12 \text{ fb}^{-1}$ 14TeV

4.5 Discussion

We have investigated diverse bounds on the parameter space of a simplified model of DM whose phenomenology could plausibly explain the low-mass and high-cross-section signal of DM scattering in the CDMS Silicon data. Our model is typical of some extensions of the SM Higgs sector that give light scalars coupling to SM fermions in an MFV pattern (*e.g.*, coupling like a Higgs). We have shown that such models can easily attain the necessary large scattering cross-sections for couplings of $\mathcal{O}(0.1 - 1)$, while also attaining the correct relic density, in many regions of this subspace. If such a model were to be supplemented with a pseudoscalar of similar mass to our messenger ϕ , essentially none of the above story would change qualitatively, except that one would have the kind of canonical s-wave annihilation rates that we may already be seeing in the Galactic Center.

We have discussed collider and low-energy B-factory bounds on our parameter space and the complementarity of these bounds. A round-up of these results is described in Figures 4.5-4.6, where all bounds are collected and plotted in the $g_\chi g_d$ vs. m_ϕ plane. Results are given for two different choices of $g_\chi = 1$ and $g_\chi = 0.1$. In Fig. 4.5 we find that, for large $g_\chi = 1$, the combination of $t\bar{t} + \text{MET}$ and $\Upsilon(nS)$ data require $g_d \lesssim 0.1$ except in the difficult region $m_{\Upsilon(3S)} < m_\phi < 2m_\chi$ where $g_d \lesssim 1$. For smaller $g_\chi = 0.1$ we see that the $t\bar{t} + \text{b-jet}$ bound (depending only on g_d) supplants the $t\bar{t} + \text{MET}$ bound (depending on $g_\chi g_d$) to require $g_d \lesssim 1$ for all m_ϕ . In Figure 4.6 we overlay the favored regions for scattering and relic density in our parameter space. We see that the isospin-violating case is more highly constrained than the isospin-preserving case, owing to the generally larger product $g_\chi g_d$ required to produce scattering signals at the CDMS level.

The fact that a light DM particle and scalar messenger coupling **so strongly** to SM fermions is even phenomenologically viable at this point is very interesting. It is completely plausible that a model like ours could be discovered first in direct detection experiments (as it may

already have been!), especially for mediator masses in the difficult range $m_{\Upsilon(3S)} < m_\phi < 2m_\chi$. From what we have shown it is also plausible that such a discovery could be corroborated (or such a model ruled out) by LHC searches for anomalous heavy flavor final states, strongly motivating a more careful look at such signatures under more generic (*i.e.*, than SM Higgs or MSSM sparticle) expectations.

4.6 Acknowledgments

The authors would like to acknowledge helpful discussions with J. Shelton, J. Zupan, C. Wagner, and L. Tao. The research of R.C.C. and A.R. is supported by the National Science Foundation under grant PHY-0970173. The research of T.M.P.T. is supported in part by NSF grant PHY-0970171 and by the University of California, Irvine through a Chancellor's fellowship.

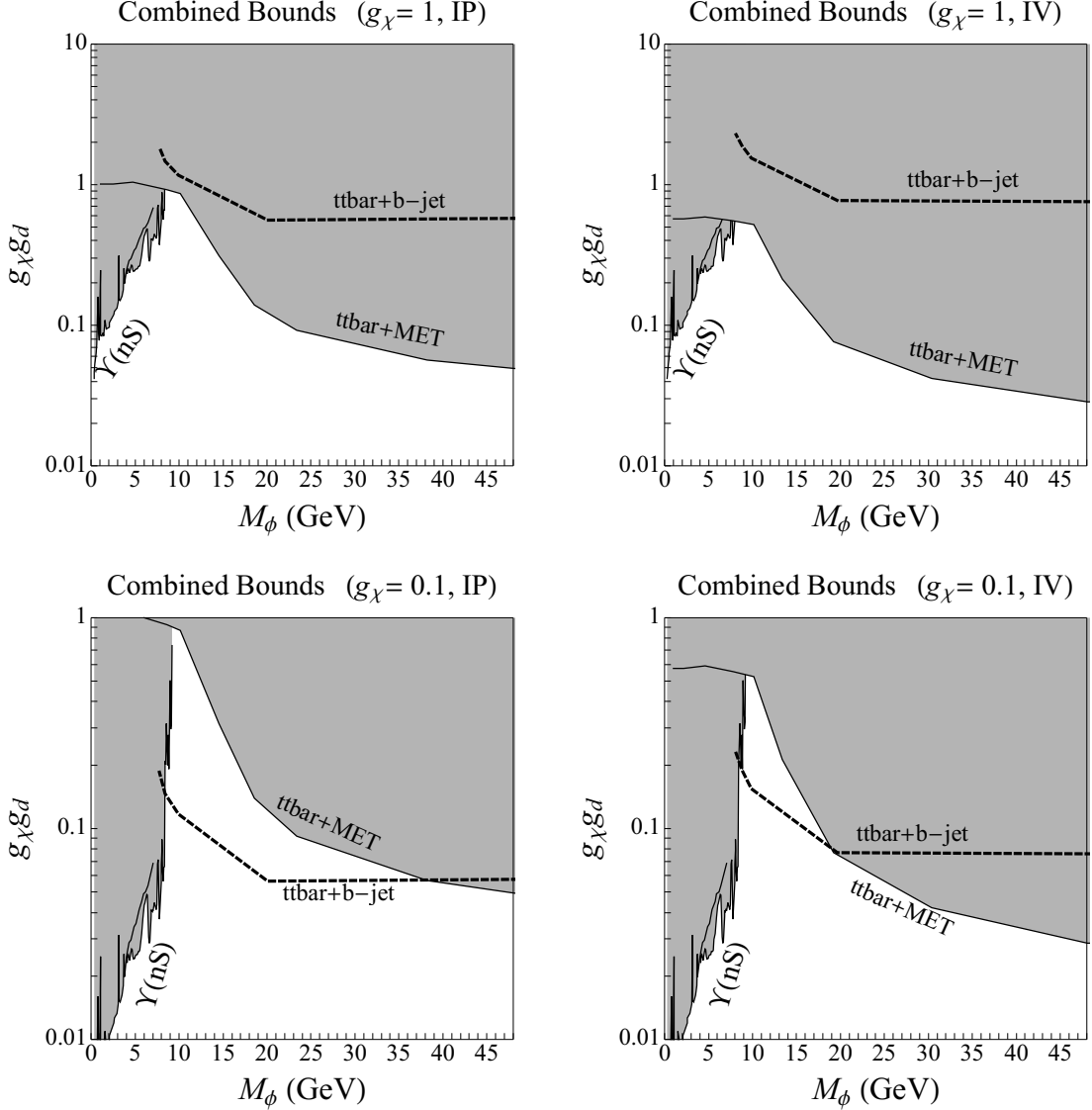
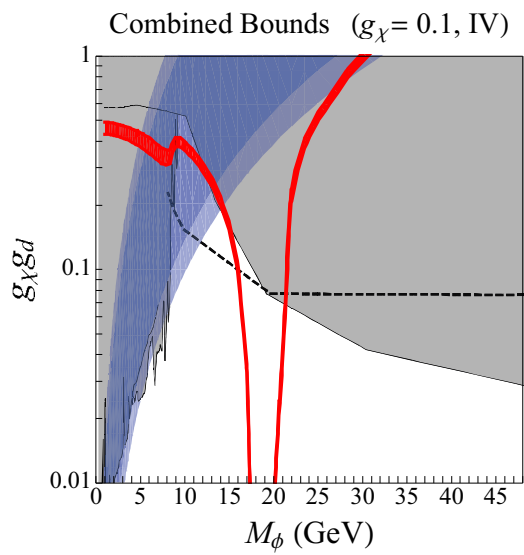
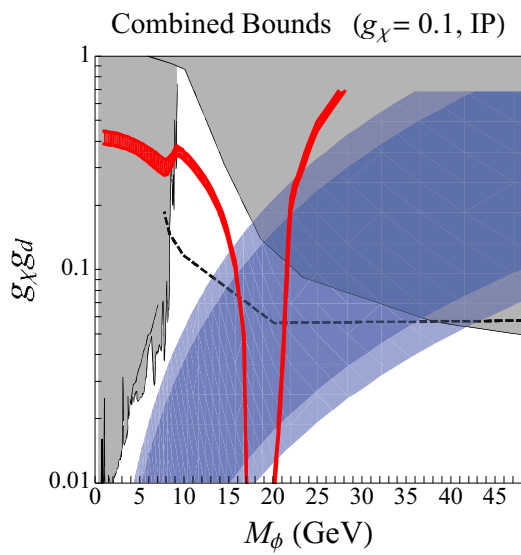
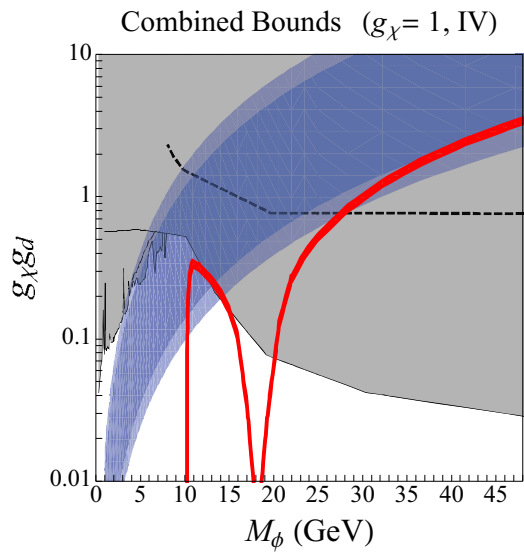
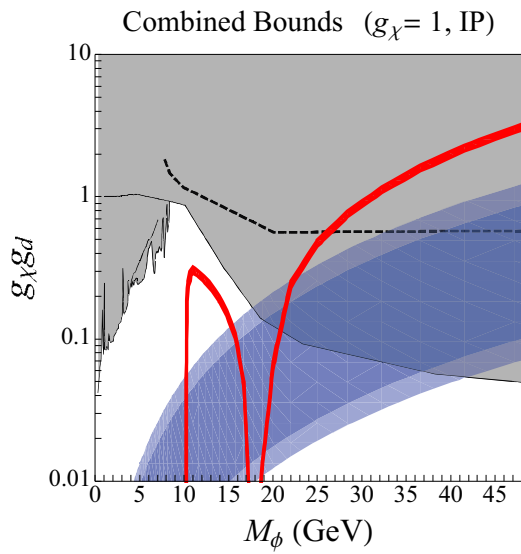


Figure 4.5: Combined bounds in the $g_\chi g_d$ vs. m_ϕ plane. Bounds from $t\bar{t} + \text{MET}$, $t\bar{t} + \text{b-jet}$ and radiative Υ decays (in both hadronic and τ channels) are labelled accordingly. Monojet bounds are irrelevant, given the axes ranges plotted. We choose $g_\chi = 1$ ($g_\chi = 0.1$) in the upper (lower) panels to translate bounds that only depend on g_d onto this plane. Left and right panels correspond to IP and IV scenarios, respectively. We use a dashed line to remind the reader that the $t\bar{t} + \text{b-jet}$ bound is particularly rough (as described in the text).



Chapter 5

Hidden On-Shell Mediators for the Galactic Center Gamma-ray Excess

Mohammad Abdullah, Anthony DiFranzo, Arvind Rajaraman, Tim M. P. Tait, Philip Tanedo, and Alexander M. Wijangco

5.1 Introduction

The particle nature of dark matter (DM) remains one of the outstanding open questions in high energy physics. Experimental probes of the dynamics that connect the dark sector and the Standard Model (SM) fall into three complimentary classes shown schematically in Fig. 5.1 See [43] for a status report.

Recent analyses of the FERMI Space Telescope data find an excess of 1–10 GeV γ -rays from the center of the galaxy. In fact, a similar excess seems to extend away from the center to high galactic latitudes [185, 186, 187]. This may be indicative of dark matter annihilating into SM final states which later shower to produce the observed excess photon spectrum [188, 189,

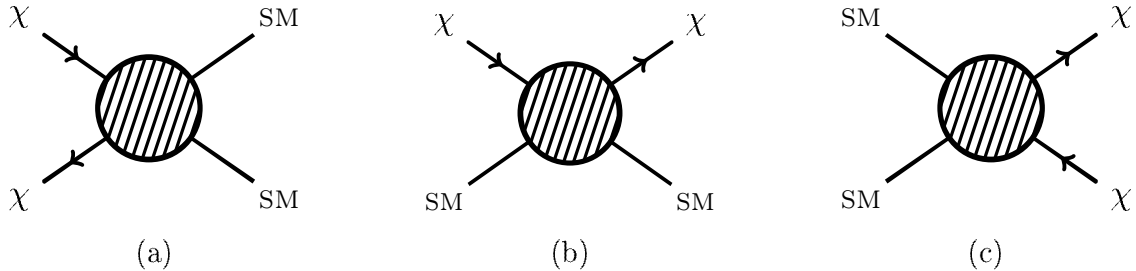


Figure 5.1: (a) Annihilation, (b) Direct Detection, (c) Collider. Complimentary modes of dark matter detection. Annihilation sets both the thermal relic abundance and the present-day indirect detection rate.

190, 169, 191, 170, 192, 193, 13, 38, 194]; see [195, 196, 197, 198, 199, 200, 201, 202, 194, 203] for recent models. While an early estimate argued that an alternate interpretation based on unidentified millisecond pulsars is unlikely [204], [13] and [205] recently demonstrated the consistency of this hypothesis with the γ -ray excess. Indeed, it may be difficult to distinguish these two possibilities since the extrapolated millisecond pulsar (MSP) profile is very similar to standard DM profiles [206]. For the remainder of this paper we assume the excess is generated by DM annihilation. The latest analyses prefer a 40 GeV dark matter candidate that annihilates into $b\bar{b}$ pairs¹ with a thermally averaged cross section $\langle\sigma v\rangle_{b\bar{b}} \approx \mathcal{O}(\text{few}) \times 10^{-26} \text{cm}^3/\text{s}$ [13, 38]. Further, because $\langle\sigma v\rangle_{b\bar{b}}$ is close to the value required to be a thermal relic from standard freeze-out, it is implausible that such a relic could produce such a γ -ray signal without having an s -wave annihilation mode. Combined with constraints from direct detection and collider experiments, this signal motivates a more detailed study of the physics encoded in the shaded regions of Fig. 5.1.

¹Annihilation of 10GeV DM into $\tau\bar{\tau}$ is also plausible fit, see [207, 208, 197, 198, 201, 209] for recent models. [210] found that a universal coupling to charged leptons may be favored after bremsstrahlung and inverse Compton scattering effects are included. In this paper we focus on the case where the γ -ray excess is generated by $b\bar{b}$ pairs; we comment on more general final states in Section 5.6.1 and Appendix 5.9.

5.1.1 From Effective Theories to Simplified Models

A simple parameterization of the SM–DM interaction is to treat the shaded blobs as effective contact interactions between dark matter particles (χ) and SM states. For example, the coupling of fermionic DM to a quark q is parameterized through nonrenormalizable operators

$$\mathcal{L} \supset \frac{1}{\Lambda^2} (\bar{\chi} \mathcal{O}_\chi \chi) (\bar{q} \mathcal{O}_q q), \quad (5.1)$$

where, for example, $\mathcal{O}_\chi \otimes \mathcal{O}_q = \gamma^\mu \otimes \gamma_\mu$ corresponds to an interaction mediated by a heavy vector mediator that has been integrated out. The coefficient Λ^{-2} can be calculated for specific DM models and allow one to apply bounds from different types of experiments in a model-independent way. This technique has been applied, for example, for collider [49, 50, 52, 53, 14, 54, 158, 171, 55, 174, 211, 172, 212, 173, 111, 213, 214, 215, 181, 216, 217], indirect detection [48, 70, 71, 218, 219, 220, 221, 97, 211] and direct detection [90, 82, 222, 223, 69, 224, 225, 226, 227] bounds on dark matter. The choice of pairwise dark matter interactions assumes the existence of a symmetry that also stabilizes the DM particle against decay while the pairwise SM interactions are assumed to be the leading order gauge-invariant operators. This need not be the case as has been demonstrated for annihilation [228] and direct detection [229]. In these cases, the structure in (5.1) fails to capture the physics of the mediator fields which couple to both the dark and visible (SM) sectors: the effective contact interaction description breaks down when the mediators do not decouple. The limitations of the contact interaction bounds were pointed out in [53] and highlighted in [230, 231, 232, 233].

This motivates a shift in the *lingua franca* used to compare experimental results to models: rather than contact interactions, light (nondecoupled) mediators suggest using ‘simplified models’ that include the renormalizable dynamics of the mediator fields [234]. This approach has been applied to colliders [235, 178, 236, 237, 175, 176, 238, 239, 232, 233, 231, 240, 241, 242] and astrophysical bounds where the physics of the mediator has been explored in DM

Name	Operator	Constraint
D2	$(\bar{\chi}\gamma_5\chi)(\bar{q}q)$	Edge of EFT validity from monojet bounds
D4	$(\bar{\chi}\gamma_5\chi)(\bar{q}\gamma_5q)$	Edge of EFT validity from monojet bounds
D5	$(\bar{\chi}\gamma^\mu\chi)(\bar{q}\gamma_\mu q)$	Spin independent direct detection
D6	$(\bar{\chi}\gamma^\mu\gamma_5\chi)(\bar{q}\gamma_\mu q)$	Related to D5, D8 in chiral basis
D7	$(\bar{\chi}\gamma^\mu\chi)(\bar{q}\gamma_\mu\gamma_5q)$	Related to D5, D8 in chiral basis
D8	$(\bar{\chi}\gamma^\mu\gamma_5\chi)(\bar{q}\gamma_\mu\gamma_5q)$	Spin dependent direct detection
D9	$(\bar{\chi}\sigma^{\mu\nu}\chi)(\bar{q}\sigma_{\mu\nu}q)$	Nontrivial spin-2 UV completion
D10	$(\bar{\chi}\sigma^{\mu\nu}\gamma^5\chi)(\bar{q}\sigma_{\mu\nu}q)$	Nontrivial spin-2 UV completion
D12	$(\bar{\chi}\gamma_5\chi)G_{\mu\nu}G^{\mu\nu}$	Monojet bounds
D14	$(\bar{\chi}\gamma_5\chi)G_{\mu\nu}\tilde{G}^{\mu\nu}$	Monojet bounds

Table 5.1: Contact operators between Dirac DM and quarks or gluons [14] that support s -wave annihilation and the constraint for the galactic center. See [15] for a recent technical analysis.

self-interactions [243, 244, 245, 246, 247, 248, 249, 250, 251, 252, 253, 254, 255, 256, 127, 257, 258, 259, 260, 261].

5.1.2 The Gamma-ray Excess Suggests Light Mediators

When the galactic center signal is combined with complementary bounds from direct detection and colliders, one is generically led to the limit where the contact interaction description (5.1) breaks down and a simplified model description is necessary. By ‘generic’ we mean no parameter tuning or additional model building is invoked.

The tension is summarized in Table 5.1, where we list the Dirac fermion dark matter contact interactions that satisfy the requirement of s -wave annihilation². Because each effective operator simultaneously encodes the various DM–SM interactions in Fig. 5.1, requiring a coupling large enough to produce the γ -ray excess automatically generates signals that are constrained by null results at direct detection [30, 262] and monojet [263] experiments. These rule out operators D5, D8, D12, and D14 in Table 5.1. The operators D2 and D4 are at

²Majorana dark matter relaxes these bounds by forcing some of these operators to vanish identically.

the edge of the validity of the effective theory [232, 233, 231]. We ignore the D9 and D10 operators since they cannot be UV completed by a renormalizable theory. Finally, the D6 and D7 operators are related to D5 and D8 by the chiral structure of the Standard Model. The fermionic $SU(2)_L \times U(1)_Y$ eigenstates are chiral so that gauge invariant interactions are naturally written in a chiral basis $\bar{q}\mathcal{O}_q P_{L,R}q$ where $P_{L,R} = \frac{1}{2}(1 \mp \gamma^5)$. Thus one generically expects that in the absence of tuning³, the presence of vector or axial couplings implies the existence of the other.

It is thus difficult to account for the γ -ray excess in the ‘heavy mediator’ limit where these contact interactions are valid. A more technical analysis of the contact interaction description was recently performed in [264, 218, 15] and includes the case of scalar dark matter. The γ -ray excess thus generically implies a dark sector with mediators that do not decouple and hence is more accurately described in a simplified model framework. Recent comprehensive studies of simplified models for the γ -ray excess have dark matter annihilating through off-shell mediators (s - and t -channel diagrams) [265, 266]; see [267, 268] for an earlier model.

5.1.3 Annihilation to On-shell Mediators

In this paper we focus on a different region in the space of simplified models where mediators are light enough that they can be produced on-shell in dark matter annihilation, henceforth referred to as the on-shell mediator scenario. This annihilation mode is largely independent of the mediator’s coupling to the SM so long the latter is nonzero. Lower limits on the SM coupling—that is, upper limits on the mediator lifetimes—are negligible since the mediator may propagate astrophysical distances before decaying to the $b\bar{b}$ pairs that subsequently yield the γ -ray excess. The SM coupling can be parametrically small which suppresses the off-shell s -channel annihilation mode as well as the direct detection and collider signals. This

³It is worth noting that such a ‘coincidental’ cancellation occurs in the Z coupling to charged leptons which is dominantly axial due to $\sin^2 \theta_W \approx 1/4$.

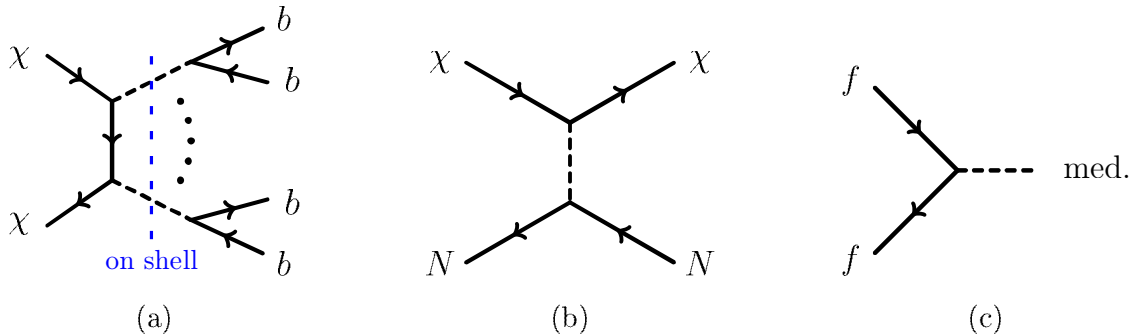


Figure 5.2: (a) Annihilation, (b) Direct Detection, (c) Collider. DM complementarity for on-shell mediators; compare to Fig. 5.1. (a) The annihilation rate is independent of the mediator coupling to the Standard Model. (b) Direct detection remains 2-to-2, here N is a target nucleon. (c) Colliders can search for the presence of the mediator independently of its DM coupling.

is shown in Fig. 5.2.

Because on-shell annihilation into mediators requires at least two final states⁴, the resulting annihilation produces at least four b quarks, as shown in Fig. 5.2a. This, in turn, requires a heavier dark matter mass in order to eject ≈ 40 GeV b quarks from each annihilation to fit the γ -ray excess. This avoids the conventional wisdom that this excess requires 10 – 40 GeV dark matter. In the limit on-shell annihilation dominates, the total excess γ -ray flux is fit by a single parameter, the mediator coupling to dark matter. Once fit, this parameter determines whether the DM may be a thermal relic. We remark that the spectrum is slightly boosted by the on-shell mediator; we address this below and explore possibilities where the mediator mass can be used as a handle to change the spectral features.

The on-shell mediator limit thus separates the physics of mediators SM and DM couplings. The former can be made parametrically small to hide DM from direct detection and collider experiments, while the latter can be used to independently fit indirect detection signals such as the galactic center γ -ray excess. Observe that these simplified models modify the standard picture of complementary DM searches for contact interactions shown schematically in

⁴One may also consider semi-annihilation processes $\chi_1\chi_2 \rightarrow \chi_3(\text{mediator})$ [269]. See [270] for a prototype model for the galactic center γ -ray excess.

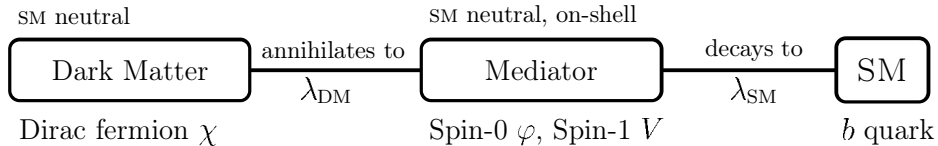


Figure 5.3: Dark matter annihilates to on-shell mediators, which in turn decay into $b\bar{b}$ pairs. Each step is controlled by a separate coupling, λ . See text for details.

Fig. 5.2. Annihilation now occurs through multiple mediator particles and is independent of the mediator coupling to the SM. Direct detection proceeds as usual through single mediator exchange between DM and SM. Collider bounds, on the other hand, need not depend on the DM coupling at all and can focus on detecting the mediator rather than the dark matter missing energy.

In this paper we explore the phenomenology of on-shell mediator simplified models for the galactic center. This paper is organized as follows. In the following two sections we present the on-shell simplified models that generate the γ -ray excess and determine the range of dark sector parameters. We then assess in Section 5.4 the extent to which the on-shell mediators must be parametrically hidden from direct detection and colliders. In Section 5.5 we discuss the viability of this scenario for thermal relics. We comment on the lessons for UV models of dark matter in Section 5.6. Appendix 5.9 briefly describes plausible variants for generating γ -ray spectra with more diverse SM final states.

5.2 On-Shell Simplified Models

Fig. 5.3 schematically represents the class of simplified models that we consider. We assume the existence of a single SM neutral spin-0 or spin-1 mediator which couples to Dirac fermion DM with coupling λ_{DM} and $b\bar{b}$ pairs with coupling λ_{SM} . Majorana fermions do not differ qualitatively in this regime. We focus on the case where mediators couple to the Dirac DM

fermion with coupling λ_{DM} and to $b\bar{b}$ pairs with coupling λ_{SM} .

5.2.1 Parity Versus Chirality

Before describing the mediator interactions, we remark on the utility of the parity and chirality bases for four-component fermion interactions. In the parity basis, one uses explicit factors of the γ^5 matrix to parameterize

$$\text{scalar } (\mathbb{1}), \quad \text{pseudoscalar } (\gamma^5), \quad \text{vector } (\gamma^\mu), \quad \text{and axial } (\gamma^\mu\gamma^5). \quad (5.2)$$

interactions. This basis is most suited for nonrelativistic interactions. Equivalently, in the chirality basis, one inserts chiral projection operators $P_{L,R} = \frac{1}{2}(1 \mp \gamma^5)$ into fermion bilinears. This is the natural description of SM gauge invariants. The spin-0 fermion bilinears are

$$\bar{\Psi}(\mathbb{1}, \gamma^5)\Psi = \bar{\Psi}P_L\Psi \pm \bar{\Psi}P_R\Psi = \psi\chi \mp \text{h.c.} \quad (5.3)$$

where we have written the Dirac spinor in terms of two-component left-handed Weyl spinors $\Psi = (\psi, \chi^\dagger)^T$, see e.g. [271]. Similarly, the spin-1 bilinears are

$$\bar{\Psi}\gamma^\mu(\mathbb{1}, \gamma^5)\Psi = \bar{\Psi}\gamma^\mu P_L\Psi \pm \bar{\Psi}\gamma^\mu P_R\Psi = \psi^\dagger\bar{\sigma}^\mu\psi \mp \chi^\dagger\bar{\sigma}^\mu\chi. \quad (5.4)$$

The γ^5 appears as a phase in the spin-0 coupling and a relative sign in the spin-1 couplings of opposite chirality fermions.

The phenomenology of the γ -ray excess suggests the use of both descriptions. DM annihilation and direct detection occur nonrelativistically so the choice of a scalar (vector) versus a pseudoscalar (axial) can dramatically affect the rate for these processes. It is thus useful to parameterize these in the language of (5.2), whether or not the DM interactions are chi-

Interaction	S (P)	V (A)	S (P)	V (A)	S (P)	V (A)
Partial Wave	p (s)	s (p/s)	p (p)	s (s)	p (s)	p (p)
On/Off-Shell	Off	Off	On	On	On	On
DM Mass [GeV]	≈ 40	≈ 40	≈ 80	≈ 80	≈ 120	≈ 120

Table 5.2: Annihilation to mediators. S,P,V,A correspond to scalar, pseudoscalar, vector, and axial vector interactions with DM. Also shown: the leading velocity (partial wave) dependence, whether the process may occur on-shell, and the approximate mass for 40 GeV final state b quarks. The off-shell axial coupling is s - or p -wave for axial/vectorlike SM coupling respectively [16].

ral. On the other hand, electroweak gauge invariance mandates chiral interactions for the mediator’s SM coupling.

We are thus led to consider a hybrid description where the mediator’s interaction with the SM is naturally described by a chiral coupling while the interaction with DM is most usefully described by a coupling of definite parity. The chiral description of the SM breaks down for direct detection; however, since chiral interactions generically include both the $\mathbb{1}$ and γ^5 terms, we focus on bounds from the parity-even interaction that yields stronger bounds. Dark matter searches at colliders probe relativistic energies without polarization information and are thus typically independent of parity. In this document we refer to the ‘spin-0’ or ‘pseudoscalar’ mediator to mean the spin-0 field which has a pseudoscalar interaction with the Dirac DM without assuming a particular parity-basis interaction to the SM.

5.2.2 Mediators Versus s-wave Annihilation

The parity basis for dark matter interactions clarifies the types of interactions that can yield s-wave annihilation for the γ -ray excess. In Table 5.2 we show annihilation modes to up to three spin-0 or spin-1 mediators for the interactions in (5.2). On-shell kinematics require at

least two final states so that the leading annihilation modes in the on-shell mediator limit are two spin-1 particles (of either parity) or three pseudoscalars. The off-shell diagrams represent the s -channel simplified models in [265, 266].

Also shown in Table 5.2 are the approximate masses for the on-shell mediator scenarios. In order to eject 40 GeV b quarks from each annihilation, the two (three) body final states require that the DM mass is approximately $m_\chi = 80$ (120) GeV. Observe that this mechanism allows one to circumvent the conventional wisdom that the galactic center signal requires DM lighter than typical electroweak scale states.

Note that these masses are back-of-the-envelope estimates that do not account for the boost in the b spectrum from the mediator momentum or the spread in mediator energies for the 3-body final state. Further, we assume only couplings to b . This is a reasonable estimate and does not violate flavor bounds for spin-0 mediators since it follows approximately from minimal flavor violation (MFV) [272, 273, 73, 144]. On the other hand, spin-1 mediators generically couple democratically to all three generations in the MFV ansatz, as can be seen when comparing (5.3) and (5.4). Finally, one should also account for the effect of the off-shell, s -channel annihilation modes for finite coupling to the SM, λ_{SM} . We account for these in Sec. 5.3 where we perform a fit to the γ -ray excess.

The amplitudes for annihilation to two spin-1 mediators via the vector and axial interactions are identical so in this case the choice of parity versus chirality basis is irrelevant. Of the spin-0 mediators, however, only pseudoscalars generate s -wave annihilation. If the dark sector is described by a chiral theory, one generically expects both parities to be present. However, since the scalar is p -wave, it is suppressed by $\langle v^2 \rangle \sim 10^{-6}$ and may be ignored for annihilation. On the other hand, this dramatically affects the direct detection rate, as discussed in Sec. 5.4.2.

5.2.3 Requirements for On-Shell Mediators

On-shell mediator models must satisfy the following conditions for the dark sector spectrum,

$$2m_\chi > \begin{cases} 2m_V & \text{for a spin-1 mediator} \\ 3m_\varphi & \text{for a spin-0 mediator} \end{cases} \quad (5.5a)$$

$$m_{V,\varphi} > 2m_b \quad (5.5b)$$

and the following requirements on the mediator couplings,

$$\lambda_{\text{DM}} \sim 1 \quad (5.5c)$$

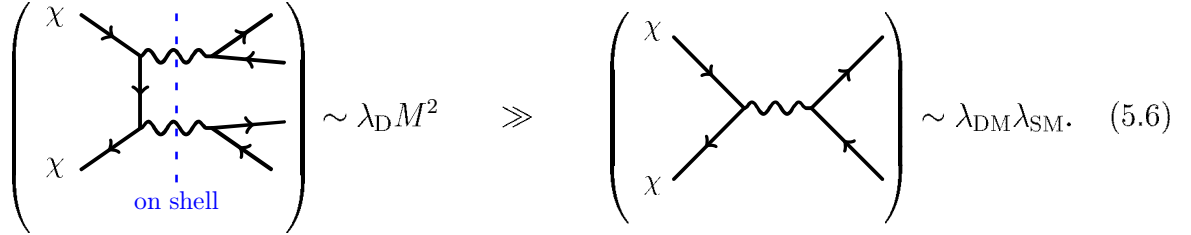
$$\lambda_{\text{SM}} \ll 1. \quad (5.5d)$$

These are interpreted as follows:

- (a) Nonrelativistic DM annihilation has enough energy to produce on-shell mediators.
- (b) The mediator may decay into b quarks to produce the spectrum of the γ -ray excess.
- (c) The additional coupling(s) in the on-shell diagrams do not suppress the amplitude nor are they so large that they are nonperturbative, $\lambda_{\text{DM}}^2 < 4\pi$.
- (d) Parametrically suppress the off-shell, s -channel mediator diagrams in annihilation and simultaneously ameliorate limits from direct detection and colliders.

We now elucidate the conditions (5.5c–5.5d) more carefully by determining the coupling scaling of the on-shell versus off-shell annihilations. For a spin-1 mediator, the on-shell annihilation mode goes through two on-shell mediators which subsequently decay into $b\bar{b}$ pairs. The key observation is that unlike the case of an off-shell s -channel mediator, the annihilation to on-shell mediators is largely independent of the coupling to the SM, λ_{SM} .

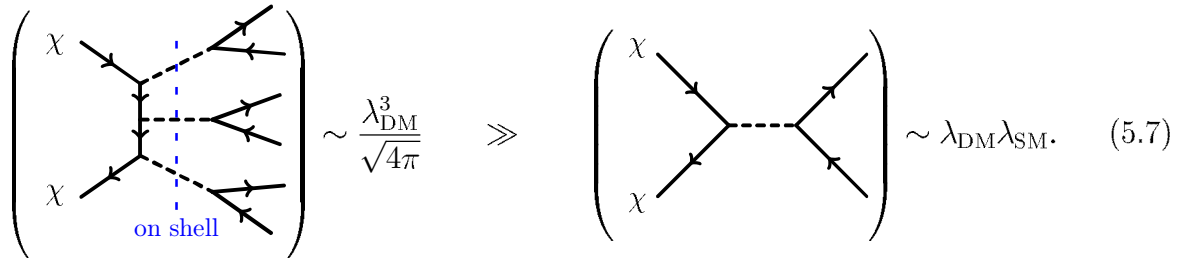
We thus focus on the limit where the on-shell mode dominates over the off-shell s -channel diagram,



$$\left(\begin{array}{c} \chi \\ \chi \end{array} \right) \sim \lambda_D M^2 \gg \left(\begin{array}{c} \chi \\ \chi \end{array} \right) \sim \lambda_{DM} \lambda_{SM}. \quad (5.6)$$

Note that this condition is trivial if the mediator has axial couplings since the s -channel diagram is p -wave. As discussed above, in a UV model that avoids flavor bounds, a spin-1 mediator is likely to couple democratically to other SM fermion generations. The annihilation rate relevant to the galactic center γ -ray excess would be multiplied by the branching ratio to $b\bar{b}$ pairs, $\text{Br}(V \rightarrow b\bar{b})$. If one insists that the γ -ray excess is generated exclusively by the decay of b quarks, then the branching ratio is an additional $\mathcal{O}(10^{-1})$ factor that must be compensated by λ_{DM} . More dangerously, one must also account for the γ -ray pollution from annihilations yielding light quarks. We address the effect of this pollution on the fit to the γ -ray spectrum in Sec. 5.6.1.

For a pseudoscalar mediator the analogous limit is



$$\left(\begin{array}{c} \chi \\ \chi \end{array} \right) \sim \frac{\lambda_{DM}^3}{\sqrt{4\pi}} \gg \left(\begin{array}{c} \chi \\ \chi \end{array} \right) \sim \lambda_{DM} \lambda_{SM}. \quad (5.7)$$

We have also inserted an explicit factor of $\sqrt{4\pi}$ for the additional phase space suppression in the cross section of a three- versus two-body final state.

Both (5.6) and (5.7) impose the limit $\lambda_{SM} \ll 1$ to suppress the s -channel off-shell mediator with λ_{DM} fixed (for given masses) to give the correct galactic center photon yield. The mag-

nitude of ‘ \gg ’ is addressed in Sec. 5.4. The limit of a very small coupling to the Standard Model is further motivated by the dearth of observational evidence for dark matter interactions at colliders and direct detection experiments. This limit also occurs naturally in models of dark photon kinetic mixing or compositeness. In our scenario, parametrically suppressing this coupling increases the lifetime of the mediator. This has little phenomenological consequence given the astronomical distance scales associated with the galactic center.

5.2.4 Estimates for the Gamma-ray Excess

Before doing a fit to the γ -ray excess, we establish a back-of-the-envelope benchmark using the DM masses in Table 5.2 and neglecting the mediator spectrum and boost. This gives a reasonable estimate while also highlighting the parametric behavior of the fit. The contact interaction fits to the galactic center γ -ray excess suggest annihilation to a pair of b quarks with a thermally averaged cross section [13],

$$\langle\sigma v\rangle_{b\bar{b}}\approx 5\times 10^{-26}\text{ cm}^3/\text{s}.\tag{5.8}$$

Note that [38] found a slightly smaller cross section, $1.5\times 10^{-26}\text{ cm}^3/\text{s}$ due to a slightly tighter DM halo (larger γ parameter in the generalized NFW profile [274, 275, 276]). The photon spectrum from this annihilation is

$$\frac{d\Phi(b,\ell)}{dE_\gamma}=\frac{\langle\sigma v\rangle_{b\bar{b}}}{2}\frac{1}{4\pi m_\chi^2}\frac{dN_\gamma}{dE_\gamma}\int_{\text{LOS}}dx\rho^2(r_{\text{gal}}(b,\ell,x)),\tag{5.9}$$

where (b,ℓ) are Galactic coordinates, ρ is the DM profile, and r_{gal} is the distance from the galactic center along the line of sight (LOS).

In on-shell mediator models, the DM annihilates into 2 (3) mediators which each decay into pairs of b quarks. In order that each of these final state b quarks to carry 40 GeV, the DM

mass must be approximately 80 (120) GeV as stated in Table 5.2. This reduces the DM number density by 4 (9) in order to maintain the observed mass density; this is manifested in the $m_{\bar{\chi}}^{-2}$ factor of (5.9). This factor is partially compensated by the multiplicity of $b\bar{b}$ pairs in the final state increases the total secondary photon flux by a factor of 2 (3). Together, these effects require that the annihilation cross section is a factor of ≈ 2 (3) times larger than $\chi\bar{\chi} \rightarrow b\bar{b}$ cross section (5.8),

$$\langle\sigma v\rangle_{\text{ann.}} \approx 2 (3) \times \langle\sigma v\rangle_{b\bar{b}}. \quad (5.10)$$

where $\langle\sigma v\rangle_{b\bar{b}}$ is the contact interaction value (5.8). Because $\langle\sigma v\rangle_{b\bar{b}}$ is already determined to be close to the thermal relic, one may worry if the additional factor in (5.10) violates the feasibility of a thermal relic. We address this in Sec. 5.5. Considering the range of kinematically allowed mediator masses and accounting for the powers of λ_{DM} in the spin-0 and spin-1 cases, (5.10) gives the estimate

$$\lambda_{\text{DM}} M \sim 1.1 - 1.4 \quad (\text{spin-0}) \quad (5.11)$$

$$\lambda_{\text{DM}} M \sim 0.27 - 0.44. \quad (\text{spin-1}) \quad (5.12)$$

These couplings indeed agree with the estimate (5.5c) while remaining perturbative, $\lambda_{\text{DM}}^2 < 4\pi$. The scale of the spin-1 coupling implies a slight suppression on the left-hand side of (5.6) which must be compensated by a stronger upper bound on λ_{SM} . We show below that direct detection also constraints λ_{SM} strongly for the spin-1 mediator.

5.3 The Gamma-Ray Excess from On-Shell Mediators

Having established the intuition developed in Sec. 5.2.4, we examine the photon spectrum predicted from the on-shell mediator scenario and fit to the observed γ -ray excess.

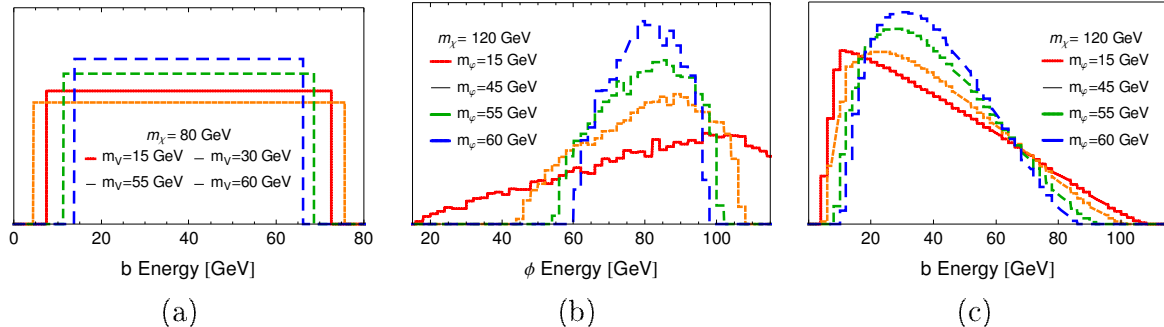


Figure 5.4: (a) $\chi\bar{\chi} \rightarrow VV \rightarrow 4b$, (b) $\chi\bar{\chi} \rightarrow 3\phi$, (c) $\chi\bar{\chi} \rightarrow 3\phi \rightarrow 6b$. Energy spectrum with arbitrary normalization from DM annihilation for (a) b quarks from two on-shell spin-1 mediators, (b) pseudoscalar mediators, (c) b quarks from three on-shell pseudoscalar mediators. (a) corresponds to $m_\chi = 80$ GeV while (b,c) corresponds to $m_\chi = 120$. Lines correspond to $m_V = 15, 30, 55, 60$ GeV or $m_\phi = 15, 45, 55, 60$ GeV from red (solid) to blue (most dashed). The ‘box’ width in (a) is not monotonically decreasing with m_V , as evidenced by the 30 GeV line (orange).

5.3.1 Mediator Spectra

In 2-to-2 scattering, the final state energies is completely determined by kinematics. This is the case for $\chi\bar{\chi} \rightarrow b\bar{b}$ from effective contact interactions or simplified models with single off-shell mediators; the monochromatic spectrum of final state b quarks yield, upon showering, a spectrum of photons which fits the observed γ -ray excess well. In the case of annihilation to on-shell mediators, however, the b quark spectrum is no longer monochromatic, as shown in Figure 5.4.

For spin-1 mediators, it is well known that the final states of a $\chi\bar{\chi} \rightarrow VV \rightarrow 4b$ cascade has box-like energy spectrum over the kinematically allowed range; see, for example, [277, 278]. The V spectrum is monochromatic in the lab frame and the $b\bar{b}$ spectrum is monochromatic in the V rest frame. The b energies in the lab frame depend on the angle of the $b\bar{b}$ axis relative to the direction of the V boost. Isotropy of the V boost washes out the angular dependence and gives a flat b spectrum over the kinematically allowed region. This is demonstrated in Fig. 5.4(a). The box becomes more sharply peaked as $m_V \rightarrow m_\chi = 40$ GeV. The case of annihilation into three spin-0 mediators is more complicated since the mediators

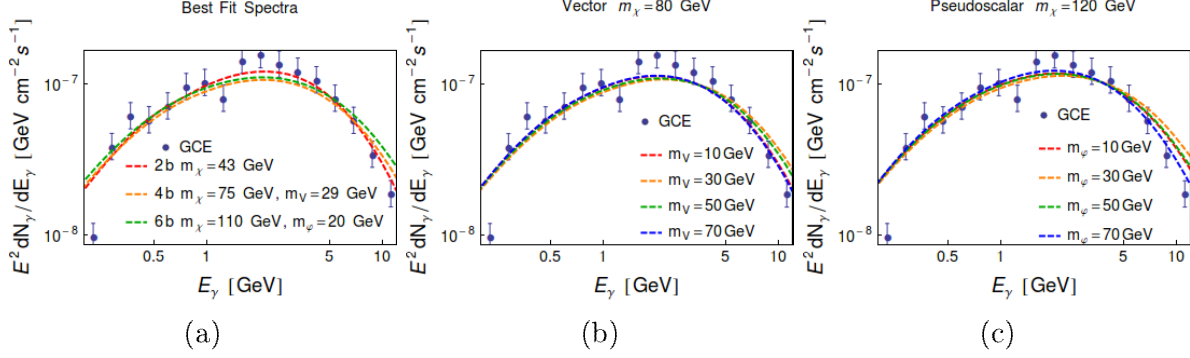


Figure 5.5: (a) Comparison, (b) Spin-1, (c) Spin-0. Predicted spectra for the galactic center γ -ray excess (GCE) for (a) the best fit models categorized by the number of final state b quarks, (b) a range of spin-1 mediator masses, (c) a range of spin-0 mediator masses. Overlaid is the measured γ -ray spectrum from [13], bars demonstrate an arbitrary measure of goodness-of-fit. See Sec. 5.3.3 for details.

have a nontrivial energy spectrum and it is no longer simple to derive the b spectrum from kinematics alone. Monte Carlo energy spectra for $\chi\bar{\chi} \rightarrow 3\varphi$ and the subsequent decay in to $6b$ are shown in Fig. 5.4(b,c) using MadGraph 5 [179].

5.3.2 Generating Gamma-Ray Spectra

γ -ray spectra for our simplified models are generated using PPPC 4 DM ID (henceforth PPPC) [279, 280], a *Mathematica* [281] package that generates indirect detection spectra based on data extracted from PYTHIA 8 [282]. Presently, PPPC only generates signals for DM annihilation into pairs of SM particles. In order to include the effects of the on-shell mediators, one must account for the boost by convolving the PPPC photon spectrum $dN_\gamma(E_b)/dE_\gamma$ with a distribution of b energies E_b which may be taken as a box for the case of two on-shell mediators or interpolated from Monte Carlo simulations such as Fig. 5.4(c).

For on-shell annihilation into spin-0 and spin-1 mediators, the shape of the photon spectrum is completely determined by the masses of the DM particle m_χ and the mediator $m_{\varphi,V}$ while the overall normalization is fit to the necessary cross section by fixing λ_{DM} , as estimated

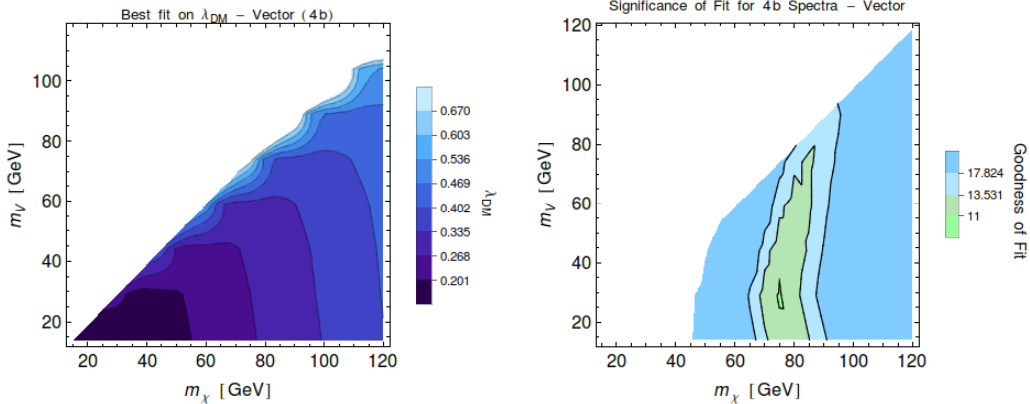


Figure 5.6: Fits for on-shell annihilation through spin-1 mediators. LEFT: best fit values of λ_{DM} . RIGHT: fit significance highlighting the best $(m_\chi, m_{\text{med.}})$ values. See text for details.

in (5.11 – 5.12). The effect of the mediator mass is fairly modest, as demonstrated in the $E_\gamma^2 dN_\gamma/dE_\gamma$ spectra in Fig. 5.5. The reason for this is that the requirement that the mediator is massive enough to decay into $b\bar{b}$ pairs (5.5d) limits the extent to which the mediators are boosted.

5.3.3 Fitting the Gamma-Ray Excess

We use the $\chi\bar{\chi} \rightarrow b\bar{b}$ γ -ray excess spectrum assuming a $\chi\bar{\chi} \rightarrow b\bar{b}$ template from Figure 8 of [13]. We note, however, that this is an approximation since the on-shell mediator scenario predicts a different spectral shape that, in principle, should be modeled and included in the fit for the γ -ray excess. The comparison of the best fit $\chi\bar{\chi} \rightarrow 2b$ spectrum versus the on-shell mediator spectra in Fig. 5.5(a) qualitatively demonstrates the degree of approximation.

Indeed, [13] showed how the spectrum of the excess (though not its existence) can depend on both the background subtraction and the choice of DM template assumed in the fit. This highlights a second caveat when building DM models for the γ -ray excess. As is standard in astrophysics literature, [13] and [38] only quote statistical errors on their fits since the systematic errors associated with fitting and subtracting background is nontrivial and in-

tractable to quantify. Both [13] and [38] make this clear in their text. Model builders from the particle physics community, however, should be careful not to interpret these statistical uncertainties in the same way as quoted uncertainties from collider data, where both statistical and systematic errors are included. [13] demonstrated some of the systematic uncertainties by exploring the differences in the spectral fits from different background subtraction. Further still, both [13] and [38] use the FERMI collaboration’s 2FGL point sources and recommended diffuse emission model `gal_2yearp7v6_v0`. These assumptions also carry an implicit systematic uncertainty that are difficult to quantify without further input from the FERMI collaboration.

That being said, one can see from the $1\sigma_{\text{stat.}}$ error bars in Fig. 5 of [38] that even just the statistical errors on the γ -ray excess can accommodate modified spectra. Combined with the estimated systematic errors in Figure 8 of [13] and additional systematic errors from the FERMI background, this suggests that more general final states beyond the standard $b\bar{b}$ and $\tau\bar{\tau}$ should be considered for the γ -ray excess. In Appendix 5.9 we present simple explorations for the range of spectra that can be generated in the on-shell mediator scenario.

Because of the unquantified systematic error associated with these spectra, we do not parameterize the statistical significance of our fits in terms of confidence intervals. Instead, we measure the goodness of fit using the χ^2 value with an arbitrarily chosen 20% error,

$$\text{goodness of fit} = \sum_i \left(\frac{\log D_i - \log(\lambda_{DM}^{2n} S_i)}{\log(0.2D_i)} \right)^2. \quad (5.13)$$

Smaller values are better fits. The index i runs over the bins in the extended source data set, D and S are the $E_\gamma^2 \frac{dN_\gamma}{dE_\gamma}$ values for the extended source data and the model spectra (assuming $\lambda_D M = 1$) respectively, and λ_{DM}^{2n} is the overall normalization of our input spectra, where $n = 2, 3$ is the number of on-shell mediators produced in each annihilation. The denominator reflects the assumed 20% error: we emphasize that this is not a statement about the total

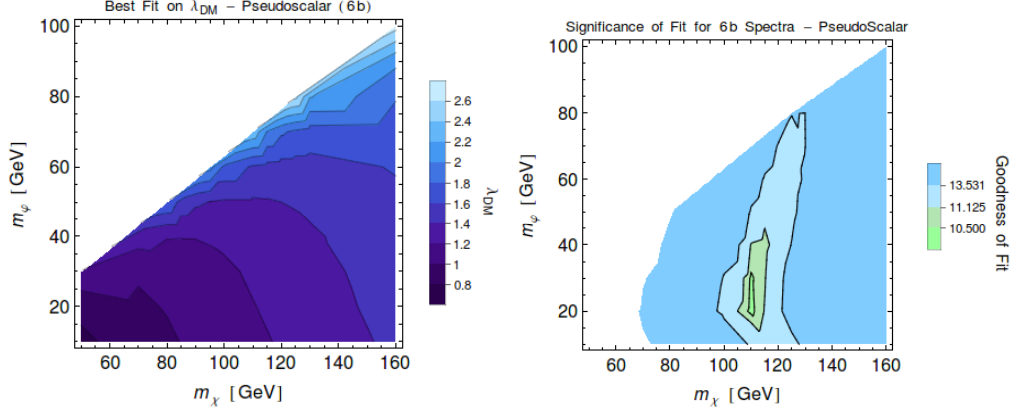


Figure 5.7: Fits for on-shell annihilation through spin-0 mediators. LEFT: best fit values of λ_{DM} . RIGHT: fit significance highlighting the best $(m_\chi, m_{\text{med.}})$ values. See text for details.

error, but rather a standard candle for quantifying the goodness-of-fit. This is shown as a bar on the data in Fig. 5.5.

In Figs. 5.6 and 5.7 we fit the spectral shape over the region of DM and mediator masses, m_χ and $m_{\text{med.}}$, estimated in Table 5.2 and (5.5a – 5.5b). The DM coupling λ_{DM} parameterizes the overall normalization and is fixed to minimize (5.13) for each value of m_χ and $m_{\text{med.}}$. The best fit values prefer a slightly lighter DM particle than the back-of-the envelope estimates in in Table 5.2 due to the on-shell mediator smearing the b spectrum. The fits are flexible over the range of mediator masses within the kinematically accessible region, as seen in Fig. 5.5(b,c). We note that these plots assume the limit of vanishing SM coupling, $\lambda_{\text{SM}} \rightarrow 0$, so that the contribution to the γ -ray spectrum from $\chi\bar{\chi} \rightarrow b\bar{b}$ via s -channel, off-shell mediators is negligible. We explore the role of finite λ_{SM} in Sec. 5.4.1. We also note that the simplest models spin-1 mediators typically have universal couplings to all quark generations; we address this in Sec. 5.6.1 and display the modified results in Fig. 5.10.

5.4 Experimental Bounds on the SM Coupling

One of the features of the on-shell mediator scenario is that the γ -ray excess annihilation mode is controlled by parameters that can be independent of the conventional experimental probes for DM–SM interactions. Following the complementarity in Fig. 5.2, we examine the effect of non-negligible mediator coupling to the SM and determine the bounds on λ_{SM} .

In contrast to effective contact interactions or models with off-shell mediators, the on-shell mediator scenario naturally includes the limit of extremely small SM coupling so that it is always possible to parametrically ‘hide’ from these bounds. In principle, one may invoke the morphology of the γ -ray excess to set a lower bound on the mediator coupling. For example, if the mediator decay were too suppressed, the observed γ -ray excess would have a spatial extent larger than the galactic center. In fact, the DM interpretations in [190, 38] found that the excess has a tighter profile ($\gamma > 1$) than the standard NFW DM density profile [274, 275, 276]. This lower bound on λ_{SM} is effectively irrelevant because of the astronomical distances associated with the galactic center.

5.4.1 Indirect Detection

In Sec. 5.3 we assumed that the contribution of s -channel diagrams to DM annihilation is negligible following (5.6 – 5.7). We can use the arbitrarily normalized goodness-of-fit measure (5.13) to assess the effect of these diagrams on the γ -ray excess fit as we parametrically increase λ_{SM} . We assume that the mediator couplings are such that the s -channel diagram supports s -wave annihilation, otherwise the contribution is negligible due to p -wave suppression by $\langle v^2 \rangle \sim 10^{-6}$. From Table 5.2, we see that non-negligible s -channel contributions may come from mediators with either pseudoscalar or vector coupling to the SM. For example, V could couple axially to both DM and the SM with a large s -channel contribution for finite

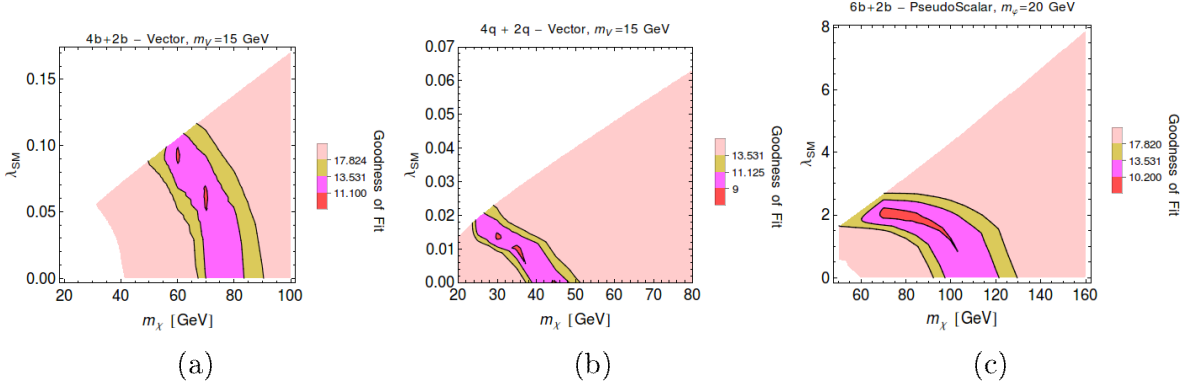


Figure 5.8: (a) Spin-1 (b -philic), (b) Spin-1 (q -democratic), (c) Spin-0. Fits including s -channel diagrams to the case of a (a) spin-1 mediator coupling only to b , (b) spin-1 mediator coupling to all quarks equally, and (c) pseudoscalar mediator. Plots assume that the s -channel diagrams are s -wave, see Tab. 5.2. Smaller values correspond to better fits, see (5.13).

λ_{SM} . On the other hand, if V couples axially to DM and vectorially to the SM, then there may be little modification to the annihilation spectrum from s -channel diagrams even for large values of λ_{SM} .

We scan over values of λ_{SM} that parametrically increases the relative fraction of s -channel off-shell DM annihilations to on-shell annihilations to mediators⁵, allowing λ_{DM} and the mediator mass to float to a best-fit value. The results of the fit are shown in Fig. 5.8, where the best fit regions have smeared into lower DM masses compared to Fig. 5.6. The s -channel contribution produces γ -ray spectrum which is a poor fit due to the larger DM mass in the on-shell mediator limit. However, because the γ -ray spectrum is smeared out relative to the b spectrum, there are intermediate masses m_χ where the harder-than-usual s -channel diagram and the softer-than-usual on-shell mediator diagram average to yield good spectral fits. From the point of view of constructing DM models for the γ -ray excess, this shows that not only can the DM particle be as heavy as 80 or 120 GeV, as shown in Sec. 5.2, but it can take on intermediate values between these values and $m_\chi \approx 40$ GeV. We further generalize

⁵ Note from (5.6 – 5.7) that the relative ratio of s -channel diagrams to on-shell mediator diagrams is determined not simply by λ_{SM} , but a ratio of λ_{SM} to a power of λ_{DM} depending on the type of mediator.

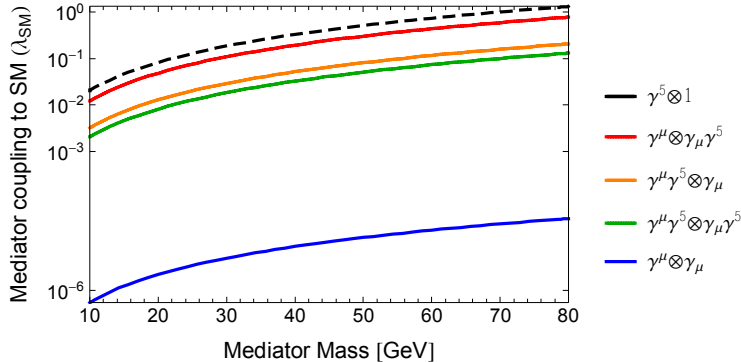


Figure 5.9: Estimated direct detection bounds on the mediator–SM coupling (λ_{SM}) for interactions $\mathcal{O}_\chi \otimes \mathcal{O}_q$ defined in (5.1). The dashed (solid) lines assume the benchmark value $m_\chi = 120$ (80) GeV for spin-0 (1) mediators and the median DM couplings in (5.11–5.12).

this in Appendix 5.9 where we find plausible fits with $m_\chi < 40$ GeV, and propose a simple mechanism to make $m_\chi > 120$ GeV.

We note that in this scenario, indirect detection bounds from cosmic antiprotons can constrain λ_{DM} . Current constraints from the PAMELA are not sensitive to the rates required in our model, though AMS-02 will access this region [283, 284]⁶.

5.4.2 Direct Detection

Unlike the other experimental options in Fig. 5.2, direct detection experiments probe WIMP–nucleon interactions at low transfer momentum, $q^2 \sim \mathcal{O}(10 \text{ MeV})$, and are accurately described in the contact interaction limit with corrections of order $\mathcal{O}(q^2/m_{\text{med}}^2) \ll 1$. The present experimental bounds on the spin-independent (SI) and spin-dependent (SD) interactions in the DM mass region of interest are set by the LUX [30] and XENON 100 [29] collaborations, respectively:

$$\sigma_{\text{SI}} \lesssim 10^{-45} \text{ cm}^2 \qquad \sigma_{\text{SD}} \lesssim 5 \times 10^{-40} \text{ cm}^2. \qquad (5.14)$$

⁶We thank KC Kong for pointing this out. See Fig. 2 and Fig. 4 of [283] for the relevant bounds, recalling (5.10) for our model. Note, however the large propagation uncertainties in Fig. 2.

In Fig. 5.9 we apply these bounds to the contact interactions in (5.1) with the identification $\Lambda^{-2} = \lambda_{\text{SM}}\lambda_{\text{DM}}/m_{\text{med.}}^2$. We use the benchmark parameters in Section 5.2.4 with the fact that the spin-0 mediator couple only to b quarks while the spin-1 mediator couples universally to all quarks.

In addition to the conventional spin-independent ($\gamma^\mu \otimes \gamma_\mu$) and spin-dependent ($\gamma^\mu \gamma^5 \otimes \gamma_\mu \gamma^5$) interactions, we present bounds on the axial-vector ($\gamma^\mu \gamma^5 \otimes \gamma_\mu$) and vector-axial ($\gamma^\mu \otimes \gamma_\mu \gamma^5$) interactions for a spin-1 mediator. These are suppressed by virtue of being higher order in the transfer momentum/DM velocity; we estimate these bounds following [224]. If the spin-1 mediator couples only to b quarks, the bound on λ_{SM} is weakened because interactions with target nucleons go through a b -quark loop that induces mixing between the mediator and the photon [266, 285].

As discussed in Sections 5.2.1 and 5.2.2, we only consider spin-0 mediators that couple as a pseudoscalar to DM. We do not include the $\gamma^5 \otimes \gamma^5$ operator since it is so suppressed by powers of the momentum transfer that the bounds on λ_{SM} are weaker than the perturbativity bound $\lambda_{\text{SM}} < \sqrt{4\pi}$. We evaluate momentum-dependent operators at $q^2 = 0.1 \text{ GeV}$ following [224]. These direct detection rates can be calculated in more detail using the nonrelativistic effective theory developed in [69, 222, 227]. Operator bounds in this formalism are presented in [286, 287] and *Mathematica* codes for these calculations are available in [287] and [223].

5.4.3 Collider bounds

The collider bounds for this class of models falls into two types: those based on processes where the mediator couples to both the SM and DM and those that only depend on the mediator's coupling to the SM.

The first type of collider bounds are epitomized by mono-object searchers with missing energy

where the DM leaves the collider. These bounds are discussed extensively in the γ -ray [off-shell, s -channel] simplified models [38, 266]. We thus only highlight the most promising proposed bound, the ‘mono- b ’ search [181]. Because of the requirement (5.5c) of on-shell annihilation into mediators, the class of models explored in this paper typically falls in the range where the effective contact interaction description breaks down [53, 230, 231, 232, 233]. We leave a detailed simplified model study for future work, but instead translate the projected scalar–scalar ($\mathbb{1} \otimes \mathbb{1}$) contact interaction bounds in [181] as a conservative estimate for the reach of this search. Over the range of dark matter masses $m_\chi \lesssim 150$ GeV, the projected bound from 8 TeV LHC data is approximately

$$M_* > 100 \text{ GeV} \quad \Rightarrow \quad \lambda_{\text{SM}}^{\text{spin-0}} \lesssim 0.2, \quad \lambda_{\text{SM}}^{\text{spin-1}} \lesssim 0.6, \quad (5.15)$$

where M_* parameterizes the scalar–scalar contact interaction,

$$\frac{m_q}{M_*^3} (\bar{\chi}\chi) (\bar{q}q). \quad (5.16)$$

To estimate this bound, we have matched this to $\lambda_{\text{SM}}\lambda_{\text{DM}}s^{-1} (\bar{\chi}\chi) (\bar{q}q)$, where we have taken $s = 225$ GeV, the cut on the minimum missing energy in [181]. We have estimated that the spin-1 bound on M_* is identical and used the smaller λ_{DM} value (5.12). Note that at high energies the distinction between operators with and without a γ^5 in the parity basis is negligible. The bound (5.15) is thus fairly robust; unlike the direct detection bounds, a judicious choice of operator cannot avoid the constraints from this search.

A second class of collider bound comes from a search for the signatures of the mediator interacting only with the SM sector. The bounds from this type of search are relatively weak in the mediator mass range of interest (15 – 70 GeV) because of large QCD backgrounds in bump searches (dijet, $4b$); see, for example, [288]. Because our only requirement is that the mediator couple to b quarks (and other quarks as mandated by MFV, for example),

a prototype for the mediator is a Z' that gauges baryon number $U(1)_B$. This has been examined originally in [289, 290] where the most stringent bounds come from the hadronic width of the Z which sets a relatively weak bound

$$\lambda_{\text{SM}} \lesssim 1. \tag{5.17}$$

This bound becomes stronger in the neighborhood of the Υ mass, but this is already at the edge of what is kinematically allowed for decay into b pairs (5.5d). See also [291] for a review including loop-level constraints from mixing and [292] for discussion of bounds combined with anomaly constraints. Another prototype for the spin-0 mediator is a gauge-phobic, leptophobic Higgs. There exist very few bounds for such an object in the mass range of interest. A preliminary estimate for the reach of a ‘Higgs’ diphoton search between 50 – 80 GeV ATLAS detector with 20/fb found weaker constraints than (5.17) [293].

5.5 Viability as a Thermal Relic

One of the appealing features of the simplest $\chi\bar{\chi} \rightarrow b\bar{b}$ mode is that the required annihilation cross section (5.8) is so close to the value required for a thermal relic. Due to the scaling in (5.9), the s -wave annihilation cross section for the on-shell mediator scenario is a factor of n larger than the thermal value where $n = 2, 3$ is the number of mediators emitted, (5.10). This comes from a factor of n enhancement due to the number of $b\bar{b}$ final states and a factor of n^2 suppression coming from a decreased DM number density. We examine the extent to which our scenario may still furnish a standard thermal relic. Observe that this sector of the model no longer has free parameters since the γ -ray excess fixes both the dark matter mass m_χ and coupling λ_{DM} .

5.5.1 s-wave Cross Section

For simplicity, let us first assume that DM annihilation at freeze-out is dominated by the same diagrams that generate the galactic center γ -ray excess at the present time. We address s -channel and p -wave corrections below. The observed Dirac DM density $\Omega_\chi h^2$ is approximately⁷ [295]

$$\Omega_\chi h^2 \approx \frac{6 \times 10^{-27} \text{ cm}^3/s}{\langle \sigma v \rangle_{\text{ann.}}} \quad (\Omega_\chi h^2)_{\text{obs.}} = 0.12 \quad [296, 297, 298] \quad (5.18)$$

where h is the Hubble constant in units of $100 \text{ km}/(\text{s} \cdot \text{Mpc})$. From (5.10), the annihilation cross section is $\langle \sigma v \rangle_{\text{ann.}} \approx n(5 \times 10^{-26} \text{ cm}^3/s)$, where $n = 2$ or 3 depending on the mediator. At face value, this gives a relic abundance that is too small. One may not mitigate this by assuming another DM component since this, in turn, reduces the galactic center signal and hence requires one to increase the annihilation cross section further.

While the value of $\Omega_\chi h^2$ is well measured, the precise value of the annihilation cross section $\langle \sigma v \rangle_{\text{ann.}}$ at freeze-out carries uncertainties from early universe parameters such as the number of effective degrees of freedom. On top of this, there are further uncertainties in our approximation (5.10) coming from uncertainties in astrophysical parameters. For example, the $\chi\bar{\chi} \rightarrow b\bar{b}$ annihilation cross section (5.8) depends on the fit to the dark matter density profile at the center of the galaxy [299]. The analysis in [38] found a tighter density profile for which $\langle \sigma v \rangle_{b\bar{b}} \approx 1.5 \times 10^{-26} \text{ cm}^3/c$. The value of $\langle \sigma v \rangle_{\text{ann.}}$ spin-1 mediators ($n = 2$) required for a thermal relic falls between these two estimates of $\langle \sigma v \rangle_{b\bar{b}}$. We may thus assume that it is consistent with the galactic center signal within the uncertainty of the DM morphology. In fact, when the boost from the on-shell mediator is taken into account, the best fit DM mass is slightly smaller than the assumed 80 GeV in our estimate. This can push the estimated relic abundance from $\Omega_\chi h^2 = 0.10$ to 0.12 so that the case of a spin-1 mediator may

⁷The thermal cross section for Dirac DM is a factor of 2 larger than Majorana DM [294].

plausibly yield the correct thermal relic abundance. On the other hand, it is difficult for a spin-0 mediator to satisfy the observed DM relic abundance and seems to require additional mechanisms to produce $\Omega_\chi h^2$.

5.5.2 s -channel and p -wave Corrections

The corrections to the above estimates include s -channel $\chi\bar{\chi} \rightarrow b\bar{b}$ diagrams and p -wave corrections from additional on-shell mediator diagrams. The s -channel modes are parametrically suppressed by $\lambda_{\text{SM}}^2 \ll 1$ in the cross section and can be ignored.

Corrections from p -wave diagrams are negligible for present day annihilation in the galactic center due to a large velocity suppression. At the time of DM freeze-out, on the other hand, this velocity suppression is much weaker and one should check for p -wave corrections to the relic abundance. For spin-1 mediators there are no additional diagrams which are not suppressed relative to the $\chi\bar{\chi} \rightarrow VV$ s -wave diagram. For pseudoscalars mediators, on the other hand, the $\chi\bar{\chi} \rightarrow 2\varphi$ mode is p -wave but not parametrically suppressed by λ_{SM} . At freeze-out these diagrams may contribute appreciably to DM annihilation,

$$\left(\begin{array}{c} \chi \\ \chi \\ \text{on shell} \end{array} \right) \sim \frac{\lambda_{\text{DM}}}{\sqrt{4\pi}} \sqrt{\frac{x_f}{3}} \left(\begin{array}{c} \chi \\ \chi \\ \text{on shell} \end{array} \right). \quad (5.19)$$

The prefactor accounts for the additional phase space and p -wave suppression. The ratio of the DM mass to the freeze-out temperature $x_f = m_\chi/T_f \approx 20$ appears when thermally averaging the annihilation cross section at freeze-out over a Maxwell–Boltzmann velocity distribution. This factor is not especially large and so one expects the pseudoscalar annihilation cross section at freeze-out to be even larger than approximated with only the s -wave

piece. This further reinforces the observation that this class of mediator requires additional mechanisms to attain the observed DM relic density. See [300, 301, 302, 303, 304, 305, 306, 307, 308, 309, 310, 311, 312, 313, 314, 315, 316, 317, 318] for a partial list of model-building tools for obtaining the correct relic abundance without the standard freeze-out mechanism.

5.5.3 MSPs Can Save Freeze-Out

As noted in the Introduction, [190, 169, 319, 192, 13, 205] have pointed out that an alternate source for the γ -ray excess is a population of hitherto unobserved millisecond pulsars (MSPs). As an estimate, a few thousand MSPs could generate the observed γ -ray flux [13]. A recent study of low-mass X-ray binaries (LMXB) may lend credence to this argument. It is thought that MSPs are old pulsars that have been spun up ‘reborn’ due to mass accretion from a binary companion and that LMXB are simply a different phase of the same binary system. During accretion, the system is X-ray luminous and is categorized as an LMXB. The X-ray flux drops when the accretion rate drops and the system is then observed as a MSP. One can thus attempt to use the spatial distribution of the LMXB as a proxy for that of MSPs. [320] found that the spatial morphology of the LMXB in M31 is consistent with both the γ -ray excess and the DM interpretation—thus making it difficult to distinguish the two [206].

This, however, can be a boon for model-building within our DM framework. [190] noted that the degeneracy between the MSP and DM interpretations of the excess suggests that the excess may come from a combination of the two sources. In this way one may take the DM annihilation cross section to be that which is required for a thermal relic—thus undershooting the expected γ -ray flux—and then posit that a MSP population accounts for the remainder of the γ -ray excess.

5.5.4 Conditions for Thermal Equilibrium

In order for the thermal freeze-out calculation for χ to be valid, we must assume that the mediator is in thermal equilibrium when the DM freezes out. This imposes a lower bound on the coupling of the mediator to the SM. In principle one must solve the Boltzmann equation for the mediator, but to good approximation it is sufficient to impose $H \ll \Gamma(\text{med} \rightarrow b\bar{b})$. For the range of mediators that can give the γ -ray excess, this imposes a very modest lower bound $\lambda_{\text{SM}} \gtrsim 10^{-9}$.

5.6 Comments on UV Completions and Model Building

Simplified models, such as those presented here, are bridges between experimental data and explicit UV models. In this section we highlight connections between our on-shell simplified models and viable UV completions.

5.6.1 Minimal Flavor Violation

The simplified models constructed in Section 5.2 couple the mediator only to b quarks to fit to the galactic center extended γ -ray source. Assuming only this coupling violates flavor symmetry and can lead to strong constraints from flavor-changing neutral currents. A standard approach to this issue in models of new physics is to impose the minimal flavor violation (MFV) ansatz where the Yukawa matrices are the only flavor spurions in the new physics sector [272, 273, 73, 144]. This prescribes a set of relative couplings to the SM fermions up to overall prefactors. We assume that the dark sector is flavor neutral, see [321, 203, 322] for models with nontrivial flavor charge.

For the pseudoscalar mediator this is a small correction as can be seen by writing out the

flavor indices in the spin-0 fermion bilinears (5.3) by which the pseudoscalar couples to the quarks. MFV mandates insertions of the Yukawa matrices between couplings of right- and left-handed fermions. After rotating to mass eigenstates this yields mediator–SM interactions

$$\mathcal{L}_{\varphi\text{-SM}} = \lambda_u \frac{m_{u_i}}{\Lambda} \varphi \bar{u}_{Li} u_{Ri} + \lambda_d \frac{m_{d_i}}{\Lambda} \varphi \bar{d}_{Li} d_{Ri} + \lambda_\ell \frac{m_{\ell_i}}{\Lambda} \varphi \bar{\ell}_{Li} \ell_{Ri}, \quad (5.20)$$

where $q_{L,R} = P_{L,R} q$, the $\lambda_{u,d,\ell}$ are overall prefactors, and Λ is a UV flavor scale. Assuming that the $\lambda_{u,d,\ell}$ are the same order naturally sets the dominant φ decay mode to be $b\bar{b}$ since the $t\bar{t}$ mode is kinematically inaccessible for the range of masses we consider. The simplified model coupling to b quarks is thus identified as

$$\lambda_{\text{SM}} = \lambda_d \frac{m_b}{\Lambda}. \quad (5.21)$$

The results of the simplified model above should be adjusted by including the effects of the other φ decay modes, though these effects are suppressed by the relative size of the other fermion masses to m_b . We remark that modest to large values of λ_u can lead to new signatures such as mediator emission off of a top quark at the LHC or gluon couplings through top loops.

The spin-1 mediators couple fermions of the same chirality, as demonstrated in (5.4). Promoting these interactions to an MFV-compliant coupling does not introduce additional factors of the Yukawa matrices since each term is a flavor singlet. Thus, unless the UV model is specifically constructed so that the spin-1 mediator couples preferentially to b quarks, the generic expectation is the spin-1 mediators have a universal coupling to each generation, for example

$$(\lambda_{\text{SM}})_d = (\lambda_{\text{SM}})_s = (\lambda_{\text{SM}})_b, \quad (5.22)$$

and similarly for the up-type quarks, leptons, and neutrinos. Unlike the case of the pseu-

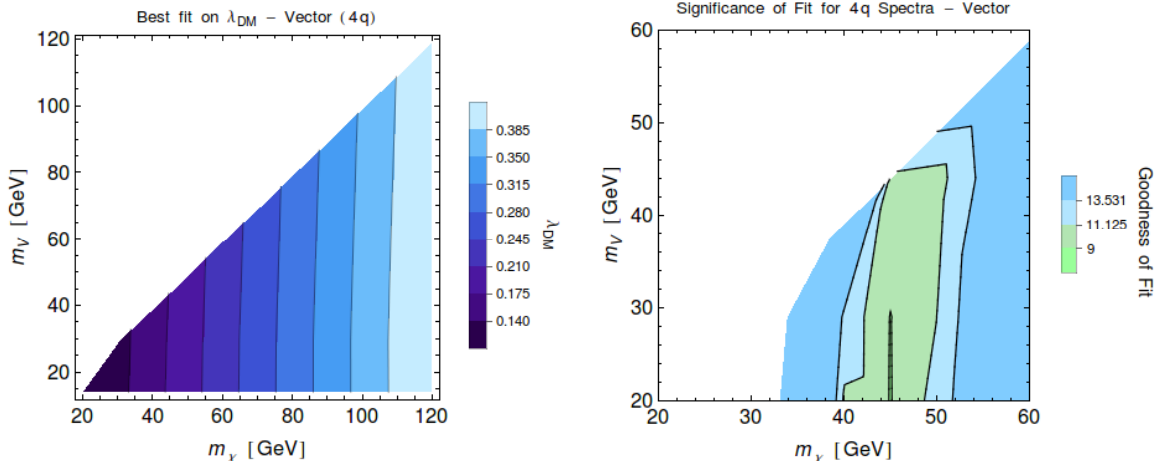


Figure 5.10: Fits for on-shell annihilation through spin-1 mediators assuming universal coupling to all quarks; compare to Fig. 5.6 which assumed a coupling to only b quarks. LEFT: best fit values of λ_{DM} . RIGHT: fit significance highlighting the best $(m_\chi, m_{\text{med.}})$ values. See Section 5.3.3 for details.

doscalar mediator, this can lead to dramatic modifications since the light quarks produce a softer spectrum of secondary photons relative to the b . This is demonstrated in Fig. 5.10 which shows that the best fit spectrum is very different from that of the case where the spin-1 mediator only couples to the b : the best fit DM mass is ≈ 45 GeV rather than ≈ 75 GeV.

As a caveat, we note that for fitting the γ -ray excess with either spin-0 or spin-1 mediators, it is sufficient that λ_d is nonzero. Thus, in principle, one can set λ_u and λ_ℓ to vanish; the latter condition suppresses the leptonic signals for the mediator at colliders and skirts the most stringent constraints on bosons in the on-shell mediator mass range (5.5a – 5.5b).

5.6.2 Gauge symmetries

Gauge invariance also constrains UV completions of these simplified models. Because the SM fermions are chiral, the parity basis spin-0 interactions on the left-hand side of (5.3) are not $\text{SU}(2)_L \times \text{U}(1)_Y$ gauge invariant. The similarity of (5.20) to the Yukawa coupling gives

a hint for how to make this interaction SM gauge invariant. The $m_b \bar{b}_R b_L$ term is implicitly $y_b (v/\sqrt{2}) \bar{b}_R b_L$, where v is the Higgs vacuum expectation value. We may promote this to a gauge invariant coupling by restoring the Higgs doublet H so that (5.20) becomes

$$\mathcal{L}_{\varphi\text{-SM}} = \frac{\lambda_u y_{ij}^u}{\Lambda} \varphi H \cdot \bar{Q} u_R + \frac{\lambda_d y_{ij}^d}{\Lambda} \varphi \tilde{H} \cdot \bar{Q} d_R + \frac{\lambda_\ell y_{ij}^\ell}{\Lambda} \varphi \tilde{H} \cdot \bar{L} \ell_R, \quad (5.23)$$

where $\tilde{H} = i\sigma^2 H^*$, Q and L are the left-handed SU(2) doublets.

UV models for the spin-1 mediators are also constrained by gauge invariance since these couplings can be assumed to be interactions of a spontaneously broken U(1) gauge symmetry. In a UV model one must be able to assign messenger charges to the SM fermions—or otherwise introduce new matter in the dark sector—to cancel all gauge anomalies with respect to the mediator gauge symmetry. The axial mediator case requires particular care since the global chiral symmetry of the SM is anomalous requiring, for example, a cancellation between the up-type and down-type quarks. See [292] for a recent analysis of anomaly constraints on the phenomenology of Z' bosons in the mass range and with the type of leptophobic/gauge-phobic couplings we consider for on-shell mediators for the γ -ray excess.

5.6.3 Renormalizability

Finally, one may push further and argue that a true ‘simplified model’ should depend only on renormalizable couplings; i.e. that it should be a UV complete theory. While the spin-1 couplings automatically satisfy this, the pseudoscalar couplings (5.23) are dimension-5. We would thus like to consider renormalizable operators that generate (5.23). Because the SM fermions are chiral, there are no renormalizable interactions with the SM singlet φ and the SM fermions. We thus left with interactions between the Higgs and the pseudoscalar,

$$\mathcal{L}_{\varphi\text{H}} = |H|^2 \lambda_H (M\varphi + \varphi^2), \quad (5.24)$$

where M is a dimensionful coupling. These couplings are reminiscent of the Higgs portal framework [323, 324] with the caveat that φ is now a mediator rather than the DM particle. At energies below m_h , (5.24) generates the couplings in (5.23) with the prediction $\lambda_u = \lambda_d = \lambda_\ell$. This is model dependent: In a two-Higgs doublet model such as the MSSM, one may have φ mix differently with the up- and down-type Higgses. These couplings introduce additional handles for dark sector bounds through the invisible width of the Higgs. See [325] for an explicit model for the γ -ray excess of this type.

5.6.4 Self-Interacting Dark Matter

The on-shell mediator scenario has nontrivial dynamics even in the limit of parametrically small coupling to the SM and may be a candidate for a model of self-interacting dark matter. However, the lower bound on the mediator mass (5.5d) is heavier than the typical scale required to address anomalies in small-scale structure [326, 327, 243, 246, 247, 252, 254, 255, 256, 127, 259, 260, 261]. A complete study of DM self-interactions through a pseudoscalar has yet to be completed, though the first steps are presented in [244] and have indicated that resonance effects may be relevant even for $m_\varphi \gtrsim 10$ GeV. Alternately, in Appendix 5.9 we address alternate final states that may match the γ -ray excess. Of particular interest is a mediator which decays into gluons—say through a loop of heavy quarks—could be made light enough to plausibly be in the regime of interesting models for self-interaction. We leave a detailed exploration for future work.

5.6.5 Prototypes for UV models

We briefly comment on directions in specific models that may be adapted to the on-shell mediator scenario. The MSSM introduces an additional pseudoscalar state which can plausibly mix with the Higgs as in (5.24), but SUSY bounds tend to rule out the mass range of

interest. Alternately, the singlet superfield of the NMSSM may be sufficiently unconstrained to furnish the required pseudoscalar. More generally, [325] recently proposed a complete non-supersymmetric UV model with two-Higgs doublets for the γ -ray excess.

A second alternate direction is to develop models with spin-1 mediators. We have shown that these typically are forced to have a constrained SM coupling if the mediator has a universal coupling to all generations, as one may generically expect for a gauged symmetry; see [139] for an explicit leptophilic model. While a Z' coupling to $U(1)_B$ and parametrically small coupling to the SM is a valid scenario within the on-shell mediator framework, one may also consider options where the spin-1 mediator does not have universal coupling, for example [328]. Inspiration for such a particle is motivated by Randall-Sundrum models [329] (gauge bosons with the 4D zero mode projected out, see e.g. [330, 331]) or their holographic duals (composite Higgs models with ρ -meson-like excitations) [332, 333].

5.6.6 Exceptions

Finally, we point out several exceptions to some of the ‘generic’ statements we have made in this document.

- In Sec. 5.1.2 we motivated the on-shell mediator scenario by exploiting how bounds on one operator ‘generically’ bound others. Some of these bounds are avoided when χ were a Majorana fermion since operators such as $\bar{\chi}\gamma^\mu\chi \equiv 0$. More generically one may also consider bosonic dark matter.
- In the MFV ansatz, we saw from the chiral structure that scalar couplings naturally follow the mass hierarchy while vector couplings tend to be universal. The latter condition is not necessary even within the MFV framework. For example, if the leading order spin-1 flavor spurion δ_{ij} were to vanish, the next-to-leading term is $y_i^\dagger y_j$ which

Mediator	MASS [GeV]		INTERACTION		COUPLING		Thermal Relic?
	m_χ	$m_{\text{mes.}}$	DM	SM	λ_{DM}	λ_{SM}	
spin-0	110	20	γ^5	$\mathbb{1}$	1.2	< 0.08	MSP?
"	"	"	γ^5	γ^5	"	$< 0.02^*$	"
spin-1	45	14	γ^μ	γ_μ	0.18	$< 10^{-6}$	$\gamma = 1.3$
"	"	"	$\gamma^\mu \gamma^5$	$\gamma_\mu \gamma^5$	"	< 0.004	"
"	"	"	$\gamma^\mu \gamma^5$	γ_μ	"	< 0.006	"
"	"	"	γ^μ	$\gamma_\mu \gamma^5$	"	< 0.02	"

Table 5.3: Best fit parameters assuming b -philic couplings for the spin-0 mediator and universal quark couplings for the spin-1 mediator. The upper bound for λ_{SM} for the $\gamma^5 \otimes \gamma^5$ is a conservative estimate for the 8 TeV mono- b reach at the LHC (see Section 5.4.3); the other bounds come from direct detection. In the last column, we indicate whether consistency with a thermal relic abundance suggests a tighter DM profile ($\gamma = 1.3$) or some population of millisecond pulsars (MSP), see Section 5.5.

has an even strongly hierarchical coupling to the third generation. Such a structure may be possible through models of partial compositeness [332, 333].

- We limited our analysis to a single class of mediator at a time. In the presence of multiple mediator fields, one can find processes that violate the relation between diagram topology and partial wave. For example, $\chi\bar{\chi} \rightarrow \varphi_1\varphi_2$ is s -wave for distinct spin-0 particles $\varphi_{1,2}$.

5.7 Conclusions and Outlook

We have presented a class of simplified models where dark matter annihilates into on-shell mediators which, in turn, decay into the SM with a typically suppressed width. This separates the sector of the model which can account for indirect detection signals—such as the FERMI galactic center γ -ray excess—and those which are bounded by direct detection and collider experiments. We have addressed γ -ray spectrum coming from these models and have compared used the γ -ray excess to identify plausible regions of parameter space for a DM interpretation; the best fit parameters and bounds on the SM coupling are shown in

Table 5.3. We have addressed the key points for UV model building and, in an appendix below, highlight further directions for modifying the γ -ray spectrum with more general SM final states.

5.8 Acknowledgements

This work is supported in part by the NSF grant PHY-1316792. We thank Kev Abazajian, Nikhil Anand, Nicolas Canac, Eugenio Del Nobile, Jonathan Feng, Shunsaku Horiuchi, Manoj Kaplinghat, Gordan Krnjaic (*'kern-ya-yitch'*), Tongyan Lin, Simona Murgia, Brian Shuve, Tracy Slatyer, Yuhsin Tsai, Daniel Whiteson, and Hai-Bo Yu for many insightful discussions. Plots in this document were generated using *Mathematica* [281]. P.T. would like to thank Southwest airlines and the airspace above the California coast where part of this work was completed.

While this paper was being prepared, [270, 196] was posted with an explicit model for on-shell vector mediators. [270] differs from the $\chi\bar{\chi} \rightarrow VV$ mode in this work in that it examines a specific UV completion which includes semi-annihilations. Their 1σ contours also do not account for the systematic uncertainties discussed in Sec. 5.3.3. Shortly after this work was posted to arXiv, [334] was posted and explores on-shell mediators with diverse SM final states and emphasizes the theme in our Figs. 5.10–5.8 and Appendix 5.9 that one need not focus only on bottom quark couplings and, further, that dark matter masses both above and below 40 GeV can yield the γ -ray excess.

5.9 Appendix: The Spectrum of Spectra

In the main text we have shown how the conventional 40 GeV DM model for the γ -ray excess can be converted into a heavier DM model ($m_\chi = 80, 120$ GeV) by taking the limit where annihilation to on-shell mediators dominates. We further showed that one can interpolate the DM masses between $m_\chi = 40$ GeV and 80, 120 GeV by parametrically increasing the SM coupling and increasing the fraction annihilations through an off-shell mediator. In this appendix we briefly demonstrate nonstandard (i.e. beyond $b\bar{b}$ and $\tau\bar{\tau}$) spectra that may also fit the γ -ray excess in the regimes $m_\chi < 40$ GeV and $m_\chi > 80, 120$ GeV. We use PPPC as described in Sec. 5.3.2 and our fits are subject to the caveats described in Sec. 5.3.3. For simplicity and consistency when comparing to other plots in this paper, we plot the data fit to the $b\bar{b}$ template from Fig. 8 of [13].

Fig. 5.11 shows sample spectra that show the range of behavior when considering different final states both for off-shell s -channel processes and for those with on-shell mediators. In each of these cases, we note that by considering either admixtures of different final states or on-shell mediator annihilation into different species, one can find viable DM models for the γ -ray excess where the DM mass is less than the 40 GeV value typically considered in the literature.

For example, we point out in (a) and (b) that gluons can give a reasonable fit to the spectrum. While the photon spectrum from monochromatic gluons takes a slightly different shape than that of the b —presumably part of the reason why gg final states were not proposed for the γ -ray excess fit—they are reasonably close to the data given the implicit systematic uncertainties. This fit is improved significantly if the [off-shell, s -channel] mediator is allowed to decay to both gluons or $b\bar{b}$ pairs. Shown in (b) is the fit for a mediator that decays to

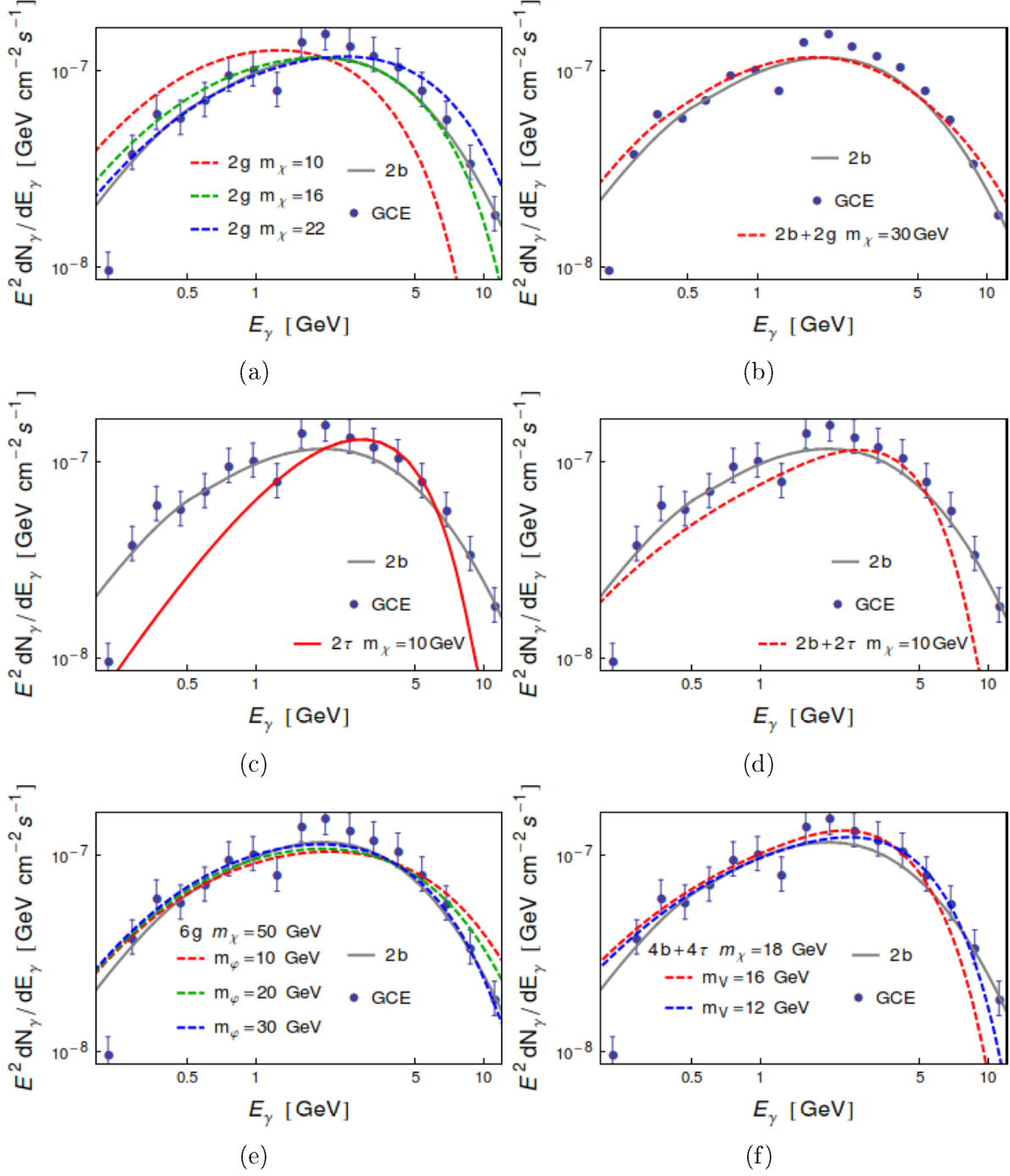


Figure 5.11: (a) $\chi\bar{\chi} \rightarrow gg$, (b) $\chi\bar{\chi} \rightarrow gg$ (67%) or $b\bar{b}$ (33%), (c) $\chi\bar{\chi} \rightarrow \tau\bar{\tau}$, (d) $\chi\bar{\chi} \rightarrow \tau\bar{\tau}$ (85%) or $b\bar{b}$ (15%), (e) $\chi\bar{\chi} \rightarrow 6g$, (f) $\chi\bar{\chi} \rightarrow 2 \times [\tau\bar{\tau}$ (85%) or $b\bar{b}$ (15%)]. Spectra for various final states, including branching ratios to different final states. 4-(6)-body final states originate from on-shell mediators with masses m_V (m_ϕ) shown. For visual comparison with other plots in this work, the gray $2b$ line is the $\chi\bar{\chi} \rightarrow b\bar{b}$ best fit spectrum and dots are the measured galactic center γ -ray excess spectrum (GCE) assuming a $b\bar{b}$ signal template from [13]. Bars demonstrate an arbitrary measure of goodness-of-fit with respect to this spectrum. Note that the γ -ray excess data depends on the template used for the DM γ -ray spectrum so these data points are mainly for comparative purposes and are not necessarily representative of the goodness-of-fit to the γ -ray excess. See Sec. 5.3.3 for details.

either gluons or $b\bar{b}$ pairs, with

$$\text{Br}(\text{mediator} \rightarrow gg) \approx 2 \text{Br}(\text{mediator} \rightarrow b\bar{b}). \quad (5.25)$$

The gluon mode is especially amenable to lighter dark matter masses since the final state is massless. Couplings to a spin-0 mediator can be generated through, for example, loops of third generation quarks.

Similarly, in Fig. 5.11(c) we show what appears to be a poor fit to 10 GeV $\tau\bar{\tau}$ pairs. This, however, is a consequence of comparing the γ -ray spectrum from $\tau\bar{\tau}$ to the γ -ray excess fit assuming a $b\bar{b}$ DM template. It is indeed well known that DM annihilating into 10 GeV $\tau\tau$ fits the excess well; this should be taken as a reminder of the systematic uncertainties implicit with the γ -ray fits. It also serves to highlight that for a specific model, a proper assessment of the fit to the γ ray excess requires a full astrophysical fit to the specific annihilation mode (along the lines of [190] and [38]) where both the model parameters and background parameters are fit simultaneously. For our purposes here, we only highlight the change in the spectrum from (c) to (d) where we introduce a 15% branching ratio of the mediator going to $b\bar{b}$ —the fit has interpolated between the two spectra and gives an intuitive handle for how to generate hybrid spectra. A similar hybrid spectrum was explored in Fig. 6 of [193].

In Fig. 5.11(e, f) we demonstrate the range of behavior for annihilation to on-shell mediators that each decay to either gluons or $\tau\bar{\tau}/b\bar{b}$. Note that an on-shell vector mediator cannot decay into two gluons by the Landau-Yang theorem so that one is forced to consider either $\chi\bar{\chi} \rightarrow 2 \times (V \rightarrow ggg)$ or $\chi\bar{\chi} \rightarrow 3 \times (\phi \rightarrow gg)$, each with six final state gluons. We plot the latter case in (e). In (f) we see an example of an on-shell vector mediator that decays to $\tau\bar{\tau}$ 85% of the time and $b\bar{b}$ the remainder. This spectrum fits the γ -ray excess spectrum for a $b\bar{b}$ template with $m_V \approx 12$ GeV.

Finally, we propose a simple extension where the DM mass can be made heavier than the

region considered in the primary text. We saw that the on-shell mediator scenario raised the DM mass by having DM annihilation go into more final state primaries (b quarks). By extending the mediator sector to include additional on-shell states between the DM and SM sectors in Fig. 5.3, one may force larger dark matter masses. For example, [277] explored the cascade where $\chi\bar{\chi} \rightarrow 2\phi_1$ with $\phi_i \rightarrow 2\phi_{i+1}$ for the PAMELA positron excess [335]. See the appendix in that paper for analytical results for the generalization of the box spectrum to a higher polynomial spectrum where the degree of the polynomial is set by the number of on-shell mediator sectors. Additionally, as we mentioned above, one may use the Landau-Yang theorem to force $V_1 \rightarrow 3g$ decays at the end of the cascade or use mediator sectors where symmetries force $\phi_i \rightarrow n\phi_{i+1}$ with $n > 2$. We remember from our analysis in Sec. 5.5, however, that increasing the number of on-shell mediators per annihilation while maintaining the γ -ray excess signal also increases the annihilation cross section beyond what is expected from a simple thermal relic.

Chapter 6

Conclusion

The particle nature of dark matter remains an open question, but it is a question on which a very large body of data has been accumulated. The theoretical efforts of the community have identified a number of very well motivated dark matter candidates, and the experimental efforts have probed quite a bit of this parameter space. The data gained is rich, and this thesis has presented some examples on how this data provides insights into how one should construct a theory of dark matter. In fact, the mixed results coming from direct detection experiments and the possible signals from indirect detection observations may indicate that new theoretical frameworks are needed. Perhaps one of the assumptions may not be sound, as illustrated in chapter 5 with two to two annihilations. Perhaps a particular kind of new physics is motivated, like in the case of chapter 4 with light mediators. In the near future a wealth of new information will be available from all the different classes of dark matter experimentation. At colliders, the LHC will begin its second run at a twice the energy and a much higher luminosity. Certainly new measures on the newly discovered higgs boson will be done, and perhaps details on the gauge hierarchy will be discovered. Concurrently, direct detection experiments continue to push their sensitivities to the neutrino floor, notably probing many higgs mediated scattering scenarios. Finally, indirect detection is probing

further into the realm of thermal cross sections, revealing more about dark matter in the early universe. There is no guarantee that the answer of dark matter will be revealed in any of these places. However, theoretical work similar to the work in this thesis will ensure that no matter the outcome, insights on dark matter interaction will be gained.

Bibliography

- [1] J. Angle et al. First Results from the XENON10 Dark Matter Experiment at the Gran Sasso National Laboratory. *Phys.Rev.Lett.*, 100:021303, 2008.
- [2] M. Felizardo, T. Morlat, A.C. Fernandes, T.A. Girard, J.G. Marques, et al. First Results of the Phase II SIMPLE Dark Matter Search. *Phys.Rev.Lett.*, 105:211301, 2010.
- [3] E. Aprile et al. First Dark Matter Results from the XENON100 Experiment. *Phys.Rev.Lett.*, 105:131302, 2010.
- [4] Z. Ahmed et al. Dark Matter Search Results from the CDMS II Experiment. *Science*, 327:1619–1621, 2010.
- [5] Z. Ahmed et al. Results from a Low-Energy Analysis of the CDMS II Germanium Data. *Phys.Rev.Lett.*, 106:131302, 2011.
- [6] C.E. Aalseth et al. Results from a Search for Light-Mass Dark Matter with a P-type Point Contact Germanium Detector. *Phys.Rev.Lett.*, 106:131301, 2011.
- [7] R. Agnese et al. Silicon Detector Dark Matter Results from the Final Exposure of CDMS II. *Phys.Rev.Lett.*, 111(25):251301, 2013.
- [8] Georges Aad et al. Search for dark matter candidates and large extra dimensions in events with a jet and missing transverse momentum with the ATLAS detector. *JHEP*, 1304:075, 2013.
- [9] Search for a supersymmetric top-quark partner in final states with two leptons in $\sqrt{s} = 8$ TeV pp collisions using 13 fb of ATLAS data. 2012.
- [10] Search for the Standard Model Higgs boson produced in association with top quarks in proton-proton collisions at $\sqrt{s} = 7$ TeV using the ATLAS detector. 2012.
- [11] J.P. Lees et al. Search for hadronic decays of a light Higgs boson in the radiative decay $\Upsilon \rightarrow \gamma A^0$. *Phys.Rev.Lett.*, 107:221803, 2011.
- [12] J.P. Lees et al. Search for a low-mass scalar Higgs boson decaying to a tau pair in single-photon decays of $\Upsilon(1S)$. *Phys.Rev.*, D88(7):071102, 2013.

- [13] Kevork N. Abazajian, Nicolas Canac, Shunsaku Horiuchi, and Manoj Kaplinghat. Astrophysical and Dark Matter Interpretations of Extended Gamma-Ray Emission from the Galactic Center. *Phys.Rev.*, D90(2):023526, 2014.
- [14] Jessica Goodman, Masahiro Ibe, Arvind Rajaraman, William Shepherd, Tim M.P. Tait, et al. Constraints on Dark Matter from Colliders. *Phys.Rev.*, D82:116010, 2010.
- [15] Alexandre Alves, Stefano Profumo, Farinaldo S. Queiroz, and William Shepherd. Effective field theory approach to the Galactic Center gamma-ray excess. *Phys.Rev.*, D90(11):115003, 2014.
- [16] Jason Kumar and Danny Marfatia. Matrix element analyses of dark matter scattering and annihilation. *Phys.Rev.*, D88(1):014035, 2013.
- [17] F. Zwicky. Die Rotverschiebung von extragalaktischen Nebeln. *Helv.Phys.Acta*, 6:110–127, 1933.
- [18] Ray G. Carlberg, H.K.C. Yee, and E. Ellingson. The Average mass and light profiles of galaxy clusters. *Astrophys.J.*, 478:462, 1997.
- [19] Douglas Clowe, Marusa Bradac, Anthony H. Gonzalez, Maxim Markevitch, Scott W. Randall, et al. A direct empirical proof of the existence of dark matter. *Astrophys.J.*, 648:L109–L113, 2006.
- [20] Raphael Gavazzi, Christophe Adami, Florence Durret, Jean-Charles Cuillandre, Olivier Ilbert, et al. A weak lensing study of the Coma cluster. *Astron.Astrophys.*, 498:L33, 2009.
- [21] Vera C. Rubin and Jr. Ford, W. Kent. Rotation of the Andromeda Nebula from a Spectroscopic Survey of Emission Regions. *Astrophys.J.*, 159:379–403, 1970.
- [22] Laurent Chemin, Claude Carignan, and Tyler Foster. HI kinematics and dynamics of Messier 31. *Astrophys.J.*, 705:1395–1415, 2009.
- [23] Edvige Corbelli, Silvio Lorenzoni, Rene A.M. Walterbos, Robert Braun, and David A. Thilker. A wide-field HI mosaic of Messier 31. II. The disk warp, rotation and the dark matter halo. *Astron.Astrophys.*, 511:A89, 2010.
- [24] W.J.G. de Blok, F. Walter, E. Brinks, C. Trachternach, S-H. Oh, et al. High-Resolution Rotation Curves and Galaxy Mass Models from THINGS. *Astron.J.*, 136:2648–2719, 2008.
- [25] Alan W. McConnachie. The observed properties of dwarf galaxies in and around the Local Group. *Astron.J.*, 144:4, 2012.
- [26] Mario Mateo. Dwarf galaxies of the Local Group. *Ann.Rev.Astron.Astrophys.*, 36:435–506, 1998.
- [27] P.A.R. Ade et al. Planck 2013 results. XVI. Cosmological parameters. *Astron.Astrophys.*, 571:A16, 2014.

- [28] Gerard Lemson. Halo and Galaxy Formation Histories from the Millennium Simulation: Public release of a VO-oriented and SQL-queryable database for studying the evolution of galaxies in the Lambda-CDM cosmogony. 2006.
- [29] E. Aprile et al. Dark Matter Results from 225 Live Days of XENON100 Data. *Phys.Rev.Lett.*, 109:181301, 2012.
- [30] D.S. Akerib et al. First results from the LUX dark matter experiment at the Sanford Underground Research Facility. *Phys.Rev.Lett.*, 112:091303, 2014.
- [31] R. Agnese et al. Search for Low-Mass Weakly Interacting Massive Particles with SuperCDMS. *Phys.Rev.Lett.*, 112(24):241302, 2014.
- [32] T.A. Girard, M. Felizardo, A.C. Fernandes, J.G. Marques, and A.R. Ramos. Reply to ‘Comments on ‘First Results of the Phase II SIMPLE Dark Matter Search’’. *Phys.Rev.Lett.*, 108:259002, 2012.
- [33] E. Behnke et al. First Dark Matter Search Results from a 4-kg CF₃I Bubble Chamber Operated in a Deep Underground Site. *Phys.Rev.*, D86(5):052001, 2012.
- [34] C.E. Aalseth et al. CoGeNT: A Search for Low-Mass Dark Matter using p-type Point Contact Germanium Detectors. *Phys.Rev.*, D88(1):012002, 2013.
- [35] G. Angloher, M. Bauer, I. Bavykina, A. Bento, C. Bucci, et al. Results from 730 kg days of the CRESST-II Dark Matter Search. *Eur.Phys.J.*, C72:1971, 2012.
- [36] R. Bernabei et al. New results from DAMA/LIBRA. *Eur.Phys.J.*, C67:39–49, 2010.
- [37] Esra Bulbul, Maxim Markevitch, Adam Foster, Randall K. Smith, Michael Loewenstein, et al. Detection of An Unidentified Emission Line in the Stacked X-ray spectrum of Galaxy Clusters. *Astrophys.J.*, 789:13, 2014.
- [38] Tansu Daylan, Douglas P. Finkbeiner, Dan Hooper, Tim Linden, Stephen K. N. Portillo, et al. The Characterization of the Gamma-Ray Signal from the Central Milky Way: A Compelling Case for Annihilating Dark Matter. 2014.
- [39] M. Ackermann et al. Searching for Dark Matter Annihilation from Milky Way Dwarf Spheroidal Galaxies with Six Years of Fermi-LAT Data. 2015.
- [40] Gañlle Giesen, Mathieu Boudaud, Yoann Genolini, Vivian Poulin, Marco Cirelli, et al. AMS-02 antiprotons, at last! Secondary astrophysical component and immediate implications for Dark Matter. 2015.
- [41] Georges Aad et al. Search for new phenomena in final states with an energetic jet and large missing transverse momentum in pp collisions at $\sqrt{s} = 8$ TeV with the ATLAS detector. 2015.
- [42] Vardan Khachatryan et al. Search for dark matter, extra dimensions, and unparticles in monojet events in proton-proton collisions at $\sqrt{s} = 8$ TeV. 2014.

- [43] Sebastian Arrenberg, Howard Baer, Vernon Barger, Laura Baudis, Daniel Bauer, et al. Working Group Report: Dark Matter Complementarity. 2013.
- [44] Daniel Bauer, James Buckley, Matthew Cahill-Rowley, Randel Cotta, Alex Drlica-Wagner, et al. Dark Matter in the Coming Decade: Complementary Paths to Discovery and Beyond. 2013.
- [45] E. Komatsu et al. Seven-Year Wilkinson Microwave Anisotropy Probe (WMAP) Observations: Cosmological Interpretation. *Astrophys.J.Suppl.*, 192:18, 2011.
- [46] Jonathan L. Feng and Jason Kumar. The WIMPless Miracle: Dark-Matter Particles without Weak-Scale Masses or Weak Interactions. *Phys.Rev.Lett.*, 101:231301, 2008.
- [47] Andreas Birkedal, Konstantin Matchev, and Maxim Perelstein. Dark matter at colliders: A Model independent approach. *Phys.Rev.*, D70:077701, 2004.
- [48] Maria Beltran, Dan Hooper, Edward W. Kolb, and Zosia C. Krusberg. Deducing the nature of dark matter from direct and indirect detection experiments in the absence of collider signatures of new physics. *Phys.Rev.*, D80:043509, 2009.
- [49] Qing-Hong Cao, Chuan-Ren Chen, Chong Sheng Li, and Hao Zhang. Effective Dark Matter Model: Relic density, CDMS II, Fermi LAT and LHC. *JHEP*, 1108:018, 2011.
- [50] Maria Beltran, Dan Hooper, Edward W. Kolb, Zosia A.C. Krusberg, and Tim M.P. Tait. Maverick dark matter at colliders. *JHEP*, 1009:037, 2010.
- [51] William Shepherd, Tim M.P. Tait, and Gabrijela Zaharijas. Bound states of weakly interacting dark matter. *Phys.Rev.*, D79:055022, 2009.
- [52] Jessica Goodman, Masahiro Ibe, Arvind Rajaraman, William Shepherd, Tim M.P. Tait, et al. Constraints on Light Majorana dark Matter from Colliders. *Phys.Lett.*, B695:185–188, 2011.
- [53] Yang Bai, Patrick J. Fox, and Roni Harnik. The Tevatron at the Frontier of Dark Matter Direct Detection. *JHEP*, 1012:048, 2010.
- [54] Patrick J. Fox, Roni Harnik, Joachim Kopp, and Yuhsin Tsai. LEP Shines Light on Dark Matter. *Phys.Rev.*, D84:014028, 2011.
- [55] Jean-Francois Fortin and Tim M.P. Tait. Collider Constraints on Dipole-Interacting Dark Matter. *Phys.Rev.*, D85:063506, 2012.
- [56] Jernej F. Kamenik and Jure Zupan. Discovering Dark Matter Through Flavor Violation at the LHC. *Phys.Rev.*, D84:111502, 2011.
- [57] C.P. Burgess, Maxim Pospelov, and Tonnis ter Veldhuis. The Minimal model of non-baryonic dark matter: A Singlet scalar. *Nucl.Phys.*, B619:709–728, 2001.

- [58] Shinya Kanemura, Shigeki Matsumoto, Takehiro Nabeshima, and Nobuchika Okada. Can WIMP Dark Matter overcome the Nightmare Scenario? *Phys.Rev.*, D82:055026, 2010.
- [59] Kingman Cheung, Kentarou Mawatari, Eibun Senaha, Po-Yan Tseng, and Tzu-Chiang Yuan. The Top Window for dark matter. *JHEP*, 1010:081, 2010.
- [60] Jian Wang, Chong Sheng Li, Ding Yu Shao, and Hao Zhang. Next-to-leading order QCD predictions for the signal of Dark Matter and photon associated production at the LHC. *Phys.Rev.*, D84:075011, 2011.
- [61] Yann Mambrini and Bryan Zaldivar. When LEP and Tevatron combined with WMAP and XENON100 shed light on the nature of Dark Matter. *JCAP*, 1110:023, 2011.
- [62] C.E. Aalseth, P.S. Barbeau, J. Colaresi, J.I. Collar, J. Diaz Leon, et al. Search for an Annual Modulation in a P-type Point Contact Germanium Dark Matter Detector. *Phys.Rev.Lett.*, 107:141301, 2011.
- [63] Frank Petriello and Kathryn M. Zurek. DAMA and WIMP dark matter. *JHEP*, 0809:047, 2008.
- [64] Jonathan L. Feng, Jason Kumar, and Louis E. Strigari. Explaining the DAMA Signal with WIMPlless Dark Matter. *Phys.Lett.*, B670:37–40, 2008.
- [65] J. Filippini. WIMP hunting with the Cryogenic Dark Matter Search. *Nuovo Cim.*, C32N5-6:45–52, 2009.
- [66] Thomas Schwetz and Jure Zupan. Dark Matter attempts for CoGeNT and DAMA. *JCAP*, 1108:008, 2011.
- [67] Patrick J. Fox, Joachim Kopp, Mariangela Lisanti, and Neal Weiner. A CoGeNT Modulation Analysis. *Phys.Rev.*, D85:036008, 2012.
- [68] Marco Farina, Duccio Pappadopulo, Alessandro Strumia, and Tomer Volansky. Can CoGeNT and DAMA Modulations Be Due to Dark Matter? *JCAP*, 1111:010, 2011.
- [69] JiJi Fan, Matthew Reece, and Lian-Tao Wang. Non-relativistic effective theory of dark matter direct detection. *JCAP*, 1011:042, 2010.
- [70] Jessica Goodman, Masahiro Ibe, Arvind Rajaraman, William Shepherd, Tim M.P. Tait, et al. Gamma Ray Line Constraints on Effective Theories of Dark Matter. *Nucl.Phys.*, B844:55–68, 2011.
- [71] Kingman Cheung, Po-Yan Tseng, and Tzu-Chiang Yuan. Cosmic Antiproton Constraints on Effective Interactions of the Dark Matter. *JCAP*, 1101:004, 2011.
- [72] Matthew R. Buckley. Asymmetric Dark Matter and Effective Operators. *Phys.Rev.*, D84:043510, 2011.

- [73] A.J. Buras, P. Gambino, M. Gorbahn, S. Jager, and L. Silvestrini. Universal unitarity triangle and physics beyond the standard model. *Phys.Lett.*, B500:161–167, 2001.
- [74] Jonathan L. Feng, Jason Kumar, Danny Marfatia, and David Sanford. Isospin-Violating Dark Matter. *Phys.Lett.*, B703:124–127, 2011.
- [75] Spencer Chang, Jia Liu, Aaron Pierce, Neal Weiner, and Itay Yavin. CoGeNT Interpretations. *JCAP*, 1008:018, 2010.
- [76] Zhaofeng Kang, Jinmian Li, Tianjun Li, Tao Liu, and Jinmin Yang. Asymmetric Sneutrino Dark Matter in the NMSSM with Minimal Inverse Seesaw. 2011.
- [77] Eugenio Del Nobile, Chris Kouvaris, and Francesco Sannino. Interfering Composite Asymmetric Dark Matter for DAMA and CoGeNT. *Phys.Rev.*, D84:027301, 2011.
- [78] Xin Gao, Zhaofeng Kang, and Tianjun Li. Origins of the Isospin Violation of Dark Matter Interactions. *JCAP*, 1301:021, 2013.
- [79] Mads T. Frandsen, Felix Kahlhoefer, John March-Russell, Christopher McCabe, Matthew McCullough, et al. On the DAMA and CoGeNT Modulations. *Phys.Rev.*, D84:041301, 2011.
- [80] Yu Gao, Jason Kumar, and Danny Marfatia. Isospin-Violating Dark Matter in the Sun. *Phys.Lett.*, B704:534–540, 2011.
- [81] Mu-Chun Chen, Kalyana T. Mahanthappa, Aurora Meroni, and S.T. Petcov. Predictions for Neutrino Masses, $\beta\beta_{0\nu}$ -Decay and Lepton Flavor Violation in a SUSY $SU(5) \times T'$ Model of Flavour. 2011.
- [82] Andriy Kurylov and Marc Kamionkowski. Generalized analysis of weakly interacting massive particle searches. *Phys.Rev.*, D69:063503, 2004.
- [83] Johan Alwall, Pavel Demin, Simon de Visscher, Rikkert Frederix, Michel Herquet, et al. MadGraph/MadEvent v4: The New Web Generation. *JHEP*, 0709:028, 2007.
- [84] Torbjorn Sjostrand, Stephen Mrenna, and Peter Z. Skands. PYTHIA 6.4 Physics and Manual. *JHEP*, 0605:026, 2006.
- [85] J. Conway et. al. Pgs 4, pretty good simulation of high-energy collisions . 2013.
- [86] T. Aaltonen et al. Search for large extra dimensions in final states containing one photon or jet and large missing transverse energy produced in $p\bar{p}$ collisions at $\sqrt{s} = 1.96$ -TeV. *Phys.Rev.Lett.*, 101:181602, 2008.
- [87] <http://www-cdf.fnal.gov/physics/exotic/r2a/20070322.monojet/public/ykk.html>.
- [88] Search for New Phenomena in Monojet plus Missing Transverse Momentum Final States using 1 fb⁻¹ of pp Collisions at sqrt(s)=7 TeV with the ATLAS Detector. 2011.

- [89] L. Vacavant and I. Hinchliffe. Signals of models with large extra dimensions in ATLAS. *J.Phys.*, G27:1839–1850, 2001.
- [90] G. Belanger, F. Boudjema, A. Pukhov, and A. Semenov. Dark matter direct detection rate in a generic model with micrOMEGAs 2.2. *Comput.Phys.Commun.*, 180:747–767, 2009.
- [91] Joel Giedt, Anthony W. Thomas, and Ross D. Young. Dark matter, the CMSSM and lattice QCD. *Phys.Rev.Lett.*, 103:201802, 2009.
- [92] A.A. Abdo, M. Ackermann, M. Ajello, W.B. Atwood, L. Baldini, et al. Fermi LAT Search for Photon Lines from 30 to 200 GeV and Dark Matter Implications. *Phys.Rev.Lett.*, 104:091302, 2010.
- [93] M. Ackermann et al. Fermi LAT Search for Dark Matter in Gamma-ray Lines and the Inclusive Photon Spectrum. *Phys.Rev.*, D86:022002, 2012.
- [94] Torsten Bringmann, Xiaoyuan Huang, Alejandro Ibarra, Stefan Vogl, and Christoph Weniger. Fermi LAT Search for Internal Bremsstrahlung Signatures from Dark Matter Annihilation. *JCAP*, 1207:054, 2012.
- [95] Christoph Weniger. A Tentative Gamma-Ray Line from Dark Matter Annihilation at the Fermi Large Area Telescope. *JCAP*, 1208:007, 2012.
- [96] Meng Su and Douglas P. Finkbeiner. Strong Evidence for Gamma-ray Line Emission from the Inner Galaxy. 2012.
- [97] Arvind Rajaraman, Tim M.P. Tait, and Daniel Whiteson. Two Lines or Not Two Lines? That is the Question of Gamma Ray Spectra. *JCAP*, 1209:003, 2012.
- [98] Elmo Tempel, Andi Hektor, and Martti Raidal. Fermi 130 GeV gamma-ray excess and dark matter annihilation in sub-haloes and in the Galactic centre. *JCAP*, 1209:032, 2012.
- [99] Andi Hektor, Martti Raidal, and Elmo Tempel. Evidence for indirect detection of dark matter from galaxy clusters in Fermi γ -Ray data. *Astrophys.J.*, 762:L22, 2013.
- [100] Meng Su and Douglas P. Finkbeiner. Double Gamma-ray Lines from Unassociated Fermi-LAT Sources. 2012.
- [101] Dan Hooper and Tim Linden. Are Lines From Unassociated Gamma-Ray Sources Evidence For Dark Matter Annihilation? *Phys.Rev.*, D86:083532, 2012.
- [102] Andi Hektor, Martti Raidal, and Elmo Tempel. Double gamma-ray lines from unassociated Fermi-LAT sources revisited. 2012.
- [103] Timothy Cohen, Mariangela Lisanti, Tracy R. Slatyer, and Jay G. Wacker. Illuminating the 130 GeV Gamma Line with Continuum Photons. *JHEP*, 1210:134, 2012.

- [104] Daniel Whiteson. Disentangling Instrumental Features of the 130 GeV Fermi Line. *JCAP*, 1211:008, 2012.
- [105] Andi Hektor, Martti Raidal, and Elmo Tempel. Fermi-LAT gamma-ray signal from Earth Limb, systematic detector effects and their implications for the 130 GeV gamma-ray excess. *Eur.Phys.J.*, C73:2578, 2013.
- [106] Douglas P. Finkbeiner, Meng Su, and Christoph Weniger. Is the 130 GeV Line Real? A Search for Systematics in the Fermi-LAT Data. *JCAP*, 1301:029, 2013.
- [107] Stefano Profumo and Tim Linden. Gamma-ray Lines in the Fermi Data: is it a Bubble? *JCAP*, 1207:011, 2012.
- [108] Alexey Boyarsky, Denys Malyshev, and Oleg Ruchayskiy. Spectral and spatial variations of the diffuse $\tilde{\chi}_1^0$ -ray background in the vicinity of the Galactic plane and possible nature of the feature at 130 GeV. *Phys.Dark Univ.*, 2:90–96, 2013.
- [109] Felix Aharonian, Dmitry Khangulyan, and Denis Malyshev. Cold ultrarelativistic pulsar winds as potential sources of galactic gamma-ray lines above 100 GeV. *Astron.Astrophys.*, 547:A114, 2012.
- [110] Serguei Chatrchyan et al. Search for heavy long-lived charged particles in pp collisions at $\sqrt{s} = 7$ TeV. *Phys.Lett.*, B713:408–433, 2012.
- [111] R.C. Cotta, J.L. Hewett, M.P. Le, and T.G. Rizzo. Bounds on Dark Matter Interactions with Electroweak Gauge Bosons. *Phys.Rev.*, D88:116009, 2013.
- [112] Mads T. Frandsen, Ulrich Haisch, Felix Kahlhoefer, Philipp Mertsch, and Kai Schmidt-Hoberg. Loop-induced dark matter direct detection signals from gamma-ray lines. *JCAP*, 1210:033, 2012.
- [113] Spencer Chang, Neal Weiner, and Itay Yavin. Magnetic Inelastic Dark Matter. *Phys.Rev.*, D82:125011, 2010.
- [114] Kunal Kumar, Arjun Menon, and Tim M.P. Tait. Magnetic Fluffy Dark Matter. *JHEP*, 1202:131, 2012.
- [115] Neal Weiner and Itay Yavin. How Dark Are Majorana WIMPs? Signals from MiDM and Rayleigh Dark Matter. *Phys.Rev.*, D86:075021, 2012.
- [116] Neal Weiner and Itay Yavin. UV completions of magnetic inelastic and Rayleigh dark matter for the Fermi Line(s). *Phys.Rev.*, D87(2):023523, 2013.
- [117] Jonathan L. Feng. Dark Matter Candidates from Particle Physics and Methods of Detection. *Ann.Rev.Astron.Astrophys.*, 48:495–545, 2010.
- [118] Jihn E. Kim and Gianpaolo Carosi. Axions and the Strong CP Problem. *Rev.Mod.Phys.*, 82:557–602, 2010.

- [119] L.J. Rosenberg and K.A. van Bibber. Searches for invisible axions. *Phys.Rept.*, 325:1–39, 2000.
- [120] Gianfranco Bertone, Dan Hooper, and Joseph Silk. Particle dark matter: Evidence, candidates and constraints. *Phys.Rept.*, 405:279–390, 2005.
- [121] Gerard Jungman, Marc Kamionkowski, and Kim Griest. Supersymmetric dark matter. *Phys.Rept.*, 267:195–373, 1996.
- [122] D.J.H. Chung, L.L. Everett, G.L. Kane, S.F. King, Joseph D. Lykken, et al. The Soft supersymmetry breaking Lagrangian: Theory and applications. *Phys.Rept.*, 407:1–203, 2005.
- [123] Geraldine Servant and Timothy M.P. Tait. Is the lightest Kaluza-Klein particle a viable dark matter candidate? *Nucl.Phys.*, B650:391–419, 2003.
- [124] Hsin-Chia Cheng, Jonathan L. Feng, and Konstantin T. Matchev. Kaluza-Klein dark matter. *Phys.Rev.Lett.*, 89:211301, 2002.
- [125] Dan Hooper and Stefano Profumo. Dark matter and collider phenomenology of universal extra dimensions. *Phys.Rept.*, 453:29–115, 2007.
- [126] Maxim Pospelov, Adam Ritz, and Mikhail B. Voloshin. Secluded WIMP Dark Matter. *Phys.Lett.*, B662:53–61, 2008.
- [127] Maxim Pospelov and Adam Ritz. Astrophysical Signatures of Secluded Dark Matter. *Phys.Lett.*, B671:391–397, 2009.
- [128] Jonathan L. Feng, Huitzu Tu, and Hai-Bo Yu. Thermal Relics in Hidden Sectors. *JCAP*, 0810:043, 2008.
- [129] David E. Kaplan, Markus A. Luty, and Kathryn M. Zurek. Asymmetric Dark Matter. *Phys.Rev.*, D79:115016, 2009.
- [130] Adam Falkowski, Joshua T. Ruderman, and Tomer Volansky. Asymmetric Dark Matter from Leptogenesis. *JHEP*, 1105:106, 2011.
- [131] Hooman Davoudiasl and Rabindra N. Mohapatra. On Relating the Genesis of Cosmic Baryons and Dark Matter. *New J.Phys.*, 14:095011, 2012.
- [132] Tongyan Lin, Hai-Bo Yu, and Kathryn M. Zurek. On Symmetric and Asymmetric Light Dark Matter. *Phys.Rev.*, D85:063503, 2012.
- [133] Silvia Galli, Fabio Iocco, Gianfranco Bertone, and Alessandro Melchiorri. Updated CMB constraints on Dark Matter annihilation cross-sections. *Phys.Rev.*, D84:027302, 2011.
- [134] Gert Hütsi, Jens Chluba, Andi Hektor, and Martti Raidal. WMAP7 and future CMB constraints on annihilating dark matter: implications on GeV-scale WIMPs. *Astron.Astrophys.*, 535:A26, 2011.

- [135] Douglas P. Finkbeiner, Silvia Galli, Tongyan Lin, and Tracy R. Slatyer. Searching for Dark Matter in the CMB: A Compact Parameterization of Energy Injection from New Physics. *Phys.Rev.*, D85:043522, 2012.
- [136] Richard H. Cyburt, Brian D. Fields, Keith A. Olive, and Evan Skillman. New BBN limits on physics beyond the standard model from He-4. *Astropart.Phys.*, 23:313–323, 2005.
- [137] Georg G. Raffelt. Particle physics from stars. *Ann.Rev.Nucl.Part.Sci.*, 49:163–216, 1999.
- [138] A. Liam Fitzpatrick, Dan Hooper, and Kathryn M. Zurek. Implications of CoGeNT and DAMA for Light WIMP Dark Matter. *Phys.Rev.*, D81:115005, 2010.
- [139] Dan Hooper, Neal Weiner, and Wei Xue. Dark Forces and Light Dark Matter. *Phys.Rev.*, D86:056009, 2012.
- [140] Sarah Andreas, Chiara Arina, Thomas Hambye, Fu-Sin Ling, and Michel H.G. Tytgat. A light scalar WIMP through the Higgs portal and CoGeNT. *Phys.Rev.*, D82:043522, 2010.
- [141] Adam Falkowski, Jose Juknevich, and Jessie Shelton. Dark Matter Through the Neutrino Portal. 2009.
- [142] Nobuchika Okada and Osamu Seto. Isospin violating dark matter being asymmetric. *Phys.Rev.*, D88:063506, 2013.
- [143] Ki-Young Choi and Osamu Seto. Light Dirac right-handed sneutrino dark matter. *Phys.Rev.*, D88(3):035005, 2013.
- [144] G. D’Ambrosio, G.F. Giudice, G. Isidori, and A. Strumia. Minimal flavor violation: An Effective field theory approach. *Nucl.Phys.*, B645:155–187, 2002.
- [145] J. Beringer et al. Review of Particle Physics (RPP). *Phys.Rev.*, D86:010001, 2012.
- [146] Search for the standard model Higgs boson at LEP. *PoS*, HEP2001:128, 2001.
- [147] Radovan Dermisek and John F. Gunion. The NMSSM Solution to the Fine-Tuning Problem, Precision Electroweak Constraints and the Largest LEP Higgs Event Excess. *Phys.Rev.*, D76:095006, 2007.
- [148] Ulrich Ellwanger, Cyril Hugonie, and Ana M. Teixeira. The Next-to-Minimal Supersymmetric Standard Model. *Phys.Rept.*, 496:1–77, 2010.
- [149] C. Balazs, Marcela Carena, A. Freitas, and C.E.M. Wagner. Phenomenology of the nMSSM from colliders to cosmology. *JHEP*, 0706:066, 2007.
- [150] Patrick Draper, Tao Liu, Carlos E.M. Wagner, Lian-Tao Wang, and Hao Zhang. Dark Light Higgs. *Phys.Rev.Lett.*, 106:121805, 2011.

- [151] Marcela Carena, Nausheen R. Shah, and Carlos E.M. Wagner. Light Dark Matter and the Electroweak Phase Transition in the NMSSM. *Phys.Rev.*, D85:036003, 2012.
- [152] Jun-Jie Cao, Ken-ichi Hikasa, Wenyu Wang, Jin Min Yang, Ken-ichi Hikasa, et al. Light dark matter in NMSSM and implication on Higgs phenomenology. *Phys.Lett.*, B703:292–297, 2011.
- [153] Debottam Das and Ulrich Ellwanger. Light dark matter in the NMSSM: upper bounds on direct detection cross sections. *JHEP*, 1009:085, 2010.
- [154] Dan Hooper and Tim M.P. Tait. Neutralinos in an extension of the minimal supersymmetric standard model as the source of the PAMELA positron excess. *Phys.Rev.*, D80:055028, 2009.
- [155] Alexander V. Belikov, John F. Gunion, Dan Hooper, and Tim M.P. Tait. CoGeNT, DAMA, and Light Neutralino Dark Matter. *Phys.Lett.*, B705:82–86, 2011.
- [156] Matthew R. Buckley, Dan Hooper, and Tim M.P. Tait. Particle Physics Implications for CoGeNT, DAMA, and Fermi. *Phys.Lett.*, B702:216–219, 2011.
- [157] Xiao-Gang He and Jusak Tandean. Low-Mass Dark-Matter Hint from CDMS II, Higgs Boson at the LHC, and Darkon Models. *Phys.Rev.*, D88:013020, 2013.
- [158] Arvind Rajaraman, William Shepherd, Tim M.P. Tait, and Alexander M. Wijangco. LHC Bounds on Interactions of Dark Matter. *Phys.Rev.*, D84:095013, 2011.
- [159] G. Belanger, F. Boudjema, P. Brun, A. Pukhov, S. Rosier-Lees, et al. Indirect search for dark matter with micrOMEGAs2.4. *Comput.Phys.Commun.*, 182:842–856, 2011.
- [160] John R. Ellis, Keith A. Olive, and Christopher Savage. Hadronic Uncertainties in the Elastic Scattering of Supersymmetric Dark Matter. *Phys.Rev.*, D77:065026, 2008.
- [161] J. Gasser, H. Leutwyler, and M.E. Sainio. Form-factor of the sigma term. *Phys.Lett.*, B253:260–264, 1991.
- [162] Veronique Bernard, Norbert Kaiser, and Ulf G. Meissner. Critical analysis of baryon masses and sigma terms in heavy baryon chiral perturbation theory. *Z.Phys.*, C60:111–120, 1993.
- [163] M.M. Pavan, I.I. Strakovsky, R.L. Workman, and R.A. Arndt. The Pion nucleon Sigma term is definitely large: Results from a G.W.U. analysis of pi nucleon scattering data. *PiN Newslett.*, 16:110–115, 2002.
- [164] R.D. Young and A.W. Thomas. Octet baryon masses and sigma terms from an SU(3) chiral extrapolation. *Phys.Rev.*, D81:014503, 2010.
- [165] Anthony W. Thomas, Phiala E. Shanahan, and Ross D. Young. Strange quarks and lattice QCD. *Few Body Syst.*, 54:123–128, 2013.

- [166] Parikshit Junnarkar and Andre Walker-Loud. Scalar strange content of the nucleon from lattice QCD. *Phys.Rev.*, D87(11):114510, 2013.
- [167] J.M. Alarcon, L.S. Geng, J. Martin Camalich, and J.A. Oller. The strangeness content of the nucleon from effective field theory and phenomenology. *Phys.Lett.*, B730:342–346, 2014.
- [168] Roberta Diamanti, Laura Lopez-Honorez, Olga Mena, Sergio Palomares-Ruiz, and Aaron C. Vincent. Constraining Dark Matter Late-Time Energy Injection: Decays and P-Wave Annihilations. *JCAP*, 1402:017, 2014.
- [169] Kevork N. Abazajian and Manoj Kaplinghat. Detection of a Gamma-Ray Source in the Galactic Center Consistent with Extended Emission from Dark Matter Annihilation and Concentrated Astrophysical Emission. *Phys.Rev.*, D86:083511, 2012.
- [170] Dan Hooper and Tim Linden. On The Origin Of The Gamma Rays From The Galactic Center. *Phys.Rev.*, D84:123005, 2011.
- [171] Patrick J. Fox, Roni Harnik, Joachim Kopp, and Yuhsin Tsai. Missing Energy Signatures of Dark Matter at the LHC. *Phys.Rev.*, D85:056011, 2012.
- [172] Yang Bai and Tim M.P. Tait. Searches with Mono-Leptons. *Phys.Lett.*, B723:384–387, 2013.
- [173] Linda M. Carpenter, Andrew Nelson, Chase Shimmin, Tim M.P. Tait, and Daniel Whiteson. Collider searches for dark matter in events with a Z boson and missing energy. *Phys.Rev.*, D87(7):074005, 2013.
- [174] Nicole F. Bell, James B. Dent, Ahmad J. Galea, Thomas D. Jacques, Lawrence M. Krauss, et al. Searching for Dark Matter at the LHC with a Mono-Z. *Phys.Rev.*, D86:096011, 2012.
- [175] Haipeng An, Xiangdong Ji, and Lian-Tao Wang. Light Dark Matter and Z' Dark Force at Colliders. *JHEP*, 1207:182, 2012.
- [176] Mads T. Frandsen, Felix Kahlhoefer, Anthony Preston, Subir Sarkar, and Kai Schmidt-Hoberg. LHC and Tevatron Bounds on the Dark Matter Direct Detection Cross-Section for Vector Mediators. *JHEP*, 1207:123, 2012.
- [177] Haipeng An, Ran Huo, and Lian-Tao Wang. Searching for Low Mass Dark Portal at the LHC. *Phys.Dark Univ.*, 2:50–57, 2013.
- [178] Ian M. Shoemaker and Luca Vecchi. Unitarity and Monojet Bounds on Models for DAMA, CoGeNT, and CRESST-II. *Phys.Rev.*, D86:015023, 2012.
- [179] Johan Alwall, Michel Herquet, Fabio Maltoni, Olivier Mattelaer, and Tim Stelzer. MadGraph 5 : Going Beyond. *JHEP*, 1106:128, 2011.

- [180] Georges Aad et al. Study of heavy-flavor quarks produced in association with top-quark pairs at $\sqrt{s} = 7\text{--}8\text{ TeV}$ using the ATLAS detector. *Phys.Rev.*, D89(7):072012, 2014.
- [181] Tongyan Lin, Edward W. Kolb, and Lian-Tao Wang. Probing dark matter couplings to top and bottom quarks at the LHC. *Phys.Rev.*, D88(6):063510, 2013.
- [182] Gagik K. Yeghyan. Upsilon Decays into Light Scalar Dark Matter. *Phys.Rev.*, D80:115019, 2009.
- [183] Yang Bai, Patrick Draper, and Jessie Shelton. Measuring the Invisible Higgs Width at the 7 and 8 TeV LHC. *JHEP*, 1207:192, 2012.
- [184] Christoph Englert, Tuhin S. Roy, and Michael Spannowsky. Ditau jets in Higgs searches. *Phys.Rev.*, D84:075026, 2011.
- [185] Dan Hooper and Tracy R. Slatyer. Two Emission Mechanisms in the Fermi Bubbles: A Possible Signal of Annihilating Dark Matter. *Phys.Dark Univ.*, 2:118–138, 2013.
- [186] Nobuchika Okada and Osamu Seto. Gamma ray emission in Fermi bubbles and Higgs portal dark matter. *Phys.Rev.*, D89(4):043525, 2014.
- [187] Wei-Chih Huang, Alfredo Urbano, and Wei Xue. Fermi Bubbles under Dark Matter Scrutiny. Part I: Astrophysical Analysis. 2013.
- [188] Lisa Goodenough and Dan Hooper. Possible Evidence For Dark Matter Annihilation In The Inner Milky Way From The Fermi Gamma Ray Space Telescope. 2009.
- [189] Dan Hooper and Lisa Goodenough. Dark Matter Annihilation in The Galactic Center As Seen by the Fermi Gamma Ray Space Telescope. *Phys.Lett.*, B697:412–428, 2011.
- [190] Kevork N. Abazajian. The Consistency of Fermi-LAT Observations of the Galactic Center with a Millisecond Pulsar Population in the Central Stellar Cluster. *JCAP*, 1103:010, 2011.
- [191] Alexey Boyarsky, Denys Malyshev, and Oleg Ruchayskiy. A comment on the emission from the Galactic Center as seen by the Fermi telescope. *Phys.Lett.*, B705:165–169, 2011.
- [192] Chris Gordon and Oscar Macias. Dark Matter and Pulsar Model Constraints from Galactic Center Fermi-LAT Gamma Ray Observations. *Phys.Rev.*, D88(8):083521, 2013.
- [193] Oscar Macias and Chris Gordon. Contribution of cosmic rays interacting with molecular clouds to the Galactic Center gamma-ray excess. *Phys.Rev.*, D89(6):063515, 2014.
- [194] Kamakshya Prasad Modak, Debasish Majumdar, and Subhendu Rakshit. A possible explanation of low energy γ -ray excess from galactic centre and Fermi bubble by a Dark Matter model with two real scalars. *JCAP*, 1503(03):011, 2015.

- [195] Luis Alfredo Anchordoqui and Brian James Vlcek. W-WIMP Annihilation as a Source of the Fermi Bubbles. *Phys.Rev.*, D88:043513, 2013.
- [196] P. Ko, Wan-Il Park, and Yong Tang. Higgs portal vector dark matter for GeV scale γ -ray excess from galactic center. *JCAP*, 1409:013, 2014.
- [197] Matthew R. Buckley, Dan Hooper, and Jonathan L. Rosner. A Leptophobic Z' And Dark Matter From Grand Unification. *Phys.Lett.*, B703:343–347, 2011.
- [198] M.S. Boucenna and S. Profumo. Direct and Indirect Singlet Scalar Dark Matter Detection in the Lepton-Specific two-Higgs-doublet Model. *Phys.Rev.*, D84:055011, 2011.
- [199] Guohuai Zhu. WIMPless dark matter and the excess gamma rays from the Galactic center. *Phys.Rev.*, D83:076011, 2011.
- [200] Bumseok Kyaee and Jong-Chul Park. Light dark matter for Fermi-LAT and CDMS observations. *Phys.Lett.*, B732:373–379, 2014.
- [201] Gardner Marshall and Reinard Primulando. The Galactic Center Region Gamma Ray Excess from A Supersymmetric Leptophilic Higgs Model. *JHEP*, 1105:026, 2011.
- [202] D.G. Cerde so, M. Peir s, and S. Robles. Low-mass right-handed sneutrino dark matter: SuperCDMS and LUX constraints and the Galactic Centre gamma-ray excess. *JCAP*, 1408:005, 2014.
- [203] Prateek Agrawal, Brian Batell, Dan Hooper, and Tongyan Lin. Flavored Dark Matter and the Galactic Center Gamma-Ray Excess. *Phys.Rev.*, D90(6):063512, 2014.
- [204] Dan Hooper, Ilias Cholis, Tim Linden, Jennifer Siegal-Gaskins, and Tracy Slatyer. Pulsars Cannot Account for the Inner Galaxy’s GeV Excess. *Phys.Rev.*, D88:083009, 2013.
- [205] Qiang Yuan and Bing Zhang. Millisecond pulsar interpretation of the Galactic center gamma-ray excess. *JHEAp*, 3-4:1–8, 2014.
- [206] Kevork N. Abazajian, Nicolas Canac, Shunsaku Horiuchi, Manoj Kaplinghat, and Anna Kwa. Discovery of a New Galactic Center Excess Consistent with Upscattered Starlight. 2014.
- [207] Kaoru Hagiwara, Satyanarayan Mukhopadhyay, and Junya Nakamura. 10 GeV neutralino dark matter and light stau in the MSSM. *Phys.Rev.*, D89(1):015023, 2014.
- [208] Matthew R. Buckley, Dan Hooper, and Jason Kumar. Phenomenology of Dirac Neutralino Dark Matter. *Phys.Rev.*, D88:063532, 2013.
- [209] Heather E. Logan. Dark matter annihilation through a lepton-specific Higgs boson. *Phys.Rev.*, D83:035022, 2011.

- [210] Thomas Lacroix, Celine Boehm, and Joseph Silk. Fitting the Fermi-LAT GeV excess: On the importance of including the propagation of electrons from dark matter. *Phys.Rev.*, D90(4):043508, 2014.
- [211] Kingman Cheung, Po-Yan Tseng, Yue-Lin S. Tsai, and Tzu-Chiang Yuan. Global Constraints on Effective Dark Matter Interactions: Relic Density, Direct Detection, Indirect Detection, and Collider. *JCAP*, 1205:001, 2012.
- [212] Ran Ding and Yi Liao. Spin 3/2 Particle as a Dark Matter Candidate: an Effective Field Theory Approach. *JHEP*, 1204:054, 2012.
- [213] Ning Zhou, David Berge, and Daniel Whiteson. Mono-everything: combined limits on dark matter production at colliders from multiple final states. *Phys.Rev.*, D87(9):095013, 2013.
- [214] Linda Carpenter, Anthony DiFranzo, Michael Mulhearn, Chase Shimmin, Sean Tulin, et al. Mono-Higgs-boson: A new collider probe of dark matter. *Phys.Rev.*, D89(7):075017, 2014.
- [215] Herbi Dreiner, Daniel Schmeier, and Jamie Tattersall. Contact Interactions Probe Effective Dark Matter Models at the LHC. *Europhys.Lett.*, 102:51001, 2013.
- [216] Zhao-Huan Yu, Qi-Shu Yan, and Peng-Fei Yin. Detecting interactions between dark matter and photons at high energy e^+e^- colliders. *Phys.Rev.*, D88(7):075015, 2013.
- [217] Asher Berlin, Tongyan Lin, and Lian-Tao Wang. Mono-Higgs Detection of Dark Matter at the LHC. *JHEP*, 1406:078, 2014.
- [218] Kingman Cheung, Po-Yan Tseng, and Tzu-Chiang Yuan. Gamma-ray Constraints on Effective Interactions of the Dark Matter. *JCAP*, 1106:023, 2011.
- [219] Arvind Rajaraman, Tim M.P. Tait, and Alexander M. Wijangco. Effective Theories of Gamma-ray Lines from Dark Matter Annihilation. *Phys.Dark Univ.*, 2:17–21, 2013.
- [220] Andrea De Simone, Alexander Monin, Andrea Thamm, and Alfredo Urbano. On the effective operators for Dark Matter annihilations. *JCAP*, 1302:039, 2013.
- [221] Jia-Ming Zheng, Zhao-Huan Yu, Jun-Wen Shao, Xiao-Jun Bi, Zhibing Li, et al. Constraining the interaction strength between dark matter and visible matter: I. fermionic dark matter. *Nucl.Phys.*, B854:350–374, 2012.
- [222] A. Liam Fitzpatrick, Wick Haxton, Emanuel Katz, Nicholas Lubbers, and Yiming Xu. Model Independent Direct Detection Analyses. 2012.
- [223] Nikhil Anand, A. Liam Fitzpatrick, and W.C. Haxton. Weakly interacting massive particle-nucleus elastic scattering response. *Phys.Rev.*, C89(6):065501, 2014.
- [224] Marat Freytsis and Zoltan Ligeti. On dark matter models with uniquely spin-dependent detection possibilities. *Phys.Rev.*, D83:115009, 2011.

- [225] Timothy Cohen, Daniel J. Phalen, and Aaron Pierce. On the Correlation Between the Spin-Independent and Spin-Dependent Direct Detection of Dark Matter. *Phys.Rev.*, D81:116001, 2010.
- [226] Moira I. Gresham and Kathryn M. Zurek. Effect of nuclear response functions in dark matter direct detection. *Phys.Rev.*, D89(12):123521, 2014.
- [227] A. Liam Fitzpatrick, Wick Haxton, Emanuel Katz, Nicholas Lubbers, and Yiming Xu. The Effective Field Theory of Dark Matter Direct Detection. *JCAP*, 1302:004, 2013.
- [228] Yonit Hochberg, Eric Kuflik, Tomer Volansky, and Jay G. Wacker. Mechanism for Thermal Relic Dark Matter of Strongly Interacting Massive Particles. *Phys.Rev.Lett.*, 113:171301, 2014.
- [229] David Curtin, Ze'ev Surujon, and Yuhsin Tsai. Direct Detection with Dark Mediators. *Phys.Lett.*, B738:477–482, 2014.
- [230] Michele Papucci, Alessandro Vichi, and Kathryn M. Zurek. Monojet versus the rest of the world I: t-channel models. *JHEP*, 1411:024, 2014.
- [231] Jessica Goodman and William Shepherd. LHC Bounds on UV-Complete Models of Dark Matter. 2011.
- [232] Giorgio Busoni, Andrea De Simone, Enrico Morgante, and Antonio Riotto. On the Validity of the Effective Field Theory for Dark Matter Searches at the LHC. *Phys.Lett.*, B728:412–421, 2014.
- [233] O. Buchmueller, Matthew J. Dolan, and Christopher McCabe. Beyond Effective Field Theory for Dark Matter Searches at the LHC. *JHEP*, 1401:025, 2014.
- [234] Daniele Alves et al. Simplified Models for LHC New Physics Searches. *J.Phys.*, G39:105005, 2012.
- [235] Patrick J. Fox and Ciaran Williams. Next-to-Leading Order Predictions for Dark Matter Production at Hadron Colliders. *Phys.Rev.*, D87(5):054030, 2013.
- [236] Alexander Friedland, Michael L. Graesser, Ian M. Shoemaker, and Luca Vecchi. Probing Nonstandard Standard Model Backgrounds with LHC Monojets. *Phys.Lett.*, B714:267–275, 2012.
- [237] Michael L. Graesser, Ian M. Shoemaker, and Luca Vecchi. A Dark Force for Baryons. 2011.
- [238] Stefano Profumo, William Shepherd, and Tim Tait. Pitfalls of dark matter crossing symmetries. *Phys.Rev.*, D88(5):056018, 2013.
- [239] Haipeng An, Lian-Tao Wang, and Hao Zhang. Dark matter with t -channel mediator: a simple step beyond contact interaction. *Phys.Rev.*, D89(11):115014, 2014.

- [240] Anthony DiFranzo, Keiko I. Nagao, Arvind Rajaraman, and Tim M.P. Tait. Simplified Models for Dark Matter Interacting with Quarks. *JHEP*, 1311:014, 2013.
- [241] Spencer Chang, Ralph Edezhath, Jeffrey Hutchinson, and Markus Luty. Effective WIMPs. *Phys.Rev.*, D89(1):015011, 2014.
- [242] Randel C. Cotta, Arvind Rajaraman, Tim M. P. Tait, and Alexander M. Wijangco. Particle Physics Implications and Constraints on Dark Matter Interpretations of the CDMS Signal. *Phys.Rev.*, D90(1):013020, 2014.
- [243] Manoj Kaplinghat, Sean Tulin, and Hai-Bo Yu. Self-interacting Dark Matter Benchmarks. 2013.
- [244] Brando Bellazzini, Mathieu Cliche, and Philip Tanedo. Effective theory of self-interacting dark matter. *Phys.Rev.*, D88(8):083506, 2013.
- [245] JiJi Fan, Andrey Katz, Lisa Randall, and Matthew Reece. Double-Disk Dark Matter. *Phys.Dark Univ.*, 2:139–156, 2013.
- [246] Sean Tulin, Hai-Bo Yu, and Kathryn M. Zurek. Beyond Collisionless Dark Matter: Particle Physics Dynamics for Dark Matter Halo Structure. *Phys.Rev.*, D87(11):115007, 2013.
- [247] Sean Tulin, Hai-Bo Yu, and Kathryn M. Zurek. Resonant Dark Forces and Small Scale Structure. *Phys.Rev.Lett.*, 110(11):111301, 2013.
- [248] Francis-Yan Cyr-Racine and Kris Sigurdson. Cosmology of atomic dark matter. *Phys.Rev.*, D87(10):103515, 2013.
- [249] R. Foot. Implications of mirror dark matter kinetic mixing for CMB anisotropies. *Phys.Lett.*, B718:745–751, 2013.
- [250] Sean Tulin, Hai-Bo Yu, and Kathryn M. Zurek. Three Exceptions for Thermal Dark Matter with Enhanced Annihilation to $\gamma\gamma$. *Phys.Rev.*, D87(3):036011, 2013.
- [251] David E. Kaplan, Gordan Z. Krnjaic, Keith R. Rehermann, and Christopher M. Wells. Dark Atoms: Asymmetry and Direct Detection. *JCAP*, 1110:011, 2011.
- [252] Abraham Loeb and Neal Weiner. Cores in Dwarf Galaxies from Dark Matter with a Yukawa Potential. *Phys.Rev.Lett.*, 106:171302, 2011.
- [253] Haipeng An, Shao-Long Chen, Rabindra N. Mohapatra, and Yue Zhang. Leptogenesis as a Common Origin for Matter and Dark Matter. *JHEP*, 1003:124, 2010.
- [254] Matthew R. Buckley and Patrick J. Fox. Dark Matter Self-Interactions and Light Force Carriers. *Phys.Rev.*, D81:083522, 2010.
- [255] Jonathan L. Feng, Manoj Kaplinghat, and Hai-Bo Yu. Halo Shape and Relic Density Exclusions of Sommerfeld-Enhanced Dark Matter Explanations of Cosmic Ray Excesses. *Phys.Rev.Lett.*, 104:151301, 2010.

- [256] Jonathan L. Feng, Manoj Kaplinghat, Huitzu Tu, and Hai-Bo Yu. Hidden Charged Dark Matter. *JCAP*, 0907:004, 2009.
- [257] Nima Arkani-Hamed, Douglas P. Finkbeiner, Tracy R. Slatyer, and Neal Weiner. A Theory of Dark Matter. *Phys.Rev.*, D79:015014, 2009.
- [258] Michael Kesden and Marc Kamionkowski. Galilean Equivalence for Galactic Dark Matter. *Phys.Rev.Lett.*, 97:131303, 2006.
- [259] Robert Foot. Mirror matter-type dark matter. *Int.J.Mod.Phys.*, D13:2161–2192, 2004.
- [260] R.N. Mohapatra, S. Nussinov, and V.L. Teplitz. Mirror matter as selfinteracting dark matter. *Phys.Rev.*, D66:063002, 2002.
- [261] David N. Spergel and Paul J. Steinhardt. Observational evidence for selfinteracting cold dark matter. *Phys.Rev.Lett.*, 84:3760–3763, 2000.
- [262] E. Aprile et al. Limits on spin-dependent WIMP-nucleon cross sections from 225 live days of XENON100 data. *Phys.Rev.Lett.*, 111(2):021301, 2013.
- [263] Search for New Phenomena in Monojet plus Missing Transverse Momentum Final States using 10fb-1 of pp Collisions at $\sqrt{s}=8$ TeV with the ATLAS detector at the LHC. 2012.
- [264] Wei-Chih Huang, Alfredo Urbano, and Wei Xue. Fermi Bubbles under Dark Matter Scrutiny Part II: Particle Physics Analysis. *JCAP*, 1404:020, 2014.
- [265] Asher Berlin, Dan Hooper, and Samuel D. McDermott. Simplified Dark Matter Models for the Galactic Center Gamma-Ray Excess. *Phys.Rev.*, D89(11):115022, 2014.
- [266] Eder Izaguirre, Gordan Krnjaic, and Brian Shuve. The Galactic Center Excess from the Bottom Up. *Phys.Rev.*, D90(5):055002, 2014.
- [267] CÄline Boehm, Matthew J. Dolan, Christopher McCabe, Michael Spannowsky, and Chris J. Wallace. Extended gamma-ray emission from Coy Dark Matter. *JCAP*, 1405:009, 2014.
- [268] Andi Hektor and Luca Marzola. Coy Dark Matter and the anomalous magnetic moment. *Phys.Rev.*, D90(5):053007, 2014.
- [269] Francesco D’Eramo and Jesse Thaler. Semi-annihilation of Dark Matter. *JHEP*, 1006:109, 2010.
- [270] Celine Boehm, Matthew J. Dolan, and Christopher McCabe. A weighty interpretation of the Galactic Centre excess. *Phys.Rev.*, D90(2):023531, 2014.
- [271] Herbi K. Dreiner, Howard E. Haber, and Stephen P. Martin. Two-component spinor techniques and Feynman rules for quantum field theory and supersymmetry. *Phys.Rept.*, 494:1–196, 2010.

- [272] L.J. Hall and Lisa Randall. Weak scale effective supersymmetry. *Phys.Rev.Lett.*, 65:2939–2942, 1990.
- [273] R. Sekhar Chivukula and Howard Georgi. Composite Technicolor Standard Model. *Phys.Lett.*, B188:99, 1987.
- [274] Julio F. Navarro, Carlos S. Frenk, and Simon D.M. White. The Structure of cold dark matter halos. *Astrophys.J.*, 462:563–575, 1996.
- [275] Julio F. Navarro, Carlos S. Frenk, and Simon D.M. White. A Universal density profile from hierarchical clustering. *Astrophys.J.*, 490:493–508, 1997.
- [276] Anatoly Klypin, HongSheng Zhao, and Rachel S. Somerville. Lambda CDM-based models for the Milky Way and M31 I: Dynamical models. *Astrophys.J.*, 573:597–613, 2002.
- [277] Jeremy Mardon, Yasunori Nomura, Daniel Stolarski, and Jesse Thaler. Dark Matter Signals from Cascade Annihilations. *JCAP*, 0905:016, 2009.
- [278] Alejandro Ibarra, Sergio Lopez Gehler, and Miguel Pato. Dark matter constraints from box-shaped gamma-ray features. *JCAP*, 1207:043, 2012.
- [279] Marco Cirelli, Gennaro Corcella, Andi Hektor, Gert Hutsi, Mario Kadastik, et al. PPC 4 DM ID: A Poor Particle Physicist Cookbook for Dark Matter Indirect Detection. *JCAP*, 1103:051, 2011.
- [280] Paolo Ciafaloni, Denis Comelli, Antonio Riotto, Filippo Sala, Alessandro Strumia, et al. Weak Corrections are Relevant for Dark Matter Indirect Detection. *JCAP*, 1103:019, 2011.
- [281] Inc. Wolfram Research. Mathematica. *Wolfram Research, Inc.*, 2010.
- [282] Torbjorn Sjostrand, Stephen Mrenna, and Peter Z. Skands. A Brief Introduction to PYTHIA 8.1. *Comput.Phys.Commun.*, 178:852–867, 2008.
- [283] Marco Cirelli and Gaele Giesen. Antiprotons from Dark Matter: Current constraints and future sensitivities. *JCAP*, 1304:015, 2013.
- [284] Kyoungchul Kong and Jong-Chul Park. Bounds on dark matter interpretation of Fermi-LAT GeV excess. *Nucl.Phys.*, B888:154–168, 2014.
- [285] Joachim Kopp, Viviana Niro, Thomas Schwetz, and Jure Zupan. DAMA/LIBRA and leptonically interacting Dark Matter. *Phys.Rev.*, D80:083502, 2009.
- [286] Moira I. Gresham and Kathryn M. Zurek. Light Dark Matter Anomalies After LUX. *Phys.Rev.*, D89(1):016017, 2014.
- [287] Marco Cirelli, Eugenio Del Nobile, and Paolo Panci. Tools for model-independent bounds in direct dark matter searches. *JCAP*, 1310:019, 2013.

- [288] Bogdan A. Dobrescu and Felix Yu. Coupling-mass mapping of dijet peak searches. *Phys.Rev.*, D88(3):035021, 2013.
- [289] Christopher D. Carone and Hitoshi Murayama. Possible light U(1) gauge boson coupled to baryon number. *Phys.Rev.Lett.*, 74:3122–3125, 1995.
- [290] Christopher D. Carone and Hitoshi Murayama. Realistic models with a light U(1) gauge boson coupled to baryon number. *Phys.Rev.*, D52:484–493, 1995.
- [291] M. Williams, C.P. Burgess, Anshuman Maharana, and F. Quevedo. New Constraints (and Motivations) for Abelian Gauge Bosons in the MeV-TeV Mass Range. *JHEP*, 1108:106, 2011.
- [292] Bogdan A. Dobrescu and Claudia Frugiuele. Hidden GeV-scale interactions of quarks. *Phys.Rev.Lett.*, 113:061801, 2014.
- [293] Daniel Whiteson. Private communication.
- [294] Mark Srednicki, Richard Watkins, and Keith A. Olive. Calculations of Relic Densities in the Early Universe. *Nucl.Phys.*, B310:693, 1988.
- [295] Edward W. Kolb and Michael S. Turner. The Early Universe. *Front.Phys.*, 69:1–547, 1990.
- [296] J. Dunkley et al. Five-Year Wilkinson Microwave Anisotropy Probe (WMAP) Observations: Likelihoods and Parameters from the WMAP data. *Astrophys.J.Suppl.*, 180:306–329, 2009.
- [297] E. Komatsu et al. Five-Year Wilkinson Microwave Anisotropy Probe (WMAP) Observations: Cosmological Interpretation. *Astrophys.J.Suppl.*, 180:330–376, 2009.
- [298] P.A.R. Ade et al. Planck 2013 results. I. Overview of products and scientific results. *Astron.Astrophys.*, 571:A1, 2014.
- [299] Mathias Pierre, Jennifer M. Siegal-Gaskins, and Pat Scott. Sensitivity of CTA to dark matter signals from the Galactic Center. *JCAP*, 1406(10):024, 2014.
- [300] Kathryn M. Zurek. Asymmetric Dark Matter: Theories, Signatures, and Constraints. *Phys.Rept.*, 537:91–121, 2014.
- [301] Richard Easther, Richard Galvez, Ogan Ozsoy, and Scott Watson. Supersymmetry, Nonthermal Dark Matter and Precision Cosmology. *Phys.Rev.*, D89(2):023522, 2014.
- [302] Kalliopi Petraki and Raymond R. Volkas. Review of asymmetric dark matter. *Int.J.Mod.Phys.*, A28:1330028, 2013.
- [303] John McDonald. Comment on the ‘Freeze-In’ Mechanism of Dark Matter Production. 2011.

- [304] Giorgio Arcadi and Piero Ullio. Accurate estimate of the relic density and the kinetic decoupling in non-thermal dark matter models. *Phys.Rev.*, D84:043520, 2011.
- [305] Pearl Sandick and Scott Watson. Constraints on a Non-thermal History from Galactic Dark Matter Spikes. *Phys.Rev.*, D84:023507, 2011.
- [306] Lawrence J. Hall, Karsten Jedamzik, John March-Russell, and Stephen M. West. Freeze-In Production of FIMP Dark Matter. *JHEP*, 1003:080, 2010.
- [307] Roberto Aloisio, V. Berezhinsky, and M. Kachelriess. On the status of superheavy dark matter. *Phys.Rev.*, D74:023516, 2006.
- [308] Jonathan L. Feng, Shu-fang Su, and Fumihiro Takayama. SuperWIMP gravitino dark matter from slepton and sneutrino decays. *Phys.Rev.*, D70:063514, 2004.
- [309] Jonathan L. Feng, Arvind Rajaraman, and Fumihiro Takayama. SuperWIMP dark matter signals from the early universe. *Phys.Rev.*, D68:063504, 2003.
- [310] Jonathan L. Feng, Arvind Rajaraman, and Fumihiro Takayama. Superweakly interacting massive particles. *Phys.Rev.Lett.*, 91:011302, 2003.
- [311] Edward A. Baltz and Hitoshi Murayama. Gravitino warm dark matter with entropy production. *JHEP*, 0305:067, 2003.
- [312] John McDonald. Thermally generated gauge singlet scalars as selfinteracting dark matter. *Phys.Rev.Lett.*, 88:091304, 2002.
- [313] Edward W. Kolb, Daniel J.H. Chung, and Antonio Riotto. WIMPzillas! pages 91–105, 1998.
- [314] Daniel J.H. Chung, Edward W. Kolb, and Antonio Riotto. Production of massive particles during reheating. *Phys.Rev.*, D60:063504, 1999.
- [315] Daniel J.H. Chung, Edward W. Kolb, and Antonio Riotto. Superheavy dark matter. *Phys.Rev.*, D59:023501, 1999.
- [316] Lev Kofman, Andrei D. Linde, and Alexei A. Starobinsky. Reheating after inflation. *Phys.Rev.Lett.*, 73:3195–3198, 1994.
- [317] John R. Ellis, G.B. Gelmini, Jorge L. Lopez, Dimitri V. Nanopoulos, and Subir Sarkar. Astrophysical constraints on massive unstable neutral relic particles. *Nucl.Phys.*, B373:399–437, 1992.
- [318] John R. Ellis, Dimitri V. Nanopoulos, and Subir Sarkar. The Cosmology of Decaying Gravitinos. *Nucl.Phys.*, B259:175, 1985.
- [319] N. Mirabal. Dark matter vs. Pulsars: Catching the impostor. *Mon.Not.Roy.Astron.Soc.*, 436:2461, 2013.

- [320] Rasmus Voss and Marat Gilfanov. Dynamical Formation of X-ray binaries in the inner bulge of M31. *Mon.Not.Roy.Astron.Soc.*, 380:1685, 2007.
- [321] Brian Batell, Josef Pradler, and Michael Spannowsky. Dark Matter from Minimal Flavor Violation. *JHEP*, 1108:038, 2011.
- [322] Prateek Agrawal, Monika Blanke, and Katrin Gemmler. Flavored dark matter beyond Minimal Flavor Violation. *JHEP*, 1410:72, 2014.
- [323] Vanda Silveira and A. Zee. SCALAR PHANTOMS. *Phys.Lett.*, B161:136, 1985.
- [324] Brian Patt and Frank Wilczek. Higgs-field portal into hidden sectors. 2006.
- [325] Seyda Ipek, David McKeen, and Ann E. Nelson. A Renormalizable Model for the Galactic Center Gamma Ray Excess from Dark Matter Annihilation. *Phys.Rev.*, D90(5):055021, 2014.
- [326] Sean Tulin. New weakly-coupled forces hidden in low-energy QCD. *Phys.Rev.*, D89(11):114008, 2014.
- [327] Manoj Kaplinghat, Sean Tulin, and Hai-Bo Yu. Direct Detection Portals for Self-interacting Dark Matter. *Phys.Rev.*, D89(3):035009, 2014.
- [328] Christopher D. Carone. Flavor-Nonuniversal Dark Gauge Bosons and the Muon $g-2$. *Phys.Lett.*, B721:118–122, 2013.
- [329] Lisa Randall and Raman Sundrum. A Large mass hierarchy from a small extra dimension. *Phys.Rev.Lett.*, 83:3370–3373, 1999.
- [330] Lisa Randall and Matthew D. Schwartz. Quantum field theory and unification in AdS5. *JHEP*, 0111:003, 2001.
- [331] Csaba Csaki, Joshua Erlich, and John Terning. The Effective Lagrangian in the Randall-Sundrum model and electroweak physics. *Phys.Rev.*, D66:064021, 2002.
- [332] Roberto Contino, David Marzocca, Duccio Pappadopulo, and Riccardo Rattazzi. On the effect of resonances in composite Higgs phenomenology. *JHEP*, 1110:081, 2011.
- [333] Brando Bellazzini, Csaba Csaki, Jay Hubisz, Javi Serra, and John Terning. Composite Higgs Sketch. *JHEP*, 1211:003, 2012.
- [334] Adam Martin, Jessie Shelton, and James Unwin. Fitting the Galactic Center Gamma-Ray Excess with Cascade Annihilations. *Phys.Rev.*, D90(10):103513, 2014.
- [335] Oscar Adriani et al. An anomalous positron abundance in cosmic rays with energies 1.5-100 GeV. *Nature*, 458:607–609, 2009.